MSS-030
30冊 29-th

Mon. Not. R. astr. Soc. (1982) 201, 569–577

Two-station television observations of Perseid meteors

Michael Hapgood, Pamela Rothwell and Ola Royrvik*
Department of Physics, The University, Southampton SO9 5NH

Received 1982 March 9; in original form 1981 December 29

Summary. The predictions of the dustball meteor ablation theory of Hawkes & Jones have been tested using data from two-station television observations of meteors made during the 1977 and 1978 displays of the Perseid meteor shower. The meteor velocities and the heights at which each meteor began and ended, together with the heights of maximum brightness, were determined for 39 Perseid meteors in the magnitude range $M_v = +4$ to -2. The beginning heights (h_B) were found to be independent of meteor magnitude; they ranged from 105 to 115 km, with a mean value of $h_B = 110 \pm 1$ km. The end heights (h_E) and the heights of maximum brightness (h_M) were independent of meteor magnitude only up to a critical magnitude $M_v = 0$ (corresponding to a meteoroid of critical mass $\sim 2 \times 10^{-4}$ kg). Their mean values were $h_E = 99 \pm 1$ km and $h_M = 103 \pm 1$ km respectively. For meteors brighter than $M_v = 0$, h_E and h_M were, on average, significantly lower than these mean levels, in good qualitative agreement with dustball theory.

By assuming that, at the critical mass, dustball meteoroids disintegrate into their constituent grains just before ablation starts, we find that $3-9 \times 10^5$ J kg^{-1} is required to disintegrate Perseid dustball material. This value is several times lower than the value adopted by Hawkes & Jones ($1-6 \times 10^6$ J kg^{-1}), suggesting that Perseid material is weaker than the material considered in the theory of dustball ablation.

1 Introduction

The orbits of most meteor showers coincide closely with the orbits of comets (Lovell 1954). This was first established in 1866 by Schiaparelli who noted the similarity of the orbit of the Perseids with that of Comet Swift–Tuttle (1862 III). Thus it is thought that shower meteoroids are particles ejected from a parent comet and so we expect them to have a structure which is consistent with a cometary origin. It is generally thought that the main component of a comet is a body (the nucleus) about 1 km in size, composed of a mixture of ices (water, carbon dioxide, ammonia) and dust; this is the 'dirty snowball' mixture first proposed by Whipple (1950). When the comet is close to the Sun (< 3 AU) the ices sublime,

* Present address: Aeronomy Laboratory, University of Illinois, Urbana, Illinois 61801, USA.

releasing dust particles into space. These dust particles are believed to be the shower meteoroids.

Jacchia (1955) was the first to propose a theory of meteoroid structure based on an origin in a 'dirty snowball' comet. He proposed the term 'fragile conglomerate' to describe this type of meteoroid, but the simpler term 'dustball' has come to be widely used in its place. The dustball theory assumes that meteoroids are composed of tiny grains (radius < 0.1 mm) of stony material which are weakly bound together. Thus on entering the atmosphere the meteoroid rapidly fragments into these fundamental grains, which then ablate independently.

Until recently, most discussion of the ablation of dustball meteoroids was qualitative but in 1975 Hawkes & Jones (1975a) published a quantitative theory for dustball ablation. They proposed a simple model in which the fundamental grains (radius ~ 0.07 mm) are held together by a comparatively low melting point 'glue' (melting temperature ~ 1300 K). In this model the meteoroid ablates in two stages. First, the glue melts releasing the grains; there is no light emission at this stage. Secondly the grains are heated to a high temperature and then ablate producing the meteoric light emission. Hawkes & Jones made two important predictions from this model.

(i) The beginning height h_B of the meteor (that is the height at which light emission starts) should be independent of the size of the meteoroid. Light emission starts when the surface temperature of the released grains reaches the boiling temperature of the grain material. For small particles (radius < 0.1 mm) this is controlled by the amount of heat lost by thermal radiation and the boiling temperature is reached at a height which is independent of the grain size and is a function only of the meteoroid velocity (Jones & Kaiser 1966). Thus all dustball meteoroids of the same velocity should become visible at the same height.

(ii) There should be a significant difference between the behaviour of large and small dustball meteoroids. Small dustballs should fragment completely before the ablation of the grains begins, whereas, in large dustballs, grains would continue to be released from the meteoroid after the onset of grain ablation. Consequently the end height h_E and the height of maximum light h_M of the meteor should be independent of mass for a small meteoroid, since its light curve is simply the sum of the light curves of a set of independently ablating grains. For larger meteoroids, as the mass increases, more and more grains are released after the onset of ablation, so h_M and h_E decrease with increasing meteoroid mass. A meteoroid of the critical mass m_c should just fragment at the beginning height h_B. These results are illustrated in Fig. 1. The critical mass is dependent on the meteor velocity and is expected to have values in the range 10^{-4} to 10^{-6} kg.

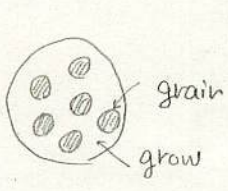

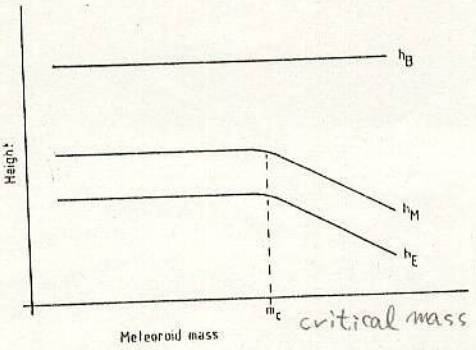

Figure 1. The mass dependence of beginning heights (h_B), heights of maximum light (h_M) and end heights (h_E) predicted for dustball meteors.

We have tested this theory by comparing its predictions against observations of Perseid meteors. For these data the meteoroid mass is the major variable and, since the velocity is constant, the mass can be represented by the meteor magnitude. We can now test the dustball ablation theory by plotting graphs of beginning height, height of maximum light and end height against the meteor magnitude. This should give a graph similar to Fig. 1. The critical magnitude at which h_M and h_E begin to decrease can be measured off the graph and the critical mass m_c, corresponding to the critical magnitude, can be estimated using the relation given by Hughes (1978).

Once we know m_c we can estimate X, the amount of energy required to fragment unit mass of dustball material. We must first derive an expression for the height h_D at which fragmentation of dustball meteoroids is complete. To do this we calculate the energy input from atmospheric heating and equate this to the energy required to fragment the meteoroid. We assume that the meteoroid is a sphere of radius r (initial value r_0) and density d and has velocity v. $\rho(h)$ is the air density at height h. The power input from atmospheric heating is

$$\frac{dE}{dt} = \tfrac{1}{2}\rho(h)v^3\pi r^2, \tag{1}$$

where we have assumed a heat transfer coefficient of unity and neglected the heat loss due to radiation. Jones & Kaiser (1966) have shown that this radiation loss is not important for large bodies ($r \gg 0.1$ mm) such as the parent meteoroid.

If Z is the zenith angle of the meteor trajectory then $v = -(dh/dt)/\cos Z$ and so we can rewrite equation (1) as

$$\frac{dE}{dt} = -\frac{\rho(h)v^2\pi r^2}{2\cos Z}\frac{dh}{dt}. \tag{2}$$

To calculate how this power ablates the meteoroid, we must consider the effect of the thermal conductivity of the meteoroid material. To simplify the problem we treat only the two extreme cases.

Case 1. The thermal conductivity is sufficiently high that heat is rapidly conducted into the interior of the meteoroid during ablation. In this case the meteoroid will heat up isothermally and will disintegrate almost instantaneously when the boiling temperature of the dustball 'glue' is reached. This requires a total energy input

$$E = \tfrac{4}{3}\pi r_0^3 X d. \tag{3}$$

By integrating equation (2) under the assumption of an exponentially scaled atmosphere of scale height H, we obtain another expression for E. By equating these we obtain the following expression

$$\rho(h_D) = \frac{8 X d \cos Z r_0}{3 H v^2}. \tag{4}$$

Case 2. The thermal conductivity of the material is very low, so that at any instant only the surface layer is heated. In this case the meteoroid fragments layer by layer and we can write

$$\frac{dE}{dt} = -4\pi r^2 X d\frac{dr}{dt}. \tag{5}$$

By combining equations (2) and (5) and integrating we obtain the expression

$$\rho(h_D) = \frac{8 X d \cos Z r_0}{H v^2}. \tag{6}$$

MSS-030

Thus we obtain a formula for X:

$$X = \frac{C\rho(h_D)Hv^2}{8 r_0 d \cos Z} \quad (7)$$

where C is a factor which varies between 1 and 3 according to the thermal conductivity of the meteoroid material.

Since $h_D = h_B$ when the meteoroid has the critical mass we can determine all the terms on the right-hand side of equation (7). The air density and scale heights are taken from standard atmosphere tables (COSPAR 1972). The meteoroid density for Perseids is taken from Hughes (1978) and the radius r_0 is then calculated from the critical mass. The velocity and zenith distance are measured directly. Thus we can estimate the value of X to within the factor of 3 set by C.

2 Experimental data

The meteor observations reported in this paper were made with a two-station low-light television camera system. One television camera was a Marconi Instruments Image Isocon. This used an English Electric P850 image isocon tube, which had a photocathode with an extended red (S25) spectral response. An $f/1.4$ Wray lens of 102-mm focal length was used, giving a 30° by 20° field of view. The other television camera was a Grant and Taylor GT50/NV Silicon Intensified Target (SIT) television camera, which used an RCA 4804 SIT tube with an S20ER photocathode spectral response (similar to S25). An $f/0.78$ Canon lens of 25-mm focal length was used, giving a 20° by 15° field of view.

These TV cameras are quite sensitive; in ideal conditions they can record stars down to visual magnitude +7.5 (SIT) and +8.5 (isocon) respectively. For observations of meteors the limiting magnitudes move to brighter levels because TV cameras respond poorly to rapidly moving objects. Both cameras can record meteors only down to a limiting magnitude +7. (The SIT camera compensates for its worse sensitivity by having a better time response than the isocon.) Finally, we must note that conditions were not ideal for these observations as atmospheric haze reduced the limiting magnitude still further to magnitude +6.

The television cameras were operated at sites in southern England during the Perseid displays of 1977 and 1978. The isocon camera was operated at Southampton (50° 56′ N, 1° 24′ W), while the SIT camera was operated at a site to the north – in 1977 Harwell (51° 35′ N, 1° 20′ W) and in 1978 South Wonston near Winchester (51° 7′ N, 1° 20′ W). The times of observations are shown in Table 1 together with the number of two-station meteors recorded during each session.

The heights, velocities and radiants of these meteors were calculated by triangulation against the star background. We estimate that our meteor heights are accurate to ± 1 km, our velocities to within ± 2 km s^{-1} and radiants to ± 3°. The peak brightness of each meteor (expressed as an apparent magnitude m_{TV}) was estimated by comparison with the stars on the TV screen (Hawkes & Jones 1975b). We estimate the error to be about half a magnitude.

Table 1. Distribution of observations.

Night of observations	Observations started at	Observations ended at	Hours of observation	Number of meteors
1977 August 11/12	2300	0100	2	4
	0145	0315	1½	10
1977 August 12/13	2300	0315	4¼	6
1978 August 12/13	0045	0315	3½	19

All times are expressed in UT.

TABLE I. VIDICON CAMERA METEORS

I.D. No.	E.S.T.	R.A.	d(R.A.)	Dec.	d(dec)	Vobs.	dV	Vinf	Vg	cos χ	Mag	log(mass)	Hb	Hm	He	Type
810506001	00:07:25	275.3	0.5	33.2	2.0	43.5	0.9	43.7	42.2	0.729	5.5	-3.77	106	98	96	C2
810506002	00:19:48	244.2	0.5	-3.3	2.0	37.9	0.5	38.1	36.4	0.661	2.5	-2.43	106	99	93	C1
810506003	00:33:33	220.8	0.5	-2.7	2.0	30.2	3.0	30.6	28.5	0.719	6.8	-3.81	99	96	94	C1
810506004	00:46:09	257.2	0.5	12.1	2.0	28.9	6.0	29.3	27.1	0.809	6.7	-3.52	97	94	90	C1
810506005	00:47:41	233.6	0.5	20.8	2.0	47.3	1.4	47.7	46.4	0.920	3.8	-4.33	99	98	87	A
810506006	00:48:40	276.3	0.5	65.2	2.0	13.8	0.3	14.7	9.5	0.879	6.9	-2.25	88	81	76	C1
810506007	00:51:42	358.3	0.5	80.0	2.0	21.4	2.6	21.8	18.7	0.640	2.3	-0.34	112	96	87	C1
810506008	00:53:03	325.2	0.5	80.0	2.0	21.9	0.5	22.5	19.5	0.710	5.7	-2.45	91	91	84	A
810506009	01:29:26	265.9	0.5	-11.3	2.0	16.6	0.3	17.1	12.9	0.619	5.9	-2.01	93	92	86	C1
810506010	01:32:46	290.6	0.5	20.0	2.0	45.5	0.7	45.7	44.3	0.690	4.7	-3.05	108	100	97	C2
810506011	01:48:08	15.5	0.5	66.6	2.0	20.2	0.6	20.8	17.5	0.520	5.0	-1.49	92	89	85	C1
810506012	01:51:44	302.3	0.5	-2.7	2.0	72.3	1.4	72.4	71.5	0.390	3.3	-3.34	117	110	105	C2
810506013	01:57:58	162.6	0.5	6.4	2.0	66.8	0.7	67.0	66.0	0.140	4.5	-1.96	-	112	-	-
810506014	02:08:35	1.4	0.5	75.4	2.0	21.0	0.5	21.6	18.5	0.661	3.6	-2.60	95	94	83	C1
810506015	02:20:47	338.5	0.5	-2.4	2.0	69.4	0.6	69.5	68.6	0.030	3.6	—	122	121	-	C2
810506016	02:31:53	312.1	0.5	75.6	2.0	19.7	0.3	20.7	17.4	0.800	6.5	-2.48	88	87	77	A
810506017	02:38:32	284.7	0.5	22.8	2.0	32.3	0.8	32.5	30.6	0.871	5.5	-3.38	102	100	100	C1
810506018	02:40:12	271.0	0.5	17.1	2.0	28.9	1.0	29.3	27.1	0.889	6.2	-3.40	97	97	90	C1
810506019	02:45:00	300.0	0.5	45.2	2.0	33.6	0.4	34.2	32.3	0.879	5.4	-2.96	95	93	81	A
810506020	02:49:31	57.6	0.5	28.6	2.0	33.3	0.3	33.7	31.8	0.200	3.1	—	-	95	92	-
810506021	02:50:42	266.8	0.5	54.0	2.0	23.5	0.8	23.8	21.0	0.979	6.6	-2.66	97	97	77	C1
810506022	03:10:37	159.2	0.5	2.3	2.0	66.4	1.0	66.6	65.6	0.170	3.9	—	108	108	-	A
810506023	03:13:04	134.8	0.5	63.8	2.0	13.7	0.5	15.1	10.1	0.570	6.0	-1.77	83	81	78	A
810506024	03:16:12	268.2	0.5	15.7	2.0	47.7	1.0	48.1	46.8	0.889	4.8	-3.30	96	87	81	A
810506025	03:17:05	142.1	0.5	31.4	2.0	64.2	0.6	64.4	63.4	0.010	1.6	-2.68	107	107	107	A
810506026	03:17:33	317.5	0.5	54.6	2.0	36.7	0.5	36.9	35.2	0.839	3.9	-2.43	107	98	90	C1
810506027	03:34:12	299.1	0.5	11.2	2.0	60.9	0.7	61.2	60.2	0.780	4.1	-3.74	100	97	90	A
810506028	03:34:15	338.8	0.5	-1.6	2.0	64.5	0.8	64.8	63.8	0.280	5.0	-3.64	104	100	97	A
810506029	03:47:41	332.4	0.5	10.3	2.0	50.4	0.4	50.6	49.3	0.619	3.9	-3.14	110	102	101	C2
810506030	03:54:24	234.5	0.5	-2.1	2.0	28.1	0.4	28.5	26.3	0.719	5.8	-3.01	99	98	92	C1
810506031	03:57:36	241.2	0.5	-6.4	2.0	27.0	0.4	27.5	25.1	0.560	5.2	-2.72	98	98	92	C1
810506032	03:58:46	210.8	0.5	46.5	2.0	18.3	0.4	19.0	15.3	0.750	5.4	-2.09	89	85	82	A
810506033	04:03:54	209.8	0.5	23.5	2.0	18.1	0.3	18.5	14.8	0.629	1.4	-0.85	99	99	88	C1
810626001	22:45:08	347.1	0.5	50.4	2.0	39.6	0.8	39.8	38.2	0.480	4.6	-3.15	110	101	95	C1
810626002	22:55:13	302.3	0.5	63.7	2.0	10.7	0.6	11.0	3.7	0.910	6.8	-1.71	85	82	76	C1

TABLE I. VIDICON CAMERA METEORS

I.D. No.	E.S.T.	R.A.	d(R.A.)	Dec.	d(dec)	Vobs.	dV	Vinf	Vg	cos χ	Mag	log(mass)	Hb	Hm	He	Type
810626003	22:55:42	261.1	0.5	50.2	2.0	12.7	0.5	13.6	7.8	0.991	4.7	-1.72	82	81	75	A
810626004	22:59:00	274.7	0.5	-15.0	2.0	21.3	0.3	22.2	19.2	0.539	4.1	-1.93	88	85	77	A
810626005	23:05:28	305.3	0.5	-15.4	2.0	40.8	0.4	41.3	39.7	0.290	3.3	-2.05	96	93	92	A
810729001	23:59:47	289.4	0.2	41.7	1.0	22.7	0.7	23.0	20.1	0.991	5.0	-2.70	103	89	83	C1
810730001	00:02:15	340.7	0.1	-17.4	0.4	40.6	0.3	41.1	39.5	0.362	3.8	—	98	91	-	A
810730002	00:03:56	302.7	0.3	-23.6	7.0	22.1	0.4	22.7	19.7	0.468	5.2	-2.50	93	91	88	C1
810730003	00:04:49	18.0	0.7	59.8	0.5	68.7	0.3	68.8	67.9	0.687	3.4	-3.32	113	102	96	C2
810730004	00:10:08	285.1	0.7	24.2	4.4	21.1	0.7	21.5	18.3	0.925	3.0	-2.51	99	98	90	C1
810730005	00:11:21	342.4	0.1	-23.7	1.3	43.4	0.3	43.7	42.2	0.275	2.6	—	-	94	87	-
810730006	00:14:45	344.0	0.4	-12.8	3.6	40.1	0.5	40.4	38.8	0.424	4.2	—	-	91	88	-
810730007	00:27:15	339.7	0.2	-22.2	0.9	39.4	0.4	39.9	38.3	0.343	4.1	-2.84	92	90	86	A
810730008	00:39:44	332.7	0.2	13.4	3.9	23.7	0.4	24.5	21.8	0.836	5.4	-2.58	86	80	75	A
810730009	00:41:41	32.2	0.3	34.8	0.7	67.3	0.6	67.6	66.7	0.498	3.9	-3.34	103	96	92	A
810730010	00:43:59	337.4	0.3	37.2	4.2	39.4	1.8	39.7	38.1	0.940	5.0	-3.23	102	97	93	C1
810730011	00:55:34	344.1	0.2	70.5	0.7	11.7	0.4	12.7	6.0	0.916	6.5	-1.79	85	76	65	C1
810730012	01:02:50	349.3	1.3	-40.3	3.8	45.1	0.6	45.4	44.0	0.058	3.1	—	102	101	-	A
810730013	01:05:58	339.9	0.3	-14.6	2.1	40.2	0.3	40.7	39.1	0.501	3.8	-2.65	96	90	85	A
810730014	01:14:31	342.6	0.1	40.3	3.5	36.2	1.8	36.7	35.0	0.957	4.5	-3.41	93	89	86	A
810730015	01:21:34	345.0	0.3	-23.8	2.8	45.6	0.5	46.0	44.7	0.356	3.6	—	98	96	-	A
810730016	01:21:49	337.8	0.1	-18.0	1.1	42.6	0.3	43.1	41.6	0.473	4.3	-2.67	99	93	85	A
810730017	01:25:29	338.5	0.1	-3.7	1.7	44.4	0.4	44.8	43.4	0.667	4.5	-2.92	98	93	84	A
810730018	01:27:40	338.2	0.1	-4.3	1.2	47.3	0.4	47.6	46.2	0.661	2.9	—	-	98	-	-
810730019	01:30:33	12.8	2.9	53.5	3.3	49.8	2.6	50.2	48.9	0.839	5.3	-3.82	94	93	88	A
810730020	01:35:03	250.2	0.6	58.1	0.4	11.4	0.9	13.0	6.7	0.811	5.9	-2.19	78	74	73	A
810730021	22:45:39	309.2	0.1	11.6	1.8	15.4	0.4	16.2	11.7	0.830	5.5	-2.02	90	85	83	C1
810730022	22:47:00	352.4	1.0	-13.6	6.5	36.2	0.5	36.5	34.8	0.144	4.2	—	-	100	-	-
810730023	22:47:28	241.4	0.5	57.6	0.4	17.2	1.1	17.9	14.0	0.895	5.8	-2.40	90	87	84	C1
810730024	22:51:55	300.6	0.1	-0.1	0.4	23.5	0.2	24.0	21.3	0.733	4.7	-2.00	95	88	81	C1
810730025	23:03:50	306.6	0.1	3.8	1.3	26.6	0.5	27.1	24.6	0.757	5.0	-2.61	97	94	87	C1
810730026	23:08:28	290.3	0.1	20.8	0.4	17.4	0.3	18.5	14.7	0.938	5.4	-2.06	82	82	68	A
810730027	23:12:34	313.0	0.1	6.5	0.4	31.7	1.2	32.1	30.1	0.760	0.1	—	-	86	82	-
810730028	23:12:54	274.0	0.2	76.0	0.1	28.1	0.8	28.4	26.1	0.847	6.3	-2.82	105	92	83	C1
810730029	23:21:40	305.3	0.1	0.7	0.3	24.7	0.3	25.2	22.6	0.745	2.5	—	-	89	81	-
810730030	23:24:03	5.8	0.4	15.6	0.9	55.4	0.4	55.5	54.4	0.408	3.5	—	117	110	-	C2
810730031	23:22:46	327.1	0.2	4.3	2.3	49.3	0.3	49.5	48.2	0.656	4.2	-3.24	112	107	102	C2

Vol. 36 (1985), No. 1

TABLE I. VIDICON CAMERA METEORS

I.D. No.	E.S.T.	R.A.	d(R.A.)	Dec.	d(dec)	Vobs.	dV	Vinf	Vg	cos χ	Mag	log(mass)	Hb	Hm	He	Type
810730032	23:22:46	327.1	0.2	4.2	2.3	49.0	0.8	49.2	47.9	0.661	4.2	-3.23	111	106	102	C2
810730033	23:36:28	340.4	0.3	-18.6	1.2	40.6	0.3	40.9	39.3	0.307	3.9	--	-	100	-	-
810730034	23:39:37	300.2	0.4	-40.7	4.1	17.3	0.2	18.4	14.6	0.272	3.7	-1.83	82	80	78	A
810730035	23:39:43	238.5	0.4	18.9	1.7	14.2	0.5	14.8	9.6	0.710	5.9	-2.06	93	91	87	C1
810730036	23:40:28	294.8	0.2	17.4	4.4	23.8	0.5	24.6	21.9	0.910	5.5	-2.49	87	76	74	A
810730037	23:43:02	325.1	0.7	69.4	0.2	40.8	1.1	41.0	39.4	0.873	5.1	-3.04	111	103	92	C2
810730038	23:44:41	339.2	0.1	-15.3	0.3	39.9	0.3	40.2	38.6	0.377	4.2	--	-	94	-	-
810730039	23:44:53	289.2	2.7	74.2	0.2	31.5	1.3	31.8	29.7	0.863	5.3	-2.96	103	98	91	C1
810730040	23:49:17	321.7	0.1	-10.2	0.4	12.5	0.3	13.5	7.5	0.705	5.9	-1.77	82	81	77	A
810730041	23:50:39	13.3	1.8	64.5	0.7	59.8	0.6	59.9	58.9	0.713	4.4	-3.27	112	103	90	C2
810730042	23:58:39	354.6	0.2	-29.5	0.8	47.7	0.4	48.0	46.6	0.075	4.2	-2.89	103	102	101	A
810731001	00:04:02	297.4	0.1	25.5	0.4	19.7	0.6	20.7	17.4	0.957	5.8	-2.38	83	79	70	A
810731002	00:06:05	7.7	2.2	79.6	0.1	43.0	0.6	43.2	41.7	0.740	4.3	-2.86	107	94	85	C2
810731003	00:17:15	316.0	0.1	1.8	0.4	33.0	0.4	33.4	31.4	0.755	5.0	-2.90	101	94	88	C1
810731004	00:20:13	312.2	0.1	-24.8	1.2	28.3	0.4	29.0	26.7	0.418	4.5	--	91	89	-	A
810731005	00:31:37	315.8	0.8	54.0	3.6	10.8	1.7	11.5	2.7	0.991	1.9	--	87	82	79	C1
810731006	00:35:07	339.0	0.1	40.3	3.2	13.4	0.8	14.0	8.4	0.951	6.2	--	89	86	83	C1
810731007	00:40:59	340.6	0.6	-12.9	6.9	22.6	0.8	23.0	20.0	0.535	4.8	--	105	102	101	C1
810731008	00:41:10	326.8	0.1	28.1	1.3	39.9	5.0	40.1	38.5	0.946	-0.1	--	113	112	84	C1
810731009	00:41:37	40.0	0.4	42.1	0.8	67.5	0.5	67.6	66.7	0.492	-0.9	--	121	111	104	C2
810731010	00:49:30	299.2	0.4	55.7	0.6	30.5	1.0	30.8	28.6	0.964	2.2	--	107	98	87	C1
810731011	00:55:45	337.5	0.1	26.6	3.4	22.1	0.6	22.7	19.7	0.923	3.7	--	95	89	86	C1
810731012	00:56:53	335.1	0.1	21.8	7.6	36.4	0.5	36.6	34.9	0.899	3.7	-2.86	107	101	89	C1
810731013	01:08:51	35.5	0.9	53.8	0.6	56.3	5.0	56.4	55.3	0.664	4.0	-3.32	110	109	101	C2
810731014	01:09:11	336.8	0.1	-17.2	2.9	31.0	0.4	31.4	29.3	0.495	4.3	--	-	87	83	-
810731015	01:16:58	65.1	0.1	9.3	0.3	8.4	0.1	9.8	0.0	0.534	5.4	-0.82	79	75	68	C1
810731016	01:20:59	338.7	0.2	-0.4	3.3	17.9	0.5	18.6	14.8	0.748	5.5	-2.23	91	88	84	C1
810731017	01:26:18	337.5	0.1	-11.5	0.7	39.8	0.3	40.1	38.5	0.575	2.2	--	-	94	81	-
810731018	01:29:31	8.6	0.4	31.2	1.6	73.7	1.0	73.8	73.0	0.805	-0.1	-2.73	117	107	96	C2
810731019	01:32:41	351.6	1.3	19.2	15.5	22.2	0.6	22.8	19.8	0.859	5.7	-2.96	95	91	87	C1
810731020	01:33:03	307.0	0.9	-18.6	5.1	15.7	0.6	16.2	11.7	0.574	5.1	-2.04	95	93	93	C1
810731021	01:35:55	293.8	0.8	-41.3	2.6	24.0	0.3	24.3	21.6	0.114	3.5	--	98	96	-	C1
810731022	01:41:29	339.1	0.1	-21.0	1.1	43.1	0.6	43.4	41.9	0.440	4.0	--	101	95	-	A
810731023	01:43:15	338.1	0.1	4.8	1.8	48.0	0.5	48.3	46.9	0.778	2.0	-2.34	103	98	84	A
810731024	01:47:39	252.6	1.5	-6.0	4.2	11.9	0.4	12.9	6.4	0.455	5.9	-1.75	87	86	85	C1

TABLE I. VIDICON CAMERA METEORS

I.D. No.	E.S.T.	R.A.	d(R.A.)	Dec.	d(dec)	Vobs.	dV	Vinf	Vg	cos χ	Mag	log(mass)	Hb	Hm	He	Type
810731025	01:47:56	338.9	0.4	-22.9	5.3	38.0	1.1	38.3	36.7	0.421	3.5	--	-	83	80	-
810731026	01:48:38	290.5	4.2	4.7	19.7	17.2	0.4	17.9	14.0	0.698	5.2	-2.06	89	87	84	A
810731027	01:51:01	259.3	1.8	66.6	0.5	16.3	1.2	17.5	13.4	0.785	1.4	-1.37	85	83	80	A
810731028	01:50:51	30.8	5.2	55.7	2.7	56.3	0.6	56.4	55.3	0.771	-0.3	--	111	98	-	C2
810731029	01:55:57	305.6	0.1	12.6	0.6	17.1	0.3	17.8	13.9	0.836	5.6	-1.92	91	84	80	C1
810731030	01:56:54	340.5	0.1	-30.2	0.9	39.0	0.3	39.3	37.7	0.308	3.8	--	-	84	83	-
810731031	01:57:55	308.8	0.3	12.3	1.0	27.4	0.2	27.7	25.3	0.818	3.8	--	104	95	-	C1
810731032	01:58:52	16.1	0.4	41.1	1.0	60.5	1.4	60.6	59.6	0.847	3.7	-3.33	112	106	99	C2
810731033	02:00:17	306.9	0.1	-10.0	1.3	25.2	0.2	25.7	23.1	0.575	2.8	--	-	94	81	-
810731034	02:02:42	302.3	0.2	46.2	0.5	30.2	0.5	30.5	28.3	0.935	4.5	-2.46	102	88	83	C1
810731035	02:05:44	19.9	1.3	5.4	5.7	53.0	1.5	53.2	52.0	0.578	3.5	--	112	107	-	C2
810731036	02:12:37	46.1	3.8	51.5	2.6	54.4	0.7	54.5	53.4	0.693	1.8	-2.80	116	105	100	C2
810731037	02:25:48	98.7	0.7	51.4	1.3	49.7	0.4	49.9	48.6	0.327	3.9	-2.83	110	105	101	C2
810731038	02:32:58	348.6	0.2	52.6	1.3	30.2	2.6	30.6	28.5	0.984	6.5	-3.41	98	94	85	C1
810731039	02:34:29	321.5	18.5	77.2	2.0	46.7	2.3	47.1	45.8	0.826	5.1	-3.59	100	94	86	A
810731040	02:38:13	45.7	0.6	45.5	1.1	67.9	1.1	68.0	67.1	0.718	4.0	-3.43	117	110	102	C2
810731041	02:40:38	74.8	1.5	17.3	4.7	57.2	0.9	57.3	56.2	0.194	4.0	-3.28	112	111	109	C2
810731042	02:42:08	29.5	1.3	-20.5	4.5	60.5	0.5	60.7	59.7	0.243	3.0	--	-	99	-	-
810731043	02:52:30	230.9	2.9	73.6	0.5	13.9	0.3	14.8	9.6	0.701	5.8	-1.70	87	81	77	C1
810731044	03:00:08	258.0	2.1	5.2	6.1	46.2	1.5	46.5	45.1	0.093	4.2	-3.36	101	101	101	A
810731045	03:01:12	287.6	6.3	42.6	11.4	22.7	1.1	23.6	20.7	0.766	4.5	--	87	85	83	A
810731046	03:01:44	312.6	0.5	-50.0	1.7	18.1	0.3	18.8	15.1	0.059	4.7	--	-	86	86	-
810731047	03:03:09	43.8	2.5	38.8	3.7	38.5	1.2	38.7	37.1	0.759	5.4	-3.47	109	108	102	C1
810731048	21:34:21	305.3	0.2	-0.3	1.6	26.0	0.4	26.3	23.8	0.604	4.3	--	100	93	-	C1
810731049	21:36:56	15.2	0.9	48.9	1.1	63.6	0.6	63.7	62.7	0.380	3.6	-3.09	116	111	106	C2
810731050	22:16:59	324.7	0.4	60.3	0.3	44.2	0.9	44.4	42.9	0.843	4.9	-3.14	106	96	91	C2
810731051	22:26:30	260.1	0.2	24.5	4.1	20.8	5.0	21.2	18.0	0.923	4.2	-1.91	108	89	81	C1
810731052	22:31:51	341.2	0.3	-14.7	0.8	43.1	0.4	43.4	41.9	0.206	3.1	--	-	94	-	-
810731053	22:48:27	235.9	0.3	47.3	0.3	19.1	0.4	19.5	16.0	0.859	4.9	-2.45	97	88	81	C1
810731054	23:51:54	321.7	0.1	12.7	1.4	36.2	0.5	36.7	35.0	0.824	4.0	-2.66	96	88	82	A
810731055	23:52:54	340.1	0.9	78.2	0.1	24.2	0.5	24.5	21.8	0.809	4.9	-2.23	104	96	85	C1
810801001	00:44:27	327.1	0.1	-20.5	0.9	29.2	0.3	29.6	27.4	0.466	3.2	-2.26	95	91	88	A
810801002	00:57:45	358.7	0.2	-22.1	1.5	32.0	0.2	32.4	30.4	0.297	3.6	--	97	92	-	A
810801003	01:02:47	350.8	0.3	-40.3	2.0	35.0	0.5	35.4	33.5	0.079	2.1	--	-	91	91	-
810801004	01:04:26	50.8	0.4	42.3	0.6	64.6	0.6	64.7	63.7	0.457	3.6	-3.05	116	110	105	C2

TABLE I. VIDICON CAMERA METEORS

I.D. No.	E.S.T.	R.A.	d(R.A.)	Dec.	d(dec)	Vobs.	dV	Vinf	Vg	cos χ	Mag	log(mass)	Hb	Hm	He	Type
810801005	01:56:45	303.2	0.2	-11.9	1.8	24.2	0.3	24.5	21.8	0.537	4.7	-2.18	103	96	93	C1
810801006	01:58:47	15.1	0.5	37.7	1.2	48.0	1.3	48.2	46.8	0.849	4.3	-3.42	114	103	101	C2
810924001	00:12:32	22.1	0.5	8.2	2.1	46.8	0.7	47.0	45.6	0.766	4.2	-3.02	110	108	100	C2
810924002	00:18:51	26.3	0.2	-8.7	4.7	25.5	0.2	25.8	23.3	0.585	4.3	-1.94	101	93	90	C1
810924003	00:19:01	45.8	0.5	28.6	1.5	52.4	1.0	52.8	51.6	0.780	4.3	-3.31	101	95	92	A
810924004	00:22:09	249.1	0.1	56.0	0.1	22.4	0.1	23.0	20.0	0.486	4.7	—	94	85	77	C1
810924005	00:26:28	49.8	0.4	30.5	2.7	14.3	0.7	15.1	10.2	0.828	6.2	-2.19	87	85	83	C1
810924006	00:26:37	214.4	0.4	45.7	1.1	30.4	0.9	30.8	28.7	0.120	4.6	-2.84	99	99	99	C1
810924007	00:29:20	17.7	0.1	-45.0	2.0	33.0	0.7	33.2	31.3	0.071	4.4	—	107	107	107	C1
810924008	00:39:29	63.9	0.8	47.2	0.9	42.5	1.1	42.7	41.2	0.769	4.9	-3.28	107	103	98	C2
810924009	00:54:22	4.9	0.5	0.1	10.9	27.9	0.4	28.2	25.9	0.750	4.5	-2.33	111	101	99	C1
810924010	00:57:37	353.1	0.1	56.8	0.4	31.8	1.4	32.4	30.4	0.957	5.6	-2.97	93	85	76	A
810924011	01:00:57	100.9	3.4	42.8	5.2	44.6	1.7	44.8	43.4	0.481	4.4	-3.38	107	106	104	C2
810924012	01:02:02	289.0	0.4	69.7	0.2	27.2	0.8	27.5	25.1	0.705	5.5	-2.63	102	97	93	C1
810924013	01:03:13	346.3	0.5	-17.8	3.0	21.5	0.3	21.9	18.8	0.495	5.3	-2.34	102	98	95	C1
810924014	01:14:09	11.2	0.2	9.7	3.4	25.7	0.2	26.0	23.5	0.847	0.9	-1.50	106	90	84	C1
810924015	01:21:37	234.3	1.6	62.8	0.9	17.0	0.6	17.5	13.4	0.485	5.6	-2.50	99	96	93	C1
810924016	01:27:49	358.8	1.1	24.0	11.9	20.1	0.6	20.7	17.4	0.925	5.6	-2.40	93	90	83	C1
810924017	01:37:13	309.6	0.1	16.5	0.2	18.4	0.3	18.8	15.1	0.535	3.0	-1.62	97	93	90	C1
810924018	01:49:33	216.5	0.6	72.0	0.5	23.6	0.2	23.9	21.2	0.495	2.6	-1.66	107	95	91	C1
810924019	01:49:38	297.4	0.2	74.6	0.1	35.0	0.7	35.2	33.4	0.692	5.3	-2.92	106	99	91	C1
810924020	01:52:31	98.6	1.0	52.1	1.2	56.9	1.0	57.1	56.0	0.664	1.9	—	-	106	103	-
810924021	01:57:20	75.8	1.6	40.9	2.6	41.7	2.9	42.0	40.5	0.802	4.2	-3.46	103	101	97	C2
810924022	01:58:23	71.0	0.6	47.4	0.9	65.9	1.2	66.0	65.1	0.849	4.3	-3.51	114	105	99	C2
810924023	02:03:33	25.2	0.1	19.7	8.6	51.2	0.9	51.4	50.2	0.918	4.3	—	-	98	86	-
810924024	02:09:56	86.7	0.5	-4.5	1.8	69.1	0.7	69.2	68.3	0.336	3.5	—	117	110	-	C2
810924025	02:12:38	110.7	0.7	48.5	0.9	52.5	1.1	52.7	51.4	0.589	4.5	-3.45	111	108	104	C2
810924026	02:20:26	109.7	0.8	50.3	0.7	62.7	0.9	62.8	61.8	0.622	4.2	-3.67	115	109	102	C2
810924027	02:22:26	297.6	1.6	77.2	0.3	35.7	1.1	35.9	34.1	0.674	4.7	-3.02	108	98	95	C1
810924028	02:23:44	71.3	0.9	-1.0	5.7	61.8	1.4	62.0	61.0	0.556	4.0	-3.76	105	104	99	A
810924029	02:26:48	344.0	1.6	-37.8	13.9	16.9	0.9	17.4	13.3	0.178	2.7	-1.77	98	97	97	C1
810924030	02:31:42	22.5	0.9	-15.9	29.7	28.8	0.5	29.1	26.8	0.538	3.9	-2.27	106	103	93	C1
810924031	02:33:19	77.4	1.1	36.6	2.0	65.7	1.4	66.0	65.0	0.836	3.9	—	105	97	-	A
810924032	02:35:33	69.8	0.5	33.0	1.4	60.4	0.9	60.5	59.5	0.875	4.2	-3.30	116	107	100	C2
810924033	02:39:44	99.1	0.2	4.3	0.5	69.4	0.4	69.5	68.6	0.385	3.4	—	118	110	-	C2

TABLE I. VIDICON CAMERA METEORS

I.D. No.	E.S.T.	R.A.	d(R.A.)	Dec.	d(dec)	Vobs.	dV	Vinf	Vg	cos χ	Mag	log(mass)	Hb	Hm	He	Type
810924034	02:53:00	100.6	0.8	30.5	1.6	70.8	1.5	71.1	70.2	0.652	3.4	-3.65	104	104	98	A
810924035	02:59:23	235.6	8.0	74.6	6.6	24.4	0.9	24.9	22.2	0.527	5.1	-2.83	94	93	89	A
810924036	03:00:29	60.9	0.4	34.0	1.3	59.7	1.3	59.9	58.9	0.951	4.3	-3.47	106	102	94	A
810924037	03:00:35	99.2	0.5	50.4	0.5	62.2	0.7	62.3	61.3	0.774	3.8	-3.20	119	109	100	C2
810924038	03:05:30	91.7	0.5	45.1	1.0	46.0	1.0	46.2	44.8	0.822	4.6	-3.17	109	102	97	C2
810924039	03:08:33	342.7	0.6	43.8	1.0	21.8	0.9	22.2	19.1	0.774	5.7	-2.51	98	95	92	C1
810924040	03:08:42	0.4	0.5	-39.8	2.1	34.5	0.3	34.9	33.0	0.025	3.7	—	102	102	102	C1
810924041	03:15:29	69.1	0.3	4.2	1.7	60.7	1.0	61.0	60.0	0.714	4.3	-3.58	98	90	90	A
810924042	03:18:01	103.5	0.7	39.4	1.4	45.8	1.0	46.0	44.6	0.736	4.6	-3.22	107	102	98	C2
810924043	03:18:08	59.6	0.1	41.0	2.4	59.2	1.8	59.5	58.5	0.982	4.8	-3.68	104	102	89	A
810924044	03:19:18	346.0	5.7	-21.3	13.8	27.5	1.4	27.8	25.4	0.168	4.7	—	102	101	-	C1
810924045	03:19:37	64.8	0.3	46.4	1.0	63.4	1.8	63.6	62.6	0.971	4.9	-3.72	107	97	90	A
810924046	03:33:39	289.8	3.6	72.3	0.6	14.7	0.4	16.0	11.4	0.661	6.3	-2.28	83	80	74	A
810924047	03:53:40	98.1	0.3	39.7	0.6	66.2	0.6	66.3	65.4	0.843	2.6	-3.07	124	103	94	C2
810924048	03:55:01	71.5	0.4	29.5	4.4	36.3	1.2	36.5	34.8	0.946	5.0	-3.29	108	102	95	C1
810924049	03:56:04	70.9	0.5	56.6	0.5	60.4	1.3	60.5	59.5	0.957	4.1	-3.35	122	110	93	C2
810924050	04:00:20	55.7	0.4	-54.2	9.4	17.7	0.4	18.4	14.6	0.081	5.3	-2.20	88	88	88	A
810924051	04:08:35	99.1	0.4	39.1	1.2	61.0	1.2	61.1	60.1	0.859	4.8	-3.62	115	99	99	C2
810924052	04:09:13	74.4	0.5	34.2	1.9	65.6	1.7	65.7	64.8	0.964	4.2	-3.61	115	112	100	C2
810924053	04:11:28	60.6	0.1	33.6	7.4	69.0	2.2	69.1	68.2	0.986	1.9	-3.33	114	114	101	C2
810924054	04:15:18	246.9	1.5	32.8	0.9	7.4	0.2	8.9	0.0	0.570	4.8	—	-	73	70	-
810924055	04:18:19	62.9	0.1	55.4	0.9	61.5	1.6	61.6	60.6	0.977	5.4	-3.64	128	106	95	C2
811104001	00:31:21	109.7	0.5	1.3	1.1	65.8	0.5	65.9	65.0	0.325	3.0	—	117	108	-	C2
811104002	00:34:01	54.2	0.4	9.1	2.7	28.3	0.6	28.7	26.5	0.830	4.8	-2.51	97	96	89	C1
811104003	00:38:12	113.7	1.2	-6.6	2.7	57.6	0.8	57.8	56.7	0.209	4.0	—	-	94	94	-
811104004	00:43:47	52.2	0.3	7.4	4.0	23.7	0.4	24.5	21.8	0.828	5.4	-2.36	87	81	78	A
811104005	00:46:08	55.7	0.3	5.8	2.7	30.2	0.4	30.5	28.3	0.802	0.7	—	107	92	-	C1
811104006	00:48:48	117.7	0.1	54.4	0.1	62.2	1.4	62.3	61.3	0.711	4.5	-3.54	114	105	103	C2
811104007	00:51:17	184.8	0.4	52.1	0.7	38.4	0.6	38.7	37.1	0.253	4.7	-2.89	101	101	99	C1
811104008	00:52:13	166.9	1.0	42.3	1.6	62.4	0.3	62.5	61.5	0.223	3.9	-2.95	118	113	110	C2
811104009	00:53:34	25.1	8.1	80.2	1.0	44.8	1.1	45.2	43.8	0.794	5.4	-3.66	99	82	76	A
811104010	01:04:17	121.4	0.1	36.7	0.2	59.0	1.4	59.1	58.1	0.624	4.1	-3.49	113	109	107	C2
811104011	01:06:34	54.5	0.1	34.2	5.1	45.9	1.0	46.2	44.8	0.989	4.8	-3.23	102	90	86	A
811104012	01:10:07	58.7	0.6	-24.5	4.1	20.7	0.4	21.3	18.1	0.462	2.2	—	-	82	80	-
811104013	01:13:09	45.5	1.0	22.8	17.5	29.0	0.4	29.3	27.0	0.935	4.9	-2.38	112	98	94	C1

TABLE I. VIDICON CAMERA METEORS

I.D. No.	E.S.T.	R.A.	d(R.A.)	Dec.	d(dec)	Vobs.	dV	Vinf	Vg	cos χ	Mag	log(mass)	Hb	Hm	He	Type
811104014	01:19:57	101.9	0.3	14.8	2.2	66.6	0.7	66.9	66.0	0.671	3.0	-3.26	104	94	90	A
811104015	01:20:58	270.4	2.0	88.5	0.1	40.0	0.5	40.2	38.6	0.681	3.4	-2.50	117	99	91	C1
811104016	01:24:47	83.2	1.1	64.5	0.8	41.8	1.2	42.1	40.6	0.904	6.0	-3.47	104	92	85	C2
811104017	01:25:13	131.3	0.1	33.9	0.1	67.4	0.4	67.6	66.7	0.556	3.3	--	-	114	97	-
811104018	01:27:26	23.6	0.5	-5.0	5.9	13.1	0.6	14.0	8.4	0.695	6.0	-2.13	84	82	80	A
811104019	01:28:14	102.3	0.7	18.3	1.6	74.6	1.2	74.8	73.9	0.714	3.7	--	-	106	104	-
811104020	01:31:58	68.4	0.5	24.4	2.3	22.1	0.5	22.5	19.5	0.944	5.4	-2.31	97	93	86	C1
811104021	01:35:20	49.8	0.6	2.7	14.0	23.0	0.7	23.5	20.7	0.778	4.8	--	-	78	73	-
811104022	01:44:24	153.0	0.1	63.1	0.1	14.1	0.3	14.7	9.5	0.723	6.5	-1.89	90	84	81	C1
811104023	01:44:41	134.6	0.1	20.3	0.3	72.5	0.8	72.6	71.7	0.453	3.9	-3.91	121	117	110	C2
811104024	01:56:24	36.2	0.3	36.7	1.8	19.7	0.6	20.7	17.4	0.935	6.1	-2.43	88	85	78	A
811104025	01:57:33	106.6	0.2	13.0	0.8	61.4	0.5	61.5	60.5	0.695	3.8	-3.15	118	108	100	C2
811104026	01:58:10	137.6	0.4	67.9	0.1	31.8	0.6	32.4	30.4	0.734	5.3	-2.89	93	87	78	A
811104027	01:58:29	15.6	2.1	63.4	0.9	18.6	1.1	19.0	15.4	0.857	6.4	-2.60	95	92	86	C1
811104028	02:04:45	154.9	0.9	29.3	1.7	66.8	0.8	66.9	66.0	0.371	4.2	-3.55	116	113	109	C2
811104029	02:06:14	162.6	0.3	33.9	0.6	66.2	0.3	66.4	65.4	0.341	3.3	--	-	109	101	-
811104030	02:07:56	106.0	0.3	15.7	0.9	68.9	0.4	69.1	68.2	0.743	3.8	--	-	105	92	-
811104031	02:09:01	105.1	0.2	19.3	0.9	70.5	0.8	70.6	69.7	0.780	3.9	-3.42	117	109	102	C2
811104032	02:12:27	127.7	0.1	-1.0	0.3	69.6	0.9	69.7	68.8	0.378	3.5	--	116	109	-	C2
811104033	02:18:20	158.3	0.2	62.7	0.1	67.7	0.7	67.8	66.9	0.627	4.1	-3.42	114	100	99	C2
811104034	02:32:44	139.3	0.1	20.8	0.1	77.4	0.4	77.5	76.7	0.537	3.4	--	122	110	-	C2
811104035	02:36:08	14.5	0.4	39.2	0.7	18.3	0.3	19.4	15.8	0.764	6.0	-2.34	87	82	77	A
811104036	02:39:59	255.7	0.1	56.3	0.7	29.1	0.2	29.4	27.2	0.226	4.5	-2.15	103	100	97	C1
811104037	02:41:39	47.9	0.4	0.2	3.7	29.1	0.5	29.5	27.3	0.670	4.4	--	-	95	89	-
811104038	02:41:54	60.3	0.4	46.2	0.9	40.1	1.1	40.6	39.0	0.979	5.5	-3.24	96	90	80	A
811104039	02:43:19	96.7	0.2	31.0	0.8	64.9	0.8	65.0	64.1	0.940	3.7	-3.21	119	105	95	C2
811104040	02:44:25	107.1	0.3	6.7	3.7	57.9	1.3	58.0	56.9	0.713	4.0	-3.39	114	113	107	C2
811104041	02:48:20	124.4	0.1	57.6	0.1	36.6	0.8	37.1	35.4	0.853	5.5	-3.10	97	88	84	A
811104042	02:58:52	49.2	0.5	-3.5	2.8	23.3	0.3	23.8	21.0	0.627	2.7	--	-	87	82	-
811104043	03:00:30	25.4	0.4	37.7	0.8	19.9	0.4	20.3	16.9	0.787	5.6	-2.10	101	95	89	C1
811104044	03:06:35	142.4	3.7	77.6	0.1	41.9	0.8	42.1	40.6	0.757	5.3	-3.18	110	106	93	C2
811104045	03:08:13	48.3	0.2	14.9	1.3	27.2	0.3	27.5	25.1	0.778	4.9	-2.27	102	93	88	C1
811104046	03:09:30	157.3	1.1	68.5	0.6	59.1	1.7	59.2	58.2	0.716	4.6	-3.53	113	107	102	C2
811104047	03:10:47	136.1	10.4	83.1	0.1	37.4	1.1	37.6	35.9	0.745	5.3	-3.09	107	100	97	C1
811104048	03:12:33	68.3	0.5	36.9	2.0	46.4	0.9	46.8	45.5	0.973	5.0	-3.27	92	86	76	A

TABLE I. VIDICON CAMERA METEORS

I.D. No.	E.S.T.	R.A.	d(R.A.)	Dec.	d(dec)	Vobs.	dV	Vinf	Vg	cos χ	Mag	log(mass)	Hb	Hm	He	Type
811104049	03:17:56	193.0	0.3	68.2	0.2	48.8	0.6	49.1	47.8	0.566	4.5	-3.20	107	100	96	C2
811104050	03:19:23	108.7	0.2	45.2	0.7	52.1	1.4	52.5	51.3	0.959	5.0	-3.46	102	96	88	A
811104051	03:19:55	123.8	0.1	4.0	0.6	64.0	0.9	64.2	63.2	0.629	3.6	--	-	98	94	-
811104052	03:22:25	108.5	0.9	20.2	2.8	78.6	3.3	78.7	77.9	0.873	3.5	--	115	112	-	C2
811104053	03:24:48	150.6	0.1	10.4	0.4	72.4	0.5	72.7	71.8	0.453	3.7	-3.35	106	98	95	A
811104054	03:26:55	56.0	0.5	-19.0	6.9	16.5	0.4	17.0	12.8	0.503	5.4	-2.03	99	97	95	C1
811104055	03:27:24	109.4	0.6	-3.7	4.1	60.4	0.8	60.5	59.5	0.638	3.8	-3.35	117	114	105	C2
811104056	03:31:36	147.0	9.9	78.3	0.4	56.5	1.2	56.9	55.7	0.753	3.5	-3.33	96	88	86	A
811104057	03:32:27	99.1	0.3	36.7	1.7	75.2	1.8	75.4	74.5	0.984	4.5	-4.07	111	103	96	C2
811104058	03:37:24	145.6	0.3	-6.0	1.2	62.0	1.1	62.2	61.2	0.355	3.4	--	-	108	105	-
811104059	03:37:33	132.0	0.1	39.9	0.1	72.3	1.6	72.4	71.5	0.859	3.3	-3.55	121	114	107	C2
811104060	03:38:11	105.2	6.0	63.7	4.4	14.6	1.0	15.9	11.3	0.944	6.2	-2.71	76	72	67	A
811104061	03:41:19	161.9	0.8	23.6	2.1	59.4	1.0	59.6	58.5	0.507	4.0	--	-	104	101	-
811104062	03:44:02	76.2	10.6	74.9	20.0	47.8	1.2	48.0	46.6	0.847	5.4	-3.43	123	113	99	C2
811104063	03:45:04	31.1	0.9	25.5	4.0	19.9	0.5	20.5	17.2	0.674	5.4	-2.31	93	89	87	C1
811104064	03:47:15	150.9	0.2	68.5	0.1	54.7	2.5	54.8	53.7	0.783	5.3	-3.75	112	105	102	C2
811104065	03:48:07	126.9	0.6	24.5	1.1	63.7	1.8	63.8	62.8	0.838	3.6	-3.70	118	112	109	C2
811104066	03:50:39	84.1	2.2	32.4	9.1	49.4	1.4	49.7	48.4	0.975	4.5	-3.33	103	97	91	A
811104067	03:54:30	120.1	0.1	11.4	2.0	52.8	1.7	53.0	51.8	0.785	4.4	-3.52	112	109	107	C2
811104068	03:58:28	132.7	0.1	-19.1	0.1	60.9	0.7	61.0	60.0	0.340	3.8	-3.26	112	111	106	C2
811104069	04:00:56	159.6	0.3	59.8	0.4	66.7	1.7	67.0	66.1	0.760	4.3	-3.67	100	88	86	A
811104070	04:01:06	120.0	0.4	26.9	1.1	66.3	1.9	66.5	65.5	0.906	4.1	-3.68	106	105	99	A
811104071	04:03:38	127.9	0.1	26.6	0.5	61.1	1.6	61.2	60.2	0.867	4.3	-3.59	114	109	104	C2
811104072	04:10:22	110.1	0.3	-21.9	4.0	55.7	1.1	55.8	54.7	0.421	4.0	-3.32	113	110	108	C2
811104073	04:20:06	117.8	1.4	-41.0	9.1	46.3	1.7	46.5	45.1	0.105	4.1	-3.20	114	113	113	C2
811104074	04:27:35	110.7	0.1	32.8	4.4	74.1	3.2	74.2	73.4	0.977	4.3	-4.00	114	108	105	C2
811104075	04:31:26	147.7	0.1	37.8	0.5	15.1	0.5	15.9	11.3	0.871	6.1	-2.03	88	86	80	C1
811104076	04:32:56	111.2	0.2	34.5	0.8	70.2	1.6	70.5	69.6	0.984	4.6	-3.76	105	92	89	A
811104077	04:38:10	83.5	0.1	39.4	0.7	27.4	0.4	27.9	25.5	0.962	4.9	-2.32	95	87	71	A
811104078	04:39:52	154.8	0.2	39.5	0.7	72.3	0.9	72.6	71.7	0.809	4.1	-3.49	107	91	89	A
811104079	04:48:21	148.1	0.6	36.5	1.3	57.3	0.9	57.4	56.3	0.859	4.1	-3.24	119	110	103	C2
811104080	04:50:09	49.9	0.8	43.7	1.4	40.0	1.1	40.2	38.6	0.759	4.6	-3.02	110	106	101	C1
811104081	04:52:04	142.6	0.1	15.6	0.4	70.6	0.9	70.9	70.0	0.773	3.8	-3.47	104	102	92	A
811104082	04:52:08	112.0	0.3	22.1	5.7	51.1	2.3	51.3	50.0	0.933	4.5	-3.47	111	108	104	C2
811104083	04:59:32	146.8	0.7	51.5	0.9	56.5	2.8	56.7	55.6	0.906	5.0	-3.79	107	104	99	C2
811104084	05:00:36	28.7	0.4	35.5	0.6	23.2	0.3	23.5	20.7	0.536	5.1	-2.06	102	94	92	C1
811104085	05:04:08	50.9	0.2	18.2	0.9	32.1	0.3	32.3	30.3	0.574	4.7	-2.32	105	100	93	C1

Vol. 36 (1985), No. 1

TABLE II. ISIT CAMERA METEORS

I.D. No.	E.S.T.	R.A.	d(R.A.)	Dec.	d(dec)	Vobs.	dV	Vinf	Vg	cos χ	Mag	log(mass)	Hb	Hm	He	Type
820720001	22:02:28	13.5	4.4	58.9	3.0	66.4	1.1	66.5	65.6	0.461	4.7	—	117	110	-	C2
820720002	22:15:03	28.3	2.3	41.1	3.4	53.8	0.7	54.0	52.9	0.175	4.9	—	-	101	99	-
820720003	22:20:20	355.4	4.3	56.1	3.3	55.4	1.3	55.5	54.4	0.590	5.8	—	119	114	-	C2
820720004	22:36:44	313.3	1.6	67.0	0.2	36.7	1.7	36.9	35.2	0.849	3.4	-2.73	111	105	90	C1
820720005	22:47:22	344.4	3.3	57.7	1.7	56.9	1.8	57.0	55.9	0.714	6.1	-4.24	111	108	104	C2
820720006	22:54:55	358.5	0.9	12.4	1.8	68.8	0.5	69.0	68.1	0.249	4.8	—	-	113	111	-
820720007	23:00:49	169.8	0.2	35.9	0.3	13.9	0.2	14.5	9.2	0.466	7.1	-2.19	93	86	85	C1
820720008	23:04:24	253.1	1.1	49.7	1.5	20.2	1.0	20.6	17.3	0.959	7.7	-3.52	95	88	85	C1
820720009	23:05:31	246.3	0.1	61.6	0.1	27.7	0.7	28.1	25.8	0.906	7.2	—	99	93	-	C1
820720010	23:06:32	308.9	0.1	-38.5	0.7	29.4	0.2	29.8	27.6	0.134	6.1	-2.88	100	98	97	C1
820720011	23:14:04	301.1	0.1	-4.9	0.4	23.2	0.2	24.0	21.3	0.662	5.7	—	89	84	-	A
820720012	23:20:49	311.5	0.1	26.1	0.6	25.4	1.1	25.7	23.1	0.883	6.8	-3.38	99	97	93	C1
820720013	23:27:16	261.4	0.3	37.7	0.6	19.0	0.4	19.6	16.1	0.962	5.3	-2.45	92	83	76	C1
820720014	23:31:36	21.6	1.4	46.6	1.2	58.3	0.8	58.4	57.4	0.451	5.7	-3.87	115	112	107	C2
820720015	23:32:56	325.7	0.1	-27.7	0.2	27.5	0.3	28.0	25.6	0.241	5.8	—	-	89	-	-
820720016	23:51:40	180.7	1.4	66.9	0.7	23.6	1.7	24.1	21.4	0.587	7.0	-3.58	96	95	94	C1
820720017	23:52:47	13.8	1.1	52.6	1.0	55.2	0.9	55.4	54.3	0.603	6.0	—	-	105	99	-
820720018	23:52:54	212.7	0.2	6.8	0.5	11.3	0.2	12.4	5.2	0.577	6.2	-1.86	84	81	78	C1
820721001	00:00:16	29.8	1.4	34.3	2.2	52.5	1.0	52.7	51.4	0.323	5.8	-4.00	111	109	108	C2
820721002	00:02:09	355.3	0.7	30.7	1.2	63.0	0.7	63.1	62.1	0.644	5.4	-3.95	116	116	103	C2
820721003	00:02:28	217.8	0.1	63.9	0.1	19.9	0.3	20.3	16.9	0.748	5.2	-2.25	99	89	84	C1
820721004	00:10:05	321.8	0.1	23.1	0.8	36.6	0.5	36.9	35.2	0.869	6.1	—	-	99	86	-
820721005	00:17:29	28.6	0.6	34.5	0.9	55.8	0.4	55.9	54.8	0.381	5.3	-3.56	112	109	102	C2
820721006	00:23:14	291.5	0.4	-20.3	6.8	19.2	0.4	20.2	16.8	0.527	7.0	-2.90	86	81	79	A
820721007	00:32:35	277.5	0.1	68.9	0.1	21.7	0.7	22.1	19.0	0.897	6.7	-2.84	99	87	83	C1
820721008	00:33:17	337.1	0.3	-15.0	2.1	37.2	0.4	37.5	35.8	0.417	5.7	—	100	98	-	A
820721009	00:37:56	322.1	0.1	11.5	1.1	24.2	0.2	24.5	21.8	0.824	6.4	-2.80	99	90	81	C1
820721010	00:47:36	318.8	0.2	11.7	2.1	45.2	0.6	45.5	44.1	0.834	6.0	—	-	85	80	-
820721011	01:01:45	276.6	1.3	40.2	2.0	20.6	0.9	21.0	17.7	0.933	7.2	-3.08	99	96	90	C1
820721012	01:05:00	42.5	1.2	35.3	1.5	53.7	0.7	53.8	52.7	0.369	5.7	—	111	108	-	C2
820721013	01:35:34	323.1	0.1	2.1	1.2	26.9	0.4	27.4	25.0	0.769	6.0	—	97	91	-	C1
820721014	01:38:19	325.3	0.1	16.6	3.9	29.0	0.8	29.4	27.2	0.893	5.6	—	97	93	-	C1
820721015	01:51:37	22.1	2.4	63.0	0.4	33.2	1.2	33.6	31.7	0.776	7.1	-3.97	101	98	89	C1
820721016	01:56:16	356.9	0.4	6.2	2.0	53.7	0.8	53.9	52.8	0.670	5.6	-3.79	108	104	98	C2
820721017	01:56:39	29.8	3.2	-5.5	7.5	56.4	1.9	56.5	55.4	0.220	5.6	—	112	111	-	C2

TABLE II. ISIT CAMERA METEORS

I.D. No.	E.S.T.	R.A.	d(R.A.)	Dec.	d(dec)	Vobs.	dV	Vinf	Vg	cos χ	Mag	log(mass)	Hb	Hm	He	Type
820721018	01:57:33	26.3	0.7	48.6	0.9	52.9	0.9	53.1	51.9	0.726	4.7	-3.71	109	100	94	C2
820721019	02:00:25	253.6	0.1	47.2	0.2	19.6	0.2	20.0	16.6	0.736	6.0	-2.32	97	90	84	C1
820721020	02:02:40	9.9	0.7	32.2	1.9	77.0	1.3	77.2	76.3	0.789	5.8	-4.35	114	104	97	C2
820721021	02:08:48	330.8	0.1	12.0	2.0	29.9	0.5	30.6	28.4	0.861	5.8	-3.23	94	89	81	A
820721022	02:10:56	327.9	0.6	21.3	4.9	28.9	1.0	29.3	27.1	0.931	6.5	-3.44	95	91	87	A
820721023	02:14:27	36.4	0.5	32.5	0.9	71.2	0.5	71.4	70.5	0.579	3.7	—	-	108	98	-
820721024	02:16:37	300.9	1.8	62.2	0.3	32.1	1.6	32.3	30.3	0.918	6.6	—	104	96	91	C1
820721025	02:17:29	23.3	1.2	50.6	0.8	59.7	1.7	59.9	58.9	0.787	6.4	-4.35	110	105	101	C2
820721026	02:28:27	354.6	0.2	17.8	1.8	60.2	1.4	60.5	59.5	0.839	5.9	-4.31	101	97	90	A
820721027	02:30:53	266.2	1.0	-33.9	2.4	13.1	0.1	14.0	8.4	0.247	3.6	—	-	85	-	-
820721028	02:31:47	24.9	1.1	25.9	3.1	62.1	0.8	62.2	61.2	0.682	5.1	-3.82	118	113	105	C2
820721029	02:35:36	21.9	0.2	24.5	0.6	70.7	0.6	70.8	69.9	0.708	6.2	-3.62	114	104	95	C2
820721030	02:35:56	8.6	0.7	32.3	1.7	59.3	1.4	59.6	58.6	0.857	6.2	-4.30	101	97	91	A
820723001	22:38:56	332.2	0.5	-5.5	1.5	47.1	0.5	47.5	46.2	0.346	5.9	-3.90	97	94	91	A
820723002	22:46:46	283.1	0.1	9.0	2.1	16.9	0.4	17.4	13.3	0.859	6.5	-2.59	94	90	86	C1
820723003	22:50:28	298.4	0.1	-4.8	0.6	21.0	0.2	21.6	18.5	0.671	5.1	—	-	88	83	-
820723004	22:57:47	322.5	0.1	-2.5	0.4	37.3	0.3	37.6	35.9	0.524	5.8	—	-	92	88	-
820723005	23:16:09	334.9	0.2	-11.5	1.4	42.8	0.5	43.1	41.6	0.340	6.0	—	-	95	-	-
820723006	23:22:47	22.3	1.0	52.1	0.9	57.7	0.9	57.8	56.7	0.500	6.1	-3.73	114	110	106	C2
820723007	23:24:27	306.9	0.1	-3.6	0.8	27.4	0.6	28.1	25.8	0.664	5.1	—	93	91	-	A
820723008	23:27:12	242.3	0.2	66.4	0.1	24.3	0.1	24.6	21.9	0.855	7.5	-3.71	98	95	92	C1
820723009	23:31:43	218.1	0.2	55.6	0.1	18.8	0.4	19.5	15.9	0.759	5.3	—	-	88	83	-
820724001	00:11:21	16.3	1.3	55.7	0.7	64.8	0.7	64.9	63.9	0.655	3.2	—	119	105	-	C2
820724002	00:31:07	314.3	0.1	40.6	0.7	13.8	0.4	15.2	10.2	0.989	5.4	-2.33	82	76	68	A
820724003	00:40:06	2.2	4.7	71.6	0.1	56.1	1.8	56.5	55.3	0.778	6.3	—	98	89	-	A
820724004	00:43:44	303.7	0.3	-36.0	3.9	24.5	0.4	25.3	22.7	0.265	6.5	—	90	88	-	A
820724005	00:44:36	14.9	1.3	55.7	0.9	71.5	1.4	71.6	70.7	0.719	4.7	-4.34	118	103	100	C2
820724006	00:47:34	334.8	0.4	-9.6	3.8	41.4	0.5	41.7	40.2	0.539	6.1	—	-	87	82	-
820724007	01:02:25	11.8	0.5	48.3	0.5	59.6	0.9	59.7	58.7	0.750	6.0	-4.01	113	107	98	C2
820724008	01:02:51	329.3	0.2	27.3	4.5	63.2	2.3	63.4	62.4	0.929	6.1	—	-	98	93	-
820724009	01:04:17	336.1	1.3	41.0	3.7	35.8	2.1	36.4	34.6	0.948	7.0	-3.98	90	87	85	A
820724010	01:08:18	241.1	0.1	2.3	0.3	14.3	0.1	14.8	9.7	0.479	6.9	-2.14	92	89	84	C1
820724011	01:13:22	291.2	0.5	23.7	2.7	26.2	0.5	26.5	24.0	0.906	6.6	-3.02	108	100	94	C1
820724012	01:15:02	11.6	0.6	37.4	1.0	71.5	1.4	71.8	70.9	0.728	5.7	-4.33	104	102	93	A
820724013	01:31:31	38.1	2.5	41.9	3.4	47.3	1.4	47.5	46.1	0.562	5.5	—	114	111	109	C2

Vol. 36 (1985), No. 1

TABLE II. ISIT CAMERA METEORS

I.D. No.	E.S.T.	R.A.	d(R.A.)	Dec.	d(dec)	Vobs.	dV	Vinf	Vg	cos χ	Mag	log(mass)	Hb	Hm	He	Type
820724014	01:38:39	252.3	1.4	48.9	1.5	17.1	0.5	17.6	13.5	0.766	7.0	-2.71	95	91	88	C1
820724015	01:43:56	35.1	2.1	0.8	5.1	58.1	0.9	58.2	57.2	0.227	5.0	—	114	111	-	C2
820724016	01:46:47	353.7	0.8	39.6	3.1	33.7	1.0	34.3	32.4	0.916	7.2	-3.81	92	86	79	A
820724017	01:48:42	21.2	0.7	2.8	1.8	53.0	0.8	53.2	52.0	0.424	5.6	—	-	105	100	-
820724018	01:50:45	44.8	0.4	38.1	0.6	73.0	0.4	73.2	72.3	0.510	3.3	—	-	108	-	-
820724019	02:09:20	278.0	0.7	5.5	1.7	22.3	0.2	22.9	19.9	0.594	3.5	—	-	91	-	-
820724020	02:09:29	321.3	0.1	-31.6	0.2	24.4	0.3	25.2	22.6	0.331	6.0	—	89	86	-	A
820724021	02:09:42	212.7	0.2	39.5	0.3	15.0	0.2	15.5	10.7	0.414	6.8	—	93	89	-	C1
820724022	02:11:48	351.3	0.2	44.8	0.6	56.4	1.1	56.5	55.4	0.957	6.0	-3.89	119	103	95	C2
820724023	02:18:18	11.1	3.1	26.0	6.6	62.2	1.0	62.4	61.4	0.794	5.9	—	-	100	95	-
820724024	02:28:27	33.7	0.8	36.0	1.3	60.2	1.2	60.3	59.3	0.690	5.8	-4.13	113	107	105	C2
820724025	02:30:13	18.5	0.4	17.3	1.6	68.8	0.5	68.9	68.0	0.693	4.8	-3.77	119	108	94	C2
820724026	02:37:44	19.1	0.3	-2.8	1.2	68.0	0.6	68.2	67.3	0.495	5.3	—	-	111	100	-
820724027	02:39:51	309.9	7.4	63.9	0.9	28.5	2.2	28.8	26.5	0.914	7.3	-3.79	101	98	94	C1
820724028	02:42:39	289.9	0.4	41.8	0.4	23.7	0.4	24.5	21.8	0.855	6.7	—	88	82	-	A
820724029	02:45:42	8.3	0.6	38.1	1.3	52.3	1.2	52.5	51.2	0.912	5.3	-3.84	112	104	98	C2
820724030	02:59:08	229.2	0.3	-10.1	0.9	12.1	0.2	13.1	6.8	0.144	6.7	—	-	84	82	-
820724031	02:59:24	17.0	1.3	-6.4	5.2	66.7	0.9	66.8	65.9	0.510	5.1	—	116	110	-	C2
820724032	03:02:26	59.0	0.8	36.4	1.3	54.2	0.7	54.3	53.2	0.537	5.6	-3.74	115	108	105	C2
820724033	03:03:05	321.3	1.0	34.0	3.4	20.0	1.5	20.4	17.0	0.962	7.2	-3.23	99	96	94	C1
820724034	22:46:35	341.7	2.5	50.8	1.9	32.7	1.2	32.9	31.0	0.746	6.9	-3.66	102	99	96	C1
820724035	23:00:42	262.7	1.7	24.2	5.1	17.7	0.7	18.1	14.3	0.931	7.2	-2.93	97	94	90	C1
820724036	23:03:18	66.6	14.4	79.0	3.7	41.7	0.8	42.0	40.5	0.573	6.5	-3.76	105	101	97	C2
820724037	23:10:14	299.1	0.2	3.0	1.8	26.2	0.5	26.7	24.2	0.759	6.4	-3.05	95	92	88	A
820724038	23:17:43	259.3	1.5	-4.1	5.0	16.8	0.2	17.3	13.1	0.690	3.1	—	106	95	-	C1
820724039	23:19:26	23.6	1.3	32.4	2.0	58.9	0.7	59.0	58.0	0.301	5.6	-4.16	112	109	107	C2
820724040	23:26:33	220.3	0.4	51.0	0.3	14.3	0.6	15.1	10.2	0.796	7.6	-2.74	84	82	79	A
820724041	23:42:38	152.7	0.1	56.0	0.1	23.0	0.3	23.3	20.5	0.345	6.7	—	101	96	-	C1
820724042	23:46:58	227.0	0.2	49.5	0.3	16.4	0.3	16.9	12.6	0.783	7.0	-2.44	92	87	81	C1
820725001	00:06:52	12.1	0.9	68.0	0.2	61.7	0.7	61.8	60.8	0.713	4.0	-3.48	119	108	94	C2
820725002	00:16:15	333.1	0.3	-5.8	1.5	45.7	0.4	46.0	44.6	0.553	5.8	—	-	91	-	-
820725003	00:16:15	303.8	0.1	11.9	1.3	31.8	0.6	32.2	30.2	0.863	6.6	—	-	90	84	-
820725004	00:19:15	332.5	0.1	-16.7	1.6	25.6	0.8	26.1	23.6	0.453	6.4	—	96	94	-	C1
820725005	00:27:15	335.3	0.2	-3.8	1.3	50.9	2.2	51.3	50.1	0.579	5.9	—	94	92	-	A
820725006	00:28:39	332.2	0.2	-4.1	1.4	48.3	0.4	48.6	47.2	0.598	5.4	—	-	92	-	-

TABLE II. ISIT CAMERA METEORS

I.D. No.	E.S.T.	R.A.	d(R.A.)	Dec.	d(dec)	Vobs.	dV	Vinf	Vg	cos χ	Mag	log(mass)	Hb	Hm	He	Type
820725007	00:31:16	35.4	0.3	-5.9	0.7	12.4	0.1	13.0	6.7	0.339	7.4	-2.03	90	88	85	C1
820725008	00:31:58	302.6	0.1	31.4	0.2	30.8	0.9	31.4	29.4	0.979	7.5	-3.68	94	88	80	A
820725009	00:36:37	165.4	0.2	40.5	1.1	44.4	0.5	44.7	43.3	0.051	6.0	—	-	86	86	-
820725010	01:00:58	322.4	1.8	64.0	1.3	28.2	2.6	28.5	26.2	0.933	7.5	-3.68	106	96	91	C1
820725011	01:21:03	22.9	0.5	0.1	1.3	54.6	1.0	54.7	53.6	0.309	5.2	—	113	110	-	C2
820725012	01:23:10	351.0	1.4	64.4	0.3	44.2	2.0	44.7	43.2	0.881	6.8	-4.07	96	88	83	A
820725013	01:28:45	327.9	0.5	42.3	6.9	36.1	3.6	36.4	34.7	0.993	5.9	—	-	96	91	-
820725014	01:42:41	341.7	0.8	-4.9	14.3	30.9	1.6	31.3	29.2	0.647	6.7	—	-	86	82	-
820725015	01:44:37	23.6	0.4	37.0	0.7	63.1	0.8	63.3	62.3	0.697	2.4	—	-	98	90	-
820725016	01:56:03	14.0	0.3	32.8	0.7	67.9	0.7	68.1	67.2	0.778	5.9	-4.04	110	100	89	C2
820725017	01:56:42	45.2	1.2	47.5	1.0	65.2	1.4	65.4	64.4	0.597	4.0	—	-	97	92	-
820725018	02:05:32	6.2	1.0	36.5	2.7	60.6	1.5	60.8	59.8	0.867	5.5	—	-	100	93	-
820725019	02:09:34	349.0	0.1	21.2	8.0	19.7	0.7	20.3	17.0	0.897	7.1	-3.09	93	91	84	C1
820725020	02:26:41	285.7	2.4	61.7	1.0	25.4	1.3	25.7	23.1	0.855	6.3	-3.14	99	95	93	C1
820725021	02:40:48	44.4	0.5	35.8	0.8	65.1	0.6	65.2	64.3	0.628	5.1	-3.76	116	108	100	C2
820725022	02:44:44	12.2	3.4	27.2	11.3	12.1	0.4	13.7	7.8	0.893	7.0	-2.23	79	76	74	A
820725023	02:54:50	21.5	2.1	57.2	1.2	77.3	2.8	77.4	76.6	0.973	4.9	—	117	108	-	C2
820811001	23:02:32	260.6	3.4	80.9	0.6	23.6	1.0	24.4	21.7	0.792	7.5	-3.51	84	81	69	A
820811002	23:11:14	228.5	4.9	22.5	8.6	18.5	0.9	18.9	15.3	0.556	6.6	—	102	99	-	C1
820811003	23:11:27	277.7	0.2	43.6	0.8	21.1	0.8	21.5	18.3	0.964	6.9	-2.80	114	100	93	C1
820811004	23:20:49	290.1	0.1	57.4	0.1	29.3	1.3	29.6	27.4	0.962	5.9	-2.99	111	100	89	C1
820811005	23:31:05	44.8	1.4	59.9	0.9	59.5	0.9	59.6	58.6	0.543	5.5	-3.95	113	109	102	C2
820811006	23:31:55	246.1	1.2	84.1	0.2	14.9	0.5	15.7	11.0	0.792	7.8	-2.49	89	83	72	C1
820811007	23:38:08	274.5	0.1	52.5	0.1	22.1	0.4	22.5	19.5	0.925	6.2	-2.66	102	89	81	C1
820811008	23:53:00	332.0	0.8	4.4	7.1	39.5	1.1	39.8	38.2	0.745	6.2	—	-	99	95	-
820811009	23:54:47	323.2	0.1	9.2	1.3	34.1	0.6	34.5	32.6	0.826	5.9	—	102	96	-	C1
820811010	23:57:12	46.9	2.9	55.0	1.6	66.0	1.0	66.1	65.2	0.541	5.6	—	117	109	-	C2
820812001	00:03:32	342.4	0.5	-25.1	2.4	27.9	0.4	28.3	26.0	0.348	6.1	—	-	96	-	-
820812002	00:12:08	62.7	5.6	43.5	7.4	60.3	1.2	60.4	59.4	0.340	5.1	—	118	115	-	C2
820812003	00:16:25	340.8	1.1	27.7	4.0	53.5	1.0	53.9	52.7	0.914	2.9	—	-	96	82	-	A
820812004	00:19:04	49.8	1.2	56.5	0.7	55.7	0.4	55.8	54.7	0.573	3.6	-2.98	123	107	98	C2
820812005	00:22:17	54.9	1.0	50.8	1.0	47.9	0.5	48.1	46.7	0.501	4.0	-3.28	112	105	99	C2
820812006	00:28:16	281.6	0.4	42.1	0.7	20.8	0.4	21.4	18.2	0.897	6.6	—	95	87	-	C1
820812007	00:33:32	293.1	0.3	30.2	0.9	21.4	0.4	22.0	18.9	0.912	6.3	—	90	83	-	A
820812008	00:38:48	306.6	1.0	7.0	3.6	26.8	0.4	27.1	24.7	0.796	5.5	—	106	94	-	C1

TABLE II. ISIT CAMERA METEORS

I.D. No.	E.S.T.	R.A.	d(R.A.)	Dec.	d(dec)	Vobs.	dV	Vinf	Vg	cos χ	Mag	log(mass)	Hb	Hm	He	Type
820812009	00:42:08	346.6	0.2	0.0	1.7	14.0	0.3	15.4	10.5	0.760	6.8	-2.36	83	82	77	A
820812010	00:44:26	347.7	0.3	-7.4	2.5	16.5	0.3	17.7	13.7	0.662	7.0	-2.54	84	83	78	A
820812011	00:58:33	76.6	2.9	32.5	5.4	42.2	0.6	42.4	40.9	0.207	5.4	-3.46	113	112	109	C2
820812012	01:06:03	55.1	3.1	-7.0	7.3	74.5	1.9	74.8	73.9	0.001	4.6	—	106	106	106	A
820812013	01:07:15	83.6	1.9	20.4	4.6	37.8	0.6	38.0	36.3	0.021	4.9	-3.16	113	113	113	C1
820812014	01:12:44	50.2	3.0	56.7	1.4	57.2	1.1	57.3	56.2	0.661	5.3	—	124	116	-	C2
820812015	01:13:33	350.9	0.8	0.5	5.1	44.2	0.9	44.7	43.2	0.706	4.9	—	98	94	-	A
820812016	01:14:00	143.3	8.9	-5.9	19.7	8.8	0.2	9.7	0.0	0.007	5.9	—	93	93	93	C1
820812017	01:16:24	350.9	0.1	-17.2	3.0	39.0	0.5	39.3	37.7	0.482	3.0	—	100	93	-	A
820812018	01:29:34	52.0	0.8	41.9	1.0	65.4	0.7	65.5	64.6	0.598	4.6	—	117	111	-	C2
820812019	01:41:19	161.8	0.4	45.3	1.4	38.0	0.7	38.3	36.7	0.018	5.5	—	-	91	-	-
820812020	01:45:27	306.5	0.4	66.1	0.1	28.9	1.1	29.2	26.9	0.883	6.7	-3.41	100	94	89	C1
820812021	01:50:48	346.0	0.1	9.2	3.6	44.9	0.9	45.3	43.9	0.832	5.3	—	99	94	-	A
820812022	01:52:53	68.4	12.0	53.1	6.3	52.3	1.3	52.5	51.2	0.586	5.5	—	113	110	-	C2
820812023	01:53:20	2.3	0.9	46.8	1.9	60.5	2.6	60.7	59.7	0.968	6.6	-4.48	109	107	99	C2
820812024	01:54:32	17.2	0.5	-10.3	6.5	60.7	1.1	60.9	59.9	0.477	5.4	—	109	106	-	C2
820812025	01:57:28	52.6	0.7	53.2	0.6	49.6	0.6	49.8	48.5	0.710	3.8	-3.14	115	104	95	C2
820812026	02:03:14	27.3	5.0	68.5	0.8	19.8	1.7	20.4	17.1	0.857	6.9	-3.26	93	91	88	C1
820812027	02:06:48	316.6	0.7	67.6	0.1	34.6	1.1	34.8	33.0	0.883	6.8	-3.56	105	98	91	C1
820812028	02:08:22	48.7	0.4	45.5	0.4	61.4	0.7	61.5	60.5	0.726	5.2	-3.73	113	101	95	C2
820812029	02:22:09	45.9	0.5	56.8	0.2	62.8	1.2	62.9	61.9	0.796	5.9	-4.07	116	107	98	C2
820812030	02:30:20	44.2	1.3	57.5	1.0	65.1	1.7	65.2	64.3	0.817	4.5	-4.02	119	103	97	C2
820812031	02:34:02	48.7	0.6	36.9	0.9	77.2	1.0	77.5	76.6	0.738	5.6	-4.32	103	96	90	A
820812032	02:35:54	116.4	1.2	38.3	2.0	40.7	0.5	41.0	39.4	0.145	5.8	—	-	91	89	-
820812033	02:38:13	52.2	0.3	15.4	0.9	74.9	1.0	75.1	74.2	0.553	5.0	—	-	109	100	-
820812034	02:42:11	50.6	1.1	56.4	0.8	57.5	1.8	57.6	56.5	0.798	5.4	-3.93	112	107	101	C2
820812035	02:43:49	48.7	2.4	57.2	1.7	58.6	2.7	58.8	57.7	0.813	4.3	—	-	105	98	-
820812036	02:50:59	13.1	1.2	68.2	0.3	33.3	1.7	33.5	31.6	0.899	7.4	-3.74	102	94	85	C1
820812037	02:54:29	57.4	1.0	54.7	0.7	58.3	1.0	58.4	57.4	0.774	5.0	-3.72	118	108	102	C2
820812038	03:02:06	48.0	0.4	24.9	1.4	72.7	1.2	73.0	72.1	0.729	5.5	-4.27	103	99	94	A
820812039	03:09:42	49.6	0.7	57.4	0.4	59.5	0.8	59.6	58.6	0.841	3.8	-3.33	121	107	96	C2
820812040	03:14:28	47.9	1.1	58.1	0.7	54.6	2.1	54.7	53.6	0.855	6.1	-4.18	113	111	104	C2

It is interesting to see how magnitude varies with meteorid mass, velocity and cos (χ) and so we have found the coefficients listed in Tab. III below.

With the vidicon camera the average absolute magnitude of the meteors was 4·6 while with the ISIT camera it was 6·1 corresponding to masses of $1{\cdot}3 \times \times 10^{-3}$ and $2{\cdot}4 \times 10^{-4}$ g respectively.

TABLE III

Magnitudes

Coefficients in the equation

$M = a + b \log(\text{mass}) + c \log(V \text{obs}) + d \log(\cos \chi)$

	Vidicon	ISIT	All meteors
a	$9{\cdot}78 \pm 0{\cdot}36$	$10{\cdot}06 \pm 0{\cdot}33$	$9{\cdot}88 \pm 0{\cdot}36$
b	$-2{\cdot}11 \pm 0{\cdot}15$	$-1{\cdot}85 \pm 0{\cdot}14$	$-2{\cdot}02 \pm 0{\cdot}15$
c	$-7{\cdot}33 \pm 0{\cdot}41$	$-6{\cdot}86 \pm 0{\cdot}39$	$-7{\cdot}17 \pm 0{\cdot}41$
d	$0{\cdot}17 \pm 0{\cdot}23$	$-0{\cdot}02 \pm 0{\cdot}24$	$0{\cdot}10 \pm 0{\cdot}24$

The variation of magnitude with mass (reduced to 30 km/s) is shown in Fig. 3 for both the present and Super-Schmidt observations.

6. Velocities

Figure 4 shows the velocity distribution for the combined TV meteors. Although there were slight differences between the vidicon and ISIT meteors we did not consider them significant. The familiar bimodal distribution is evident with the ratio between the low and high velocity peaks being about 1·3. This is considerably less than for the Super-Schmidt meteors for which this ratio is about 2·7. The greater proportion of high velocity meteors in the TV sample may be the result of the mechanism of ejection of the dust particles from the parent comet (Whipple, 1951) or even mutual collisions in interplanetary space which will cause the smaller particles to have greater velocities provided that the collisions are not perfectly elastic.

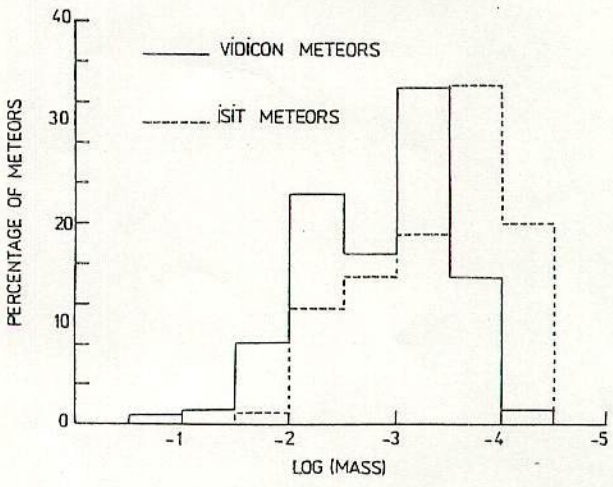

Fig. 2.

DOUBLE-STATION OBSERVATIONS OF 454 TV METEORS

II. *Orbits*

J. Jones, T. Sarma

Department of Physics, University of Western Ontario, London, Ontario, Canada N6A 3K7

Received 22 May 1984

НАБЛЮДЕНИЯ 454 ТЕЛЕВИЗИОННЫХ МЕТЕОРОВ С ДВУХ СТАНЦИЙ

II. *Орбиты*

Даются орбитальные элементы и их вероятные ошибки для 454 слабых метеоров, охватывающих область абсолютных величин от 0.5 до 8.5. Наблюдения были выполнены двумя высокочувствительными телевизионными системами с мая 1981 по август 1982 гг. На сей день это не только самое большое собрание данных по телевизионным метеорам, но и самое точное.

Как кометная, так и астероидальная группы метеоров, обнаруженные в фотографических метеорных обследованиях присутствуют в телевизионных данных, но кометная группа со случайными наклонами орбит представляется более рассеянной, чем для фотографических метеоров. Многие телевизионные метеоры имеют обратные движения с афелием >3 АЕ, а также большая часть орбит имеет малые перигелийные расстояния, если сравнить с супер-шмидтовскими метеорами. Эти особенности указывают на то, что население метеорных тел находится в состоянии динамического равновесия с источником телевизионных метеорных тел, пополняя убытки путем возмущений от Юпитера и солнечного нагрева.

The orbital elements together with their probable errors for 454 faint meteors spanning the range 0·5 to 8·5 in absolute magnitude are presented. The observations were made with two very sensitive television systems between May 1981 and August 1982. Not only is this the largest collection of television meteor data to date, it is also the most accurate.

Both the cometary and asteroidal groups of meteors discovered in photographic meteor surveys are also present in the TV data but the cometary group with randomly inclined orbits appears to be more diffuse than for the photographic meteors. Many TV meteors have retrograde orbits with aphelia > 3 A.U. and also a greater proportion of orbits have very small perihelia when compared with the Super-Schmidt meteors. These features seem to suggest that the meteoroid population is in a state of dynamic equilibrium with a source of TV meteoroids replenishing those lost by Jovian perturbations and solar heating.

38MSS 1-7

1. Introduction

This paper is the second in a series reporting the results of observations of faint meteors made with very sensitive television cameras. Detailed descriptions of the systems are given in the first paper of the series (Sarma and Jones, 1984) which is concerned mainly with the trajectory analysis. In the present paper we list the orbital elements of each of the television meteors and discuss the distribution of these elements.

The importance of this data lies in the faintness of the meteors observed and it constitutes the first substantial database for such faint meteors. Previously such data had been available only for meteors brighter than magnitude +3 (Jacchia, Verniani and Briggs, 1967; McCrosky and Posen, 1961) from observations made with Super-Schmidt cameras. More recently Hawkes, Jones and Ceplecha (1983) published the results of television meteor observations based on a small number of meteors of mean magnitude +3. But even though this set of observations was small it gave a glimpse of the possibility of exciting new discoveries in the population distribution of the orbits of meteoroids.

The faintest meteors in the present series are +8·5 magnitude and so are about 3 magnitudes fainter than those of Hawkes, Jones and Ceplecha and about 5 magnitudes fainter than the Super-Schmidt meteors.

Besides being less accurate than the Super-Schmidt observations, our data does not comprise a random sample since it was collected on only 11 nights between May and November and so does not include the winter months.

2. Orbital Elements

Whipple and Jacchia's (1957) method was used to extract the orbital elements from the trajectory information given in Paper I. These are given for each of the TV meteors in Tabs I and II for the vidicon and ISIT cameras respectively in which the symbols have the following meanings:

I.D.No. Is a nine digit number in which is encoded the date and which meteor it is on that day. The digits are as follows

Bull. Astron. Inst. Czechosl. 36 (1985), 103—115.

Vol. 36 (1985), No. 2

TABLE I. Vidicon camera meteors.

I.D. No.	E.S.T.	a	da	e	de	q	Ω	i	di	ω	dω	Mag	log(mass)	Type
810506001	00:07:25	4.1	2.0	0.79	0.07	0.87	45.2	72.8	1.4	226.4	5.5	5.5	-3.77	C2
810506002	00:19:48	4.2	0.8	0.93	0.01	0.29	45.2	30.4	2.2	299.0	3.4	2.5	-2.43	C1
810506003	00:33:33	5.8	---	0.91	0.10	0.52	45.2	14.4	2.2	270.7	2.4	6.8	-3.81	C1
810506004	00:46:09	1.1	0.4	0.62	0.10	0.41	45.2	39.9	9.7	302.8	9.3	6.7	-3.52	C1
810506005	00:47:41	-0.7	0.1	1.95	0.11	0.67	45.2	44.3	1.2	240.3	2.8	3.8	-4.33	A
810506006	00:48:40	1.1	0.0	0.07	0.02	1.01	45.2	18.2	0.6	161.7	2.1	6.9	-2.25	C1
810506007	00:51:42	2.4	1.3	0.61	0.14	0.95	45.2	27.7	2.9	147.6	3.3	2.3	-0.34	C1
810506008	00:53:03	2.4	0.3	0.59	0.05	0.97	45.2	30.2	0.8	152.5	2.0	5.7	-2.45	A
810506009	01:29:26	0.7	0.0	0.53	0.01	0.35	45.2	7.4	1.1	334.9	0.5	5.9	-2.01	C1
810506010	01:32:46	1.1	0.1	0.35	0.02	0.74	45.2	93.6	2.0	272.2	13.4	4.7	-3.05	C2
810506011	01:48:08	1.7	0.1	0.50	0.03	0.86	45.2	24.7	0.7	123.7	3.8	5.0	-1.49	C1
810506012	01:51:44	-3.5	1.2	1.27	0.14	0.93	45.2	150.9	3.1	209.9	3.1	3.3	-3.34	C2
810506013	01:57:58	-0.1	0.0	8.46	0.15	0.95	225.2	1.4	0.1	20.1	179.4	4.5	-1.96	-
810506014	02:08:35	2.0	0.2	0.55	0.03	0.92	45.2	27.7	0.6	139.6	3.5	3.6	-2.60	C1
810506015	02:20:47	-5.4	1.7	1.11	0.04	0.61	45.2	167.3	3.9	104.9	2.1	3.6	—	C2
810506016	02:31:53	1.6	0.1	0.40	0.04	0.97	45.3	29.1	0.7	150.0	2.1	6.5	-2.48	A
810506017	02:38:32	0.8	0.0	0.42	0.04	0.46	45.3	65.1	1.8	324.8	4.8	5.5	-3.38	C1
810506018	02:40:12	0.9	0.0	0.54	0.03	0.39	45.3	50.2	2.1	318.0	4.0	6.2	-3.40	C1
810506019	02:45:00	1.3	0.1	0.22	0.07	1.00	45.3	62.4	1.3	159.7	2.7	5.4	-2.96	A
810506020	02:49:31	-1.3	0.1	1.51	0.03	0.68	45.3	7.0	1.5	117.4	1.1	3.1	—	-
810506021	02:50:42	1.5	0.1	0.32	0.04	0.99	45.3	37.4	1.2	203.3	5.3	6.6	-2.66	C1
810506022	03:10:37	-0.1	0.0	8.47	0.21	0.96	225.3	4.6	1.3	18.7	0.7	3.9	—	A
810506023	03:13:04	2.3	0.2	0.57	0.04	1.00	45.3	11.1	0.6	167.9	0.6	6.0	-1.77	A
810506024	03:16:12	5.3	3.7	0.90	0.04	0.54	45.3	80.4	1.6	268.7	6.3	4.8	-3.30	A
810506025	03:17:05	-0.1	0.0	8.66	0.13	1.01	45.3	10.8	1.3	179.0	0.6	1.6	-2.68	A
810506026	03:17:33	2.8	0.8	0.67	0.07	0.92	45.3	60.6	1.4	140.9	3.0	3.9	-2.43	C1
810506027	03:34:12	3.6	1.4	0.74	0.08	0.93	45.3	123.8	2.7	214.3	4.9	4.1	-3.74	A
810506028	03:34:15	4.5	2.2	0.89	0.04	0.52	45.3	165.0	4.2	87.7	3.3	5.0	-3.64	A
810506029	03:47:41	0.9	0.1	0.66	0.01	0.32	45.3	127.6	4.0	43.5	4.2	3.9	-3.14	C2
810506030	03:54:24	0.6	0.0	0.84	0.02	0.09	45.3	48.7	2.3	348.7	0.9	5.8	-3.01	C1
810506031	03:57:36	1.4	0.0	0.72	0.01	0.38	45.3	14.9	1.8	298.9	2.2	5.2	-2.72	C1
810506032	03:58:46	2.9	0.2	0.67	0.02	0.97	45.3	19.2	0.5	203.9	1.8	5.4	-2.09	A
810506033	04:03:54	2.6	0.1	0.65	0.02	0.91	45.3	13.6	0.6	220.5	1.6	1.4	-0.85	C1
810626001	22:45:08	1.1	0.1	0.17	0.04	0.87	94.0	80.0	2.0	91.7	19.4	4.6	-3.15	C1
810626002	22:55:13	1.0	0.0	0.05	0.00	0.92	94.0	7.3	1.2	12.7	5.3	6.8	-1.71	C1

TABLE I. Vidicon camera meteors.

I.D. No.	E.S.T.	a	da	e	de	q	Ω	i	di	ω	dω	Mag	log(mass)	Type
810626003	22:55:42	1.1	0.0	0.13	0.02	1.00	94.0	13.9	0.8	213.2	3.3	4.7	-1.72	A
810626004	22:59:00	1.7	0.0	0.63	0.01	0.61	94.0	5.6	1.3	271.9	1.0	4.1	-1.93	A
810626005	23:05:28	1.9	0.1	0.97	0.00	0.06	94.0	16.2	7.6	336.3	1.1	3.3	-2.05	A
810729001	23:59:47	2.0	0.1	0.54	0.03	0.92	126.5	30.9	0.9	223.8	1.1	5.0	-2.70	C1
810730001	00:02:15	2.1	0.1	0.96	0.00	0.08	306.5	29.7	1.0	150.9	0.7	3.8	—	A
810730002	00:03:56	2.5	0.2	0.73	0.02	0.67	306.5	2.5	0.1	78.3	182.8	5.2	-2.50	C1
810730003	00:04:49	-0.9	0.1	2.17	0.09	1.00	126.5	108.3	0.7	168.9	0.7	3.4	-3.32	C2
810730004	00:10:08	2.6	0.4	0.66	0.05	0.88	126.5	22.0	1.8	228.7	2.1	3.0	-2.51	C1
810730005	00:11:21	4.1	0.6	0.97	0.00	0.13	306.5	47.2	1.2	140.5	2.9	2.6	—	-
810730006	00:14:45	1.4	0.1	0.97	0.01	0.04	306.5	25.6	13.5	160.7	3.9	4.2	—	-
810730007	00:27:15	2.3	0.2	0.94	0.00	0.14	306.5	33.4	1.4	141.3	1.6	4.1	-2.84	A
810730008	00:39:44	0.8	0.0	0.66	0.02	0.28	126.5	24.9	3.4	323.7	0.4	5.4	-2.58	A
810730009	00:41:41	9.9	11.5	0.90	0.06	0.99	126.5	144.6	1.1	162.5	1.1	3.9	-3.34	A
810730010	00:43:59	1.3	0.2	0.58	0.06	0.53	126.5	73.3	2.7	287.1	12.4	5.0	-3.23	C1
810730011	00:55:34	0.9	0.0	0.15	0.01	0.75	126.5	11.5	0.8	0.5	0.8	6.5	-1.79	C1
810730012	01:02:50	-8.5	---	1.05	0.05	0.41	306.6	61.2	1.9	99.2	10.2	3.1	—	A
810730013	01:05:58	1.9	0.1	0.96	0.00	0.07	306.6	20.8	6.1	153.7	2.6	3.8	-2.65	A
810730014	01:14:31	1.0	0.1	0.49	0.07	0.50	126.6	71.8	3.2	304.0	10.1	4.5	-3.41	A
810730015	01:21:34	6.1	2.5	0.98	0.00	0.12	306.6	58.2	1.5	140.7	6.7	3.6	—	A
810730016	01:21:49	4.2	0.5	0.98	0.00	0.09	306.6	27.8	2.5	146.9	1.8	4.3	-2.67	A
810730017	01:25:29	2.6	0.2	0.99	0.00	0.03	126.6	30.7	9.0	341.8	1.0	4.5	-2.92	A
810730018	01:27:40	5.7	1.2	1.00	0.00	0.02	126.6	35.2	7.7	343.4	0.9	2.9	—	-
810730019	01:30:33	1.5	0.6	0.33	0.21	1.02	126.6	100.6	4.1	178.7	12.1	5.3	-3.82	A
810730020	01:35:03	1.2	0.0	0.13	0.03	1.02	126.6	12.1	1.5	182.1	0.8	5.9	-2019	A
810730021	22:45:39	1.1	0.0	0.34	0.01	0.70	127.4	11.6	0.7	281.5	0.5	5.5	-2.02	C1
810730022	22:47:00	0.9	0.1	0.95	0.03	0.05	307.4	38.6	18.5	162.9	6.5	4.2	—	-
810730023	22:47:28	1.9	0.2	0.45	0.06	1.01	127.4	22.2	1.4	175.4	0.4	5.8	-2.40	C1
810730024	22:51:55	2.7	0.1	0.75	0.01	0.67	127.4	13.2	0.3	258.0	0.2	4.7	-2.00	C1
810730025	23:03:50	2.7	0.2	0.78	0.02	0.58	127.4	18.3	1.0	268.8	0.3	5.0	-2.61	C1
810730026	23:08:28	1.6	0.0	0.48	0.01	0.86	127.4	17.5	0.3	239.1	0.3	5.4	-2.06	A
810730027	23:12:34	3.5	1.2	0.87	0.03	0.46	127.4	25.8	1.1	280.1	0.6	0.1	—	-
810730028	23:12:54	2.3	0.2	0.57	0.04	1.01	127.4	44.3	1.0	167.4	0.4	6.3	-2.82	C1
810730029	23:21:40	2.4	0.1	0.74	0.01	0.61	127.4	14.6	0.3	266.9	0.2	2.5	—	-
810730030	23:24:03	1.2	0.0	0.74	0.01	0.31	127.4	148.6	1.8	308.3	2.1	3.5	—	C2
810730031	23:22:46	-2.4	0.4	1.07	0.01	0.17	127.4	51.3	4.4	307.1	3.4	4.2	-3.24	C2

TABLE I. Vidicon camera meteors.

I.D. No.	E.S.T.	a	da	e	de	q	Ω	i	di	ω	dω	Mag	log(mass)	Type
810730032	23:22:46	-2.5	0.4	1.07	0.01	0.17	127.4	50.6	4.5	307.4	3.3	4.2	-3.23	C2
810730033	23:36:28	2.4	0.2	0.96	0.00	0.10	307.5	29.7	2.4	146.8	2.0	3.9	—	-
810730034	23:39:37	1.8	0.0	0.56	0.01	0.80	307.5	8.7	1.6	64.9	2.3	3.7	-1.83	A
810730035	23:39:43	2.4	0.2	0.58	0.04	1.01	127.5	9.3	0.5	188.3	0.4	5.9	-2.06	C1
810730036	23:40:28	3.2	0.4	0.76	0.04	0.77	127.5	23.4	2.3	243.6	1.8	5.5	-2.49	A
810730037	23:43:02	6.9	7.3	0.85	0.08	1.01	127.5	66.9	1.1	183.9	0.5	5.1	-3.04	C2
810730038	23:44:41	2.1	0.1	0.96	0.00	0.09	307.5	19.5	0.8	149.9	0.4	4.2	—	-
810730039	23:44:53	3.1	1.0	0.67	0.08	1.01	127.5	50.0	1.5	173.9	0.5	5.3	-2.96	C1
810730040	23:49:17	1.0	0.0	0.27	0.01	0.70	127.5	1.8	0.1	298.4	0.3	5.9	-1.77	A
810730041	23:50:39	-1.8	0.2	1.55	0.07	1.00	127.5	97.8	0.9	168.4	1.6	4.4	-3.27	C2
810730042	23:58:39	6.8	1.9	0.96	0.01	0.24	307.5	75.8	1.0	123.7	2.2	4.2	-2.89	A
810731001	00:04:02	1.6	0.1	0.49	0.02	0.80	127.5	22.8	0.7	248.8	0.7	5.8	-2.38	A
810731002	00:06:05	7.7	3.6	0.87	0.04	0.96	127.5	70.8	0.6	152.6	1.1	4.3	-2.86	C2
810731003	00:17:15	3.7	0.4	0.89	0.01	0.39	127.5	22.3	0.6	287.7	0.3	5.0	-2.90	C1
810731004	00:20:13	5.1	0.8	0.90	0.01	0.53	307.5	6.3	1.0	91.1	0.9	4.5	—	A
810731005	00:31:37	1.0	0.0	0.07	0.03	0.89	127.5	5.0	3.1	331.8	4.4	1.9	—	C1
810731006	00:35:07	0.8	0.0	0.29	0.02	0.57	127.5	13.5	1.6	337.8	1.3	6.2	—	C1
810731007	00:40:59	0.8	0.0	0.69	0.02	0.26	307.5	4.7	2.2	145.3	183.5	4.8	—	C1
810731008	00:41:10	2.4	8.6	0.80	0.15	0.48	127.5	62.0	6.7	280.9	9.6	-0.1	—	C1
810731009	00:41:37	-7.8	2.5	1.12	0.05	0.91	127.5	135.9	1.2	144.2	1.1	-0.9	—	C2
810731010	00:49:30	2.9	0.6	0.67	0.05	0.96	127.5	47.2	1.2	209.8	1.3	2.2	—	C1
810731011	00:55:45	0.8	0.0	0.58	0.03	0.33	127.5	30.8	2.3	329.2	0.4	3.7	—	C1
810731012	00:56:53	1.2	0.0	0.77	0.09	0.27	127.5	58.8	4.7	313.7	9.5	3.7	-2.86	C1
810731013	01:08:51	2.7	---	0.67	0.36	0.90	127.5	111.5	3.6	135.2	10.8	4.0	-3.32	C2
810731014	01:09:11	1.2	0.1	0.84	0.01	0.19	307.5	11.8	4.2	140.5	2.6	4.3	—	-
810731015	01:16:58	1.0	0.0	0.02	0.00	0.98	307.5	1.3	0.0	315.0	150.1	5.4	-0.82	C1
810731016	01:20:59	0.8	0.0	0.56	0.01	0.34	127.5	5.6	2.1	326.7	1.1	5.5	-2.23	C1
810731017	01:26:18	2.1	0.1	0.96	0.00	0.08	307.5	6.5	2.0	151.4	0.7	2.2	—	-
810731018	01:29:31	-1.2	0.1	1.74	0.11	0.90	127.5	137.6	2.0	215.3	2.8	-0.1	-2.73	C2
810731019	01:32:41	0.7	0.0	0.73	0.11	0.18	127.5	25.8	11.0	343.1	1.0	5.7	-2.96	C1
810731020	01:33:03	1.2	0.0	0.41	0.02	0.74	127.5	1.3	1.2	266.9	2.7	5.1	-2.04	C1
810731021	01:35:55	31.7	62.5	0.98	0.02	0.79	307.5	11.4	1.4	56.9	1.5	3.5	—	C1
810731022	01:41:29	6.1	2.2	0.98	0.01	0.12	307.5	34.9	2.0	141.2	2.2	4.0	—	A
810731023	01:43:15	5.1	1.2	0.99	0.01	0.07	127.5	70.5	3.6	330.4	3.1	2.0	-2.34	A
810731024	01:47:39	1.6	0.1	0.39	0.03	0.99	127.5	3.2	0.7	202.1	1.2	5.9	-1.75	C1

TABLE I. Vidicon camera meteors.

I.D. No.	E.S.T.	a	da	e	de	q	Ω	i	di	ω	dω	Mag	log(mass)	Type
810731025	01:47:56	2.3	0.6	0.93	0.02	0.17	307.5	29.6	8.3	137.2	8.3	3.5	—	-
810731026	01:48:38	1.8	0.3	0.53	0.11	0.83	127.5	10.9	7.0	241.7	7.7	5.2	-2.06	A
810731027	01:51:01	1.3	0.1	0.24	0.04	1.01	127.5	24.0	1.8	175.9	1.3	1.4	-1.37	A
810731028	01:50:51	3.5	2.6	0.73	0.12	0.94	127.5	108.5	3.4	146.2	9.9	-0.3	—	C2
810731029	01:55:57	1.2	0.0	0.41	0.01	0.71	127.5	14.2	0.4	271.7	0.3	5.6	-1.92	C1
810731030	01:56:54	3.5	0.3	0.93	0.01	0.25	307.5	39.9	0.7	124.4	2.0	3.8	—	-
810731031	01:57:55	2.2	0.1	0.74	0.01	0.58	127.5	25.4	0.7	271.1	0.8	3.8	—	C1
810731032	01:58:52	2.9	1.4	0.66	0.11	0.99	127.5	124.5	1.5	199.5	3.3	3.7	-3.33	C2
810731033	02:00:17	2.7	0.1	0.79	0.01	0.58	127.5	6.9	1.0	268.6	0.4	2.8	—	-
810731034	02:02:42	2.8	0.2	0.69	0.02	0.88	127.5	45.0	0.6	226.9	0.9	4.5	-2.46	C1
810731035	02:05:44	0.8	0.1	0.64	0.06	0.30	307.6	172.8	1.4	145.1	181.6	3.5	—	C2
810731036	02:12:37	1.8	0.4	0.60	0.08	0.72	127.6	113.4	3.8	102.3	9.6	1.8	-2.80	C2
810731037	02:25:48	-6.0	1.3	1.05	0.02	0.32	127.6	73.0	0.9	71.0	3.4	3.9	-2.83	C2
810731038	02:32:58	0.8	0.1	0.32	0.05	0.57	127.6	60.9	5.1	327.2	11.4	6.5	-3.41	C1
810731039	02:34:29	-2.2	1.6	1.47	0.28	1.01	127.6	70.1	3.4	170.8	4.7	5.1	-3.59	A
810731040	02:38:13	-3.0	0.8	1.28	0.10	0.85	127.6	131.6	1.8	135.2	2.0	4.0	-3.43	C2
810731041	02:40:38	2.6	0.8	0.94	0.02	0.15	307.6	160.4	16.7	220.6	4.2	4.0	-3.28	C2
810731042	02:42:08	4.8	2.4	0.83	0.14	0.82	307.6	123.0	7.0	54.8	6.3	3.0	—	-
810731043	02:52:30	1.1	0.0	0.13	0.01	0.99	127.6	17.4	0.5	142.8	2.2	5.8	-1.70	C1
810731044	03:00:08	-0.3	0.0	4.11	0.24	0.93	127.6	19.4	4.0	206.6	2.4	4.2	-3.36	A
810731045	03:01:12	2.3	0.7	0.59	0.16	0.93	127.6	31.5	3.6	219.4	13.8	4.5	—	A
810731046	03:01:44	1.6	0.0	0.50	0.01	0.79	307.6	14.2	0.6	71.1	1.8	4.7	—	-
810731047	03:03:09	0.6	0.0	0.79	0.06	0.13	127.6	106.8	6.9	10.4	3.3	5.4	-3.47	C1
810731048	21:34:21	3.0	0.2	0.80	0.02	0.60	128.3	14.4	1.2	265.0	0.4	4.3	—	C1
810731049	21:36:56	-5.2	1.6	1.19	0.07	1.01	128.3	116.7	1.3	185.7	2.1	3.6	-3.09	C2
810731050	22:16:59	-30.9	24.0	1.03	0.07	0.98	128.4	70.9	0.8	202.1	0.8	4.9	-3.14	C2
810731051	22:26:30	999.9	---	1.00	0.40	0.98	128.4	18.9	3.6	201.4	1.3	4.2	-1.91	C1
810731052	22:31:51	3.1	0.3	0.98	0.00	0.06	308.4	26.1	2.5	153.6	1.3	3.1	—	-
810731053	22:48:27	4.0	0.5	0.75	0.03	1.01	128.4	21.6	0.4	177.4	0.2	4.9	-2.45	C1
810731054	23:51:54	3.1	0.3	0.88	0.01	0.36	128.4	39.9	1.6	292.2	1.2	4.0	-2.66	A
810731055	23:52:54	1.0	0.0	0.09	0.00	0.93	128.4	43.0	0.9	91.0	8.1	4.9	-2.23	C1
810801001	00:44:27	1.7	0.1	0.80	0.01	0.34	308.5	8.3	0.9	119.3	0.9	3.2	-2.26	A
810801002	00:57:45	0.8	0.0	0.84	0.01	0.14	308.5	44.4	1.0	154.2	1.9	3.6	—	A
810801003	01:02:47	1.9	0.2	0.79	0.01	0.41	308.5	46.6	0.8	110.6	5.1	2.1	—	-
810801004	01:04:26	16.9	133.8	0.96	0.04	0.75	128.5	135.7	1.1	117.7	1.9	3.6	-3.05	C2

TABLE I. Vidicon camera meteors.

I.D. No.	E.S.T.	a	da	e	de	q	Ω	i	di	ω	dω	Mag	log(mass)	Type
810801005	01:56:45	3.2	0.2	0.80	0.01	0.65	128.5	5.5	1.2	259.5	0.5	4.7	-2.18	C1
810801006	01:58:47	0.8	0.0	0.34	0.05	0.55	128.5	116.6	2.2	325.8	9.2	4.3	-3.42	C2
810924001	00:12:32	-6.4	2.8	1.01	0.01	0.07	359.6	4.2	0.9	147.9	181.9	4.2	-3.02	C2
810924002	00:18:51	1.1	0.1	0.68	0.02	0.35	359.7	18.7	3.6	127.3	5.5	4.3	-1.94	C1
810924003	00:19:01	1.6	0.2	0.93	0.01	0.12	179.7	136.1	3.9	326.9	3.5	4.3	-3.31	A
810924004	00:22:09	2.8	0.0	0.65	0.01	0.99	179.7	30.6	0.1	166.7	0.1	4.7	—	C1
810924005	00:26:28	0.7	0.0	0.50	0.03	0.35	179.7	5.7	1.3	342.7	0.5	6.2	-2.19	C1
810924006	00:26:37	-15.7	12.3	1.06	0.06	0.87	179.7	36.1	1.0	137.1	0.6	4.6	-2.84	C1
810924007	00:29:20	-3.4	0.7	1.23	0.05	0.79	359.7	35.6	0.6	51.5	3.0	4.4	—	C1
810924008	00:39:29	0.7	0.0	0.67	0.03	0.23	179.7	107.2	2.6	336.6	2.8	4.9	-3.28	C2
810924009	00:54:22	2.7	0.7	0.83	0.04	0.47	359.7	2.2	6.1	100.1	188.0	4.5	-2.33	C1
810924010	00:57:37	2.0	0.3	0.64	0.05	0.72	179.7	48.6	1.8	254.5	2.6	5.6	-2.97	A
810924011	01:00:57	0.6	0.0	0.64	0.12	0.23	179.7	126.2	9.7	10.6	4.6	4.4	-3.38	C2
810924012	01:02:02	2.4	0.3	0.59	0.04	0.99	179.7	41.8	1.0	193.7	0.5	5.5	-2.63	C1
810924013	01:03:13	5.6	1.0	0.86	0.02	0.79	359.7	5.9	1.3	57.7	2.0	5.3	-2.34	C1
810924014	01:14:09	1.3	0.1	0.72	0.01	0.38	179.7	4.6	3.1	299.4	2.0	0.9	-1.50	C1
810924015	01:21:37	1.2	0.0	0.21	0.02	0.98	179.7	23.6	1.0	147.0	2.4	5.6	-2.50	C1
810924016	01:27:49	1.2	0.1	0.53	0.06	0.58	179.7	13.8	6.4	283.3	5.0	5.6	-2.40	C1
810924017	01:37:13	6.0	0.9	0.84	0.02	0.94	179.7	12.4	0.2	210.7	0.1	3.0	-1.62	C1
810924018	01:49:33	1.3	0.0	0.25	0.01	0.94	179.7	38.4	0.3	135.0	1.0	2.6	-1.66	C1
810924019	01:49:38	8.7	5.8	0.89	0.05	0.99	179.7	53.6	0.7	193.6	0.3	5.3	-2.92	C1
810924020	01:52:31	1.4	0.2	0.30	0.07	0.95	179.7	125.2	1.9	142.3	7.9	1.9	—	-
810924021	01:57:20	0.6	0.0	0.76	0.09	0.14	179.7	123.0	7.8	350.0	4.0	4.2	-3.46	C2
810924022	01:58:23	22.2	---	0.96	0.10	0.88	179.7	135.3	1.5	221.9	3.0	4.3	-3.51	C2
810924023	02:03:33	-5.3	7.0	1.01	0.00	0.04	179.7	60.4	19.0	335.3	16.6	4.3	—	-
810924024	02:09:56	-4.3	2.0	1.23	0.09	1.00	359.7	133.8	2.7	9.6	1.5	3.5	—	C2
810924025	02:12:38	1.0	0.1	0.40	0.02	0.59	179.7	123.2	1.8	64.5	9.6	4.5	-3.45	C2
810924026	02:20:26	4.0	1.7	0.78	0.07	0.88	179.7	128.9	1.2	135.3	3.1	4.2	-3.67	C2
810924027	02:22:26	6.2	4.8	0.84	0.07	0.99	179.7	55.8	1.1	192.3	0.8	4.7	-3.02	C1
810924028	02:23:44	3.2	2.2	0.78	0.11	0.70	359.7	133.9	10.2	71.6	11.6	4.0	-3.76	A
810924029	02:26:48	2.5	0.5	0.64	0.06	0.90	359.7	10.2	4.2	42.6	8.9	2.7	-1.77	C1
810924030	02:31:42	1.7	0.7	0.75	0.06	0.43	359.7	24.5	18.4	109.5	212.4	3.9	-2.27	C1
810924031	02:33:19	2.6	1.2	0.66	0.11	0.88	179.7	154.8	3.5	225.6	6.2	3.9	—	A
810924032	02:35:33	1.4	0.1	0.57	0.02	0.59	179.7	157.0	2.8	278.1	6.2	4.2	-3.30	C2
810924033	02:39:44	-79.7	---	1.01	0.04	0.94	359.7	147.2	0.8	331.0	0.9	3.4	—	C2

TABLE I. Vidicon camera meteors.

I.D. No.	E.S.T.	a	da	e	de	q	Ω	i	di	ω	dω	Mag	log(mass)	Type
810924034	02:53:00	19.2	---	0.95	0.13	0.93	179.8	166.9	2.8	148.7	3.4	3.4	-3.65	A
810924035	02:59:23	1.4	0.2	0.29	0.15	0.99	179.8	40.1	2.4	158.1	6.7	5.1	-2.83	A
810924036	03:00:29	1.8	0.4	0.75	0.03	0.45	179.8	149.7	2.6	287.1	6.4	4.3	-3.47	A
810924037	03:00:35	2.5	0.4	0.62	0.06	0.97	179.8	131.1	0.9	155.9	2.0	3.8	-3.20	C2
810924038	03:05:39	0.7	0.0	0.53	0.04	0.31	179.8	125.8	2.3	1.5	0.7	4.6	-3.17	C2
810924039	03:08:33	1.5	0.1	0.49	0.03	0.74	179.8	26.1	1.2	257.4	1.6	5.7	-2.51	C1
810924040	03:08:42	-1.3	0.1	1.62	0.04	0.78	359.8	27.3	0.9	50.0	2.3	3.7	—	C1
810924041	03:15:29	2.1	0.4	0.73	0.04	0.58	359.8	142.2	3.4	90.3	5.4	4.3	-3.58	A
810924042	03:18:01	0.6	0.0	0.67	0.04	0.21	179.8	134.2	3.3	13.4	1.9	4.6	-3.22	C2
810924043	03:18:08	2.1	0.8	0.74	0.06	0.54	179.8	135.7	4.0	275.0	10.0	4.8	-3.68	A
810924044	03:19:18	-2.9	2.9	1.26	0.18	0.76	359.8	9.2	7.9	55.2	10.5	4.7	—	C1
810924045	03:19:37	5.8	51.1	0.87	0.12	0.77	179.8	132.9	1.8	240.0	5.6	4.9	-3.72	A
810924046	03:33:39	1.1	0.0	0.08	0.01	0.98	179.8	21.7	0.7	228.2	7.9	6.3	-2.28	A
810924047	03:53:40	2.8	0.5	0.66	0.05	0.96	179.8	150.4	1.0	153.9	1.7	2.6	-3.07	C2
810924048	03:55:01	0.5	0.0	0.97	0.03	0.02	179.8	129.4	16.1	356.3	1.5	5.0	-3.29	C1
810924049	03:56:04	4.5	4.1	0.80	0.10	0.92	179.8	119.1	1.1	216.6	2.9	4.1	-3.35	C2
810924050	04:00:20	1.1	0.2	0.21	0.01	0.91	359.8	26.2	0.7	64.0	41.1	5.3	-2.20	A
810924051	04:08:35	1.3	0.2	0.31	0.07	0.90	179.8	149.2	2.2	123.4	10.6	4.8	-3.62	C2
810924052	04:09:13	2.5	1.5	0.68	0.11	0.81	179.8	158.1	3.4	237.9	7.1	4.2	-3.61	C2
810924053	04:11:28	-4.4	2.5	1.14	0.17	0.62	179.8	154.1	12.5	253.3	12.8	1.9	-3.33	C2
810924054	04:15:18	1.0	0.0	0.02	0.00	0.98	359.8	1.3	0.0	270.0	7.0	4.8	—	-
810924055	04:18:19	18.1	---	0.95	0.12	0.85	179.8	118.6	1.5	226.6	3.8	5.4	-3.64	C2
811104001	00:31:21	9.5	7.0	0.92	0.04	0.74	40.3	140.0	1.8	62.1	2.8	3.0	—	C2
811104002	00:34:01	1.6	0.1	0.78	0.01	0.37	40.3	11.0	2.7	116.3	2.4	4.8	-2.51	C1
811104003	00:38:12	1.5	0.2	0.47	0.05	0.79	40.3	125.3	4.1	67.9	12.1	4.0	—	-
811104004	00:43:47	1.4	0.1	0.67	0.01	0.45	40.3	9.4	3.0	110.9	3.2	5.4	-2.36	A
811104005	00:46:08	1.9	0.1	0.81	0.01	0.35	40.3	16.1	2.8	115.9	2.8	0.7	—	C1
811104006	00:48:48	-131.7	134.3	1.01	0.10	0.79	220.3	118.4	0.9	234.1	2.9	4.5	-3.54	C2
811104007	00:51:17	1.0	0.0	0.35	0.01	0.68	220.3	74.3	0.9	76.7	4.7	4.7	-2.89	C1
811104008	00:52:13	32.8	---	0.97	0.05	0.83	220.3	118.5	1.8	132.7	4.4	3.9	-2.95	C2
811104009	00:53:34	-2.3	0.6	1.37	0.10	0.86	220.3	63.5	1.4	220.2	2.2	5.4	-3.66	A
811104010	01:04:17	1.2	0.2	0.47	0.03	0.63	220.3	146.3	0.9	278.1	10.4	4.1	-3.49	C2
811104011	01:06:34	-3.4	0.9	1.06	0.01	0.19	220.3	36.2	9.2	304.9	5.9	4.8	-3.23	A
811104012	01:10:07	1.3	0.1	0.46	0.02	0.71	40.3	24.1	1.4	83.9	7.0	2.2	—	-
811104013	01:13:09	2.2	0.5	0.82	0.06	0.41	220.3	5.8	17.4	288.1	2.4	4.9	-2.38	C1

TABLE I. Vidicon camera meteors.

I.D. No.	E.S.T.	a	da	e	de	q	Ω	i	di	ω	dω	Mag	log(mass)	Type
811104014	01:19:57	-16.3	9.8	1.03	0.03	0.46	40.3	161.0	4.9	93.8	3.1	3.0	-3.26	A
811104015	01:20:58	17.6	27.0	0.95	0.03	0.94	220.3	62.0	0.5	207.9	0.4	3.4	-2.50	C1
811104016	01:24:47	1.7	0.2	0.69	0.03	0.51	220.3	73.1	1.8	280.8	4.2	6.0	-3.47	C2
811104017	01:25:13	3.2	0.4	0.70	0.03	0.95	220.3	152.6	0.2	204.6	0.8	3.3	—	-
811104018	01:27:26	1.4	0.1	0.36	0.03	0.88	40.3	3.7	1.3	54.7	3.4	6.0	-2.13	A
811104019	01:28:14	-1.2	0.2	1.45	0.09	0.56	40.3	170.2	3.3	74.7	2.8	3.7	—	-
811104020	01:31:58	0.8	0.0	0.67	0.01	0.27	220.3	2.6	2.0	324.1	0.7	5.4	-2.31	C1
811104021	01:35:20	1.5	0.2	0.64	0.02	0.52	40.3	11.3	9.5	102.1	10.7	4.8	—	-
811104022	01:44:24	0.8	0.0	0.32	0.01	0.51	220.3	16.5	0.6	355.9	0.1	6.5	-1.89	C1
811104023	01:44:41	19.5	---	0.95	0.08	0.99	220.3	174.6	0.5	177.9	0.4	3.9	-3.91	C2
811104024	01:56:24	1.3	0.0	0.54	0.02	0.61	220.3	12.5	1.1	275.9	0.7	6.1	-2.43	A
811104025	01:57:33	1.8	0.1	0.76	0.01	0.44	40.3	157.8	1.8	106.5	2.5	3.8	-3.15	C2
811104026	01:58:10	0.8	0.0	0.34	0.01	0.52	220.3	65.0	1.2	331.0	2.0	5.3	-2.89	A
811104027	01:58:29	1.2	0.1	0.36	0.03	0.79	220.3	22.4	1.5	256.1	3.0	6.4	-2.60	C1
811104028	02:04:45	4.8	2.6	0.83	0.06	0.81	220.3	146.9	2.6	126.1	4.9	4.2	-3.55	C2
811104029	02:06:14	-65.0	54.4	1.01	0.02	0.77	220.3	133.8	0.8	124.1	1.7	3.3	—	-
811104030	02:07:56	-8.9	2.4	1.06	0.02	0.57	40.3	165.4	1.8	80.3	1.5	3.8	—	-
811104031	02:09:01	-3.6	0.8	1.15	0.05	0.55	40.3	172.7	1.9	80.1	2.3	3.9	-3.42	C2
811104032	02:12:27	17.0	---	0.94	0.08	0.99	40.3	146.9	0.5	1.1	0.4	3.5	—	C2
811104033	02:18:20	-1.0	0.1	2.03	0.07	0.99	220.3	106.0	0.3	181.2	0.2	4.1	-3.42	C2
811104034	02:32:44	-2.1	0.2	1.46	0.04	0.98	220.3	172.0	0.2	167.2	0.3	3.4	—	C2
811104035	02:36:08	1.9	0.1	0.58	0.01	0.79	220.4	13.8	0.4	244.0	0.6	6.0	-2.34	A
811104036	02:39:59	9.2	1.6	0.89	0.02	0.97	220.4	40.6	0.3	164.4	0.6	4.5	-2.15	C1
811104037	02:41:39	3.4	0.5	0.85	0.02	0.50	40.4	16.1	2.9	94.9	4.1	4.4	—	-
811104038	02:41:54	2.8	0.7	0.90	0.02	0.27	220.4	50.2	2.0	302.4	1.8	5.5	-3.24	A
811104039	02:43:19	-7.9	3.0	1.04	0.03	0.31	220.4	158.9	2.1	290.4	2.6	3.7	-3.21	C2
811104040	02:44:25	1.3	0.2	0.67	0.03	0.44	40.4	143.1	7.7	113.1	9.1	4.0	-3.39	C2
811104041	02:48:20	0.7	0.0	0.54	0.01	0.33	220.4	81.7	1.8	335.5	1.8	5.5	-3.10	A
811104042	02:58:52	1.6	0.1	0.65	0.01	0.57	40.4	15.0	1.7	94.4	3.2	2.7	—	-
811104043	03:00:30	1.6	0.1	0.56	0.02	0.70	220.4	13.2	0.5	258.7	0.7	5.6	-2.10	C1
811104044	03:06:35	2.0	0.2	0.54	0.04	0.91	220.4	74.0	0.9	219.1	3.2	5.3	-3.18	C2
811104045	03:08:13	1.8	0.1	0.77	0.01	0.42	40.4	3.1	1.0	109.0	0.9	4.9	-2.27	C1
811104046	03:09:30	-2.2	0.6	1.45	0.16	0.98	220.4	96.0	1.2	188.9	1.0	4.6	-3.53	C2
811104047	03:10:47	1.8	0.2	0.51	0.05	0.90	220.4	64.4	1.3	224.0	4.6	5.3	-3.09	C1
811104048	03:12:33	5.0	2.3	0.98	0.01	0.10	220.4	59.6	3.7	324.5	3.8	5.0	-3.27	A

TABLE I. Vidicon camera meteors.

I.D. No.	E.S.T.	a	da	e	de	q	Ω	i	di	ω	dω	Mag	log(mass)	Type
811104049	03:17:56	-11.0	3.8	1.09	0.05	0.98	220.4	79.1	0.5	170.6	0.4	4.5	-3.20	C2
811104050	03:19:23	1.1	0.1	0.68	0.01	0.36	220.4	122.2	2.1	304.9	6.2	5.0	-3.46	A
811104051	03:19:55	1.7	0.2	0.43	0.06	0.94	40.4	151.3	1.1	32.6	3.8	3.6	—	-
811104052	03:22:25	-1.0	0.3	1.72	0.31	0.71	40.4	175.8	2.4	56.7	180.9	3.5	—	C2
811104053	03:24:48	-5.4	1.1	1.14	0.04	0.75	40.4	176.9	0.6	302.9	1.2	3.7	-3.35	A
811104054	03:26:55	1.1	0.0	0.35	0.02	0.73	40.4	15.3	2.1	92.4	8.4	5.4	-2.03	C1
811104055	03:27:24	2.3	0.6	0.69	0.05	0.72	40.4	128.8	6.5	71.0	12.0	3.8	-3.35	C2
811104056	03:31:36	-1.5	0.2	1.65	0.12	0.95	220.4	86.3	1.1	200.7	3.6	3.5	-3.33	A
811104057	03:32:27	-0.8	0.1	1.62	0.14	0.53	220.4	150.5	3.4	255.8	3.4	4.5	-4.07	C2
811104058	03:37:24	2.0	0.4	0.68	0.05	0.65	40.4	141.6	2.3	278.9	5.4	3.4	—	-
811104059	03:37:33	-3.4	1.2	1.28	0.16	0.96	220.4	144.4	0.5	199.3	1.2	3.3	-3.55	C2
811104060	03:38:11	0.7	0.0	0.39	0.04	0.46	220.4	18.0	2.2	340.1	3.1	6.2	-2.71	A
811104061	03:41:19	1.5	0.2	0.70	0.03	0.45	220.4	145.6	3.6	71.2	6.7	4.0	—	-
811104062	03:44:02	-8.8	---	1.09	0.54	0.76	220.4	74.7	7.4	236.0	38.0	5.4	-3.43	C2
811104063	03:45:04	1.7	0.1	0.60	0.02	0.66	220.4	6.8	2.1	263.0	2.3	5.4	-2.31	C1
811104064	03:47:15	-41.9	38.2	1.02	0.20	0.97	220.4	94.0	1.8	195.8	1.4	5.3	-3.75	C2
811104065	03:48:07	1.3	0.3	0.35	0.10	0.87	220.4	169.8	2.1	238.3	13.1	3.6	-3.70	C2
811104066	03:50:39	1.7	0.4	0.98	0.05	0.04	220.4	114.8	17.5	340.6	18.1	4.5	-3.33	A
811104067	03:54:30	0.7	0.1	0.52	0.06	0.35	40.4	158.3	4.6	152.9	7.5	4.4	-3.52	C2
811104068	03:58:28	4.9	1.9	0.81	0.05	0.93	40.4	117.6	0.5	330.5	1.2	3.8	-3.26	C2
811104069	04:00:56	-1.2	0.2	1.83	0.18	0.99	220.4	108.0	0.9	177.1	0.5	4.3	-3.67	A
811104070	04:01:06	2.3	1.4	0.67	0.12	0.77	220.4	167.9	2.1	244.3	7.9	4.1	-3.68	A
811104071	04:03:38	1.1	0.2	0.25	0.05	0.81	220.4	164.9	1.0	264.2	20.6	4.3	-3.59	C2
811104072	04:10:22	4.6	3.5	0.80	0.15	0.92	40.4	102.6	4.5	33.6	10.7	4.0	-3.32	C2
811104073	04:20:06	4.5	5.8	0.78	0.40	0.99	40.4	79.0	8.0	355.5	350.8	4.1	-3.20	C2
811104074	04:27:35	-1.7	0.7	1.42	0.28	0.69	220.4	159.6	8.1	240.8	5.7	4.3	-4.00	C2
811104075	04:31:26	0.6	0.0	0.54	0.02	0.29	220.4	12.8	0.9	1.6	0.1	6.1	-2.03	C1
811104076	04:32:56	-4.2	1.7	1.16	0.11	0.66	220.4	155.5	1.6	247.4	3.8	4.6	-3.76	A
811104077	04:38:10	0.7	0.0	0.81	0.01	0.13	220.4	28.7	1.3	338.8	0.4	4.9	-2.32	A
811104078	04:39:52	-1.9	0.3	1.51	0.09	0.94	220.4	135.2	0.9	156.0	1.3	4.1	-3.49	A
811104079	04:48:21	1.1	0.1	0.20	0.03	0.85	220.4	135.7	2.1	98.9	17.4	4.1	-3.24	C2
811104080	04:50:09	18.1	---	0.98	0.03	0.34	220.4	40.5	2.1	239.3	2.1	4.6	-3.02	C1
811104081	04:52:04	6.2	6.7	0.85	0.08	0.91	220.4	178.1	0.6	145.5	1.9	3.8	-3.47	A
811104082	04:52:08	0.7	0.1	0.76	0.05	0.18	220.4	178.6	15.9	333.8	7.6	4.5	-3.47	C2
811104083	04:59:32	1.7	1.0	0.43	0.21	0.99	220.5	115.1	2.3	184.8	2.8	5.0	-3.79	C2
811104084	05:00:36	2.1	0.1	0.69	0.01	0.64	220.5	14.5	0.4	262.1	0.7	5.1	-2.06	C1
811104085	05:04:08	2.6	0.1	0.87	0.01	0.32	40.5	1.4	0.0	116.6	180.5	4.7	-2.32	C1

TABLE II. ISIT camera meteors.

I.D. No.	E.S.T.	a	da	e	de	q	Ω	i	di	ω	dω	Mag	log(mass)	Type
820720001	22:02:28	-1.0	0.2	1.99	0.20	0.98	117.6	105.7	3.4	161.8	4.5	4.7	—	C2
820720002	22:15:03	1.2	0.2	0.38	0.07	0.73	117.6	123.6	5.3	87.5	14.3	4.9	—	-
820720003	22:20:20	-12.0	64.2	1.08	0.18	1.02	117.6	96.4	3.3	180.5	6.8	5.8	—	C2
820720004	22:36:44	3.7	2.4	0.73	0.11	1.01	117.6	60.3	1.8	184.3	0.5	3.4	-2.73	C1
820720005	22:47:22	-2.0	0.7	1.49	0.19	1.01	117.6	91.8	2.1	186.9	3.5	6.1	-4.24	C2
820720006	22:54:55	-4.7	1.1	1.14	0.04	0.65	117.6	155.9	3.0	251.1	3.7	4.8	—	-
820720007	23:00:49	1.7	0.0	0.44	0.01	0.96	117.6	7.5	0.1	146.0	0.2	7.1	-2.19	C1
820720008	23:04:24	3.0	0.7	0.66	0.06	1.01	117.6	25.5	1.1	190.1	1.2	7.7	-3.52	C1
820720009	23:05:31	-13.0	5.1	1.08	0.05	1.02	117.6	36.4	0.6	177.4	0.1	7.2₀	—	C1
820720010	23:06:32	4.1	0.2	0.87	0.01	0.53	297.6	18.3	0.5	92.2	0.8	6.1	-2.88	C1
820720011	23:14:04	1.7	0.0	0.67	0.01	0.55	117.6	11.4	0.3	277.6	0.2	5.7	—	A
820720012	23:20:49	1.1	0.0	0.51	0.02	0.55	117.6	35.3	1.7	290.4	2.0	6.8	-3.38	C1
820720013	23:27:16	2.8	0.2	0.65	0.02	0.98	117.6	22.1	0.5	203.5	0.4	5.3	-2.45	C1
820720014	23:31:36	2.8	0.7	0.67	0.07	0.94	117.7	117.7	1.7	144.1	4.1	5.7	-3.87	C2
820720015	23:32:56	1.2	0.0	0.75	0.01	0.30	297.7	16.1	0.3	130.6	0.3	5.8	—	-
820720016	23:51:40	4.3	3.5	0.78	0.10	0.93	117.7	28.6	1.7	144.1	1.0	7.0	-3.58	C1
820720017	23:52:47	3.3	1.1	0.71	0.08	0.98	117.7	105.9	1.4	156.1	2.7	6.0	—	-
820720018	23:52:54	1.6	0.0	0.34	0.02	1.02	117.7	3.1	0.1	181.1	0.2	6.2	-1.86	C1
820721001	00:00:16	0.9	0.1	0.39	0.04	0.54	117.7	134.2	4.0	48.0	10.5	5.8	-4.00	C2
820721002	00:02:09	39.3	—	0.98	0.06	0.84	117.7	125.3	1.5	229.6	3.6	5.4	-3.95	C2
820721003	00:02:28	2.5	0.1	0.61	0.02	1.00	117.7	25.1	0.3	162.7	0.1	5.2	-2.25	C1
820721004	00:10:05	1.4	0.1	0.73	0.01	0.40	117.7	58.3	0.9	296.7	1.6	6.1	—	-
820721005	00:17:29	1.1	0.0	0.33	0.02	0.72	117.7	136.2	1.6	80.7	5.5	5.3	-3.56	C2
820721006	00:23:14	1.9	0.1	0.62	0.02	0.71	117.7	1.5	3.1	257.2	1.4	7.0	-2.90	A
820721007	00:32:35	1.5	0.1	0.32	0.03	1.02	117.7	34.0	1.0	178.7	0.2	6.7	-2.84	C1
820721008	00:33:17	1.1	0.0	0.95	0.01	0.05	297.7	20.3	6.9	161.4	1.9	5.7	—	A
820721009	00:37:56	0.9	0.0	0.64	0.01	0.32	117.7	25.7	1.0	319.2	0.2	6.4	-2.80	C1
820721010	00:47:36	172.4	---	1.00	0.01	0.29	117.7	60.6	2.2	295.2	3.7	6.0	—	-
820721011	01:01:45	2.0	0.2	0.53	0.05	0.95	117.7	26.7	1.2	216.3	2.3	7.2	-3.08	C1
820721012	01:05:00	1.1	0.1	0.64	0.02	0.39	117.7	135.7	3.1	54.7	4.5	5.7	—	C2
820721013	01:35:34	1.0	0.0	0.75	0.01	0.24	117.7	20.9	1.5	321.3	0.2	6.0	—	C1
820721014	01:38:19	0.9	0.0	0.70	0.04	0.27	117.7	40.6	3.5	320.4	2.2	5.6	—	C1
820721015	01:51:37	0.9	0.0	0.34	0.02	0.58	117.7	67.3	2.2	44.5	6.3	7.1	-3.97	C1
820721016	01:56:16	1.1	0.1	0.81	0.02	0.21	117.7	159.4	4.7	320.6	3.4	5.6	-3.79	C2
820721017	01:56:39	1.0	0.2	0.09	0.09	0.87	297.7	146.4	13.8	135.6	123.1	5.6	—	C2

TABLE II. ISIT camera meteors.

I.D. No.	E.S.T.	a	da	e	de	q	Ω	i	di	ω	dω	Mag	log(mass)	Type
820721018	01:57:33	1.5	0.2	0.45	0.05	0.81	117.7	111.4	1.5	111.1	6.1	4.7	-3.71	C2
820721019	02:00:25	2.9	0.1	0.65	0.01	1.01	117.7	24.2	0.2	192.1	0.1	6.0	-2.32	C1
820721020	02:02:40	-1.0	0.1	2.04	0.16	1.00	117.8	140.0	2.4	190.7	2.4	5.3	-4.35	C2
820721021	02:08:48	0.8	0.0	0.79	0.02	0.18	117.8	40.8	2.5	330.6	0.9	5.8	-3.23	A
820721022	02:10:56	0.9	0.0	0.67	0.06	0.29	117.8	45.2	3.8	322.5	3.2	6.5	-3.44	A
820721023	02:14:27	-3.0	0.4	1.29	0.05	0.85	117.8	149.4	1.5	134.8	1.4	3.7	—	-
820721024	02:16:37	2.7	0.9	0.62	0.09	1.00	117.8	51.9	1.9	195.6	1.2	6.6	—	C1
820721025	02:17:29	13.3	—	0.93	0.14	0.93	117.8	113.8	1.5	144.9	3.4	6.4	-4.35	C2
820721026	02:28:27	2.7	1.2	0.80	0.05	0.53	117.8	139.0	2.7	274.0	7.2	5.9	-4.31	A
820721027	02:30:53	1.6	0.0	0.40	0.01	0.94	297.8	2.9	0.5	43.6	1.0	3.6	—	-
820721028	02:31:47	1.5	0.2	0.34	0.09	0.97	117.8	152.7	5.2	146.7	7.6	5.1	-3.82	C2
820721029	02:35:36	-31.2	21.6	1.03	0.06	1.01	117.8	155.9	0.9	175.1	0.9	6.2	-3.62	C2
820721030	02:35:56	1.7	0.4	0.44	0.10	0.97	117.8	131.7	2.5	212.5	8.3	6.2	-4.30	A
820723001	22:38:56	5.6	1.6	1.00	0.00	0.03	120.5	41.1	8.4	342.1	1.8	5.9	-3.90	A
820723002	22:46:46	1.7	0.1	0.49	0.02	0.65	120.5	12.3	0.8	239.3	0.4	6.5	-2.59	C1
820723003	22:50:28	1.7	0.0	0.62	0.01	0.65	120.5	9.7	0.4	266.9	0.2	5.1	—	-
820723004	22:57:47	2.2	0.1	0.92	0.00	0.17	120.5	25.4	0.9	317.0	0.2	5.8	—	-
820723005	23:16:09	2.0	0.2	0.98	0.00	0.03	300.5	5.9	3.8	162.6	181.0	6.0	—	-
820723006	23:22:47	4.6	2.4	0.79	0.08	0.95	120.5	110.9	1.3	149.1	2.5	6.1	-3.73	C2
820723007	23:24:27	2.1	0.2	0.78	0.02	0.47	120.5	14.5	0.8	283.3	0.2	5.1	—	A
820723008	23:27:12	3.9	11.4	0.74	0.19	1.01	120.5	33.6	3.2	170.8	0.4	7.5	-3.71	C1
820723009	23:31:43	3.1	0.3	0.68	0.02	1.01	120.5	22.0	0.4	166.8	0.1	5.3	—	-
820724001	00:11:21	-1.6	0.2	1.61	0.03	0.99	120.5	109.6	0.9	163.7	1.6	3.2	—	C2
820724002	00:31:07	0.9	0.0	0.22	0.01	0.71	120.6	17.8	0.7	314.5	0.8	5.4	-2.33	A
820724003	00:40:06	-1.4	0.3	1.72	0.18	0.99	120.6	86.0	1.3	162.4	2.6	6.3	—	A
820724004	00:43:44	2.9	0.3	0.79	0.02	0.62	300.6	11.6	2.6	82.8	3.0	6.5	—	A
820724005	00:44:36	-0.7	0.1	2.34	0.17	1.00	120.6	112.4	1.2	167.4	1.4	4.7	-4.34	C2
820724006	00:47:34	1.7	0.2	0.98	0.00	0.03	120.6	4.4	19.4	342.2	1.0	6.1	—	-
820724007	01:02:25	8.1	12.0	0.87	0.08	1.01	120.6	113.6	0.8	174.8	1.2	6.0	-4.01	C2
820724008	01:02:51	-0.8	0.1	1.72	0.20	0.61	120.6	96.6	1.9	248.4	9.4	6.1	—	-
820724009	01:04:17	1.0	0.1	0.44	0.07	0.57	120.6	70.0	3.6	295.5	14.2	7.0	-3.98	A
820724010	01:08:18	2.7	0.1	0.63	0.01	1.00	120.6	5.8	0.1	197.2	0.1	6.9	-2.14	C1
820724011	01:13:22	3.4	0.4	0.77	0.03	0.78	120.6	29.5	1.4	241.5	2.1	6.6	-3.02	C1
820724012	01:15:02	-1.7	0.3	1.61	0.15	1.01	120.6	132.6	1.4	188.8	1.6	5.7	-4.33	A
820724013	01:31:31	0.8	0.1	0.55	0.06	0.37	120.6	116.9	5.9	38.1	10.6	5.5	—	C2

TABLE II. ISIT camera meteors.

I.D. No.	E.S.T.	a	da	e	de	q	Ω	i	di	ω	dω	Mag	log(mass)	Type
820724014	01:38:39	1.9	0.1	0.48	0.03	1.01	120.6	20.8	0.7	189.8	1.3	7.0	-2.71	C1
820724015	01:43:56	1.0	0.1	0.08	0.10	0.92	300.6	155.0	9.5	253.9	45.8	5.0	—	C2
820724016	01:46:47	0.7	0.0	0.54	0.07	0.32	120.6	75.9	2.6	339.9	2.2	7.2	-3.81	A
820724017	01:48:42	0.8	0.0	0.49	0.03	0.39	300.6	166.6	4.0	151.8	4.2	5.6	—	-
820724018	01:50:45	-1.3	0.1	1.58	0.04	0.78	120.6	143.0	1.0	128.1	0.9	3.3	—	-
820724019	02:09:20	8.0	1.4	0.90	0.02	0.84	120.6	15.0	0.8	230.9	1.0	3.5	—	-
820724020	02:09:29	1.3	0.0	0.67	0.01	0.44	300.6	14.1	0.3	114.1	0.3	6.0	—	A
820724021	02:09:42	2.3	0.1	0.56	0.01	1.01	120.6	12.6	0.2	170.6	0.2	6.8	—	C1
820724022	02:11:48	11.7	—	0.92	0.08	0.93	120.6	103.6	0.9	213.5	2.3	6.0	-3.89	C2
820724023	02:18:18	1.9	0.8	0.54	0.13	0.90	120.6	143.5	9.6	228.1	22.7	5.9	—	-
820724024	02:28:27	1.7	0.3	0.51	0.07	0.82	120.6	138.9	2.3	114.7	7.2	5.8	-4.13	C2
820724025	02:30:13	5.2	1.6	0.81	0.04	0.97	120.6	164.5	2.5	207.1	3.2	4.8	-3.77	C2
820724026	02:37:44	7.4	4.9	0.89	0.05	0.84	300.6	161.4	2.1	51.0	2.0	5.3	—	-
820724027	02:39:51	1.5	0.3	0.32	0.13	1.00	120.6	48.8	3.3	200.2	6.3	7.3	-3.79	C1
820724028	02:42:39	2.0	0.1	0.55	0.02	0.90	120.6	34.0	0.5	225.6	0.9	6.7	—	A
820724029	02:45:42	1.1	0.1	0.18	0.04	0.90	120.6	117.9	2.0	256.3	22.7	5.3	-3.84	C2
820724030	02:59:08	1.9	0.1	0.47	0.02	1.01	120.7	1.9	0.1	191.8	0.2	6.7	—	-
820724031	02:59:24	6.6	7.8	0.88	0.11	0.76	300.7	155.8	9.3	62.3	4.8	5.1	—	C2
820724032	03:02:26	1.6	0.2	0.85	0.01	0.24	120.7	132.6	3.2	48.4	3.3	5.6	-3.74	C2
820724033	03:03:05	0.9	0.0	0.39	0.03	0.53	120.7	29.0	3.1	314.9	3.0	7.2	-3.23	C1
820724034	22:46:35	0.9	0.1	0.26	0.04	0.67	121.4	65.0	2.3	309.2	12.4	6.9	-3.66	C1
820724035	23:00:42	2.9	0.5	0.67	0.06	0.97	121.4	16.5	1.6	208.4	2.4	7.2	-2.93	C1
820724036	23:03:18	9.9	—	0.92	0.14	0.82	121.5	65.9	2.8	127.3	8.4	6.5	-3.76	C2
820724037	23:10:14	2.9	0.3	0.79	0.02	0.61	121.5	18.2	1.3	264.5	0.6	6.4	-3.05	A
820724038	23:17:43	4.0	0.4	0.76	0.03	0.95	121.5	6.5	1.6	211.8	1.6	3.1	—	C1
820724039	23:19:26	1.3	0.1	0.21	0.07	1.00	121.5	140.1	3.2	156.5	11.3	5.6	-4.16	C2
820724040	23:26:33	1.7	0.1	0.41	0.03	1.01	121.5	14.8	0.7	169.7	0.3	7.6	-2.74	A
820724041	23:42:38	2.8	0.1	0.71	0.01	0.82	121.5	22.9	0.3	122.3	0.2	6.7	—	C1
820724042	23:46:58	2.2	0.1	0.54	0.02	1.01	121.5	17.8	0.3	174.2	0.2	7.0	-2.44	C1
820725001	00:06:52	-1.0	0.1	1.96	0.07	0.98	121.5	94.2	0.4	161.2	0.6	4.0	-3.48	C2
820725002	00:16:15	3.6	0.5	0.99	0.00	0.03	121.5	32.1	8.2	341.4	1.1	5.8	—	-
820725003	00:16:15	5.1	1.2	0.89	0.02	0.56	121.5	31.0	1.2	267.8	1.0	6.6	—	-
820725004	00:19:15	0.9	0.0	0.75	0.02	0.23	301.5	6.5	1.8	142.8	1.1	6.4	—	C1
820725005	00:27:15	146.5	—	1.00	0.00	0.02	121.5	76.2	14.0	345.1	2.8	5.9	—	A
820725006	00:28:39	12.8	8.1	1.00	0.00	0.03	121.5	48.2	6.6	339.6	1.8	5.4	—	-

TABLE II. ISIT camera meteors.

I.D. No.	E.S.T.	a	da	e	de	q	Ω	i	di	ω	dω	Mag	log(mass)	Type
820725007	00:31:16	0.7	0.0	0.39	0.01	0.45	301.5	5.6	0.2	179.1	0.2	7.4	-2.03	C1
820725008	00:31:58	3.1	0.6	0.76	0.04	0.74	121.5	42.2	1.0	248.6	1.1	7.5	-3.68	A
820725009	00:36:37	-0.4	0.0	2.83	0.06	0.81	121.5	25.8	0.9	137.0	0.2	6.0	—	-
820725010	01:00:58	1.2	0.2	0.17	0.10	0.99	121.5	50.6	3.9	212.0	12.8	7.5	-3.68	C1
820725011	01:21:03	0.8	0.0	0.42	0.03	0.48	301.5	160.2	2.7	140.7	7.1	5.2	—	C2
820725012	01:23:10	2.6	1.4	0.62	0.13	1.01	121.5	79.4	2.0	175.6	1.6	6.8	-4.07	A
820725013	01:28:45	1.3	0.4	0.48	0.12	0.69	121.5	65.1	5.0	269.6	25.2	5.9	—	-
820725014	01:42:41	0.8	0.1	0.91	0.04	0.07	121.6	7.3	33.2	342.2	1.7	6.7	—	-
820725015	01:44:37	2.9	0.7	0.66	0.07	1.00	121.6	135.4	1.1	163.8	1.7	2.4	—	-
820725016	01:56:03	-14.0	7.3	1.07	0.07	1.00	121.6	138.4	1.0	195.2	1.4	5.9	-4.04	C2
820725017	01:56:42	-3.3	1.1	1.23	0.11	0.75	121.6	124.5	1.7	121.9	3.3	4.0	—	-
820725018	02:05:32	3.2	2.3	0.71	0.13	0.95	121.6	124.9	3.3	213.3	8.4	5.5	—	-
820725019	02:09:34	0.7	0.0	0.67	0.05	0.22	121.6	22.9	5.2	345.0	0.6	7.1	-3.09	C1
820725020	02:26:41	2.0	0.3	0.49	0.07	1.00	121.6	39.6	1.7	195.0	2.3	6.3	-3.14	C1
820725021	02:40:48	8.1	6.3	0.91	0.04	0.71	121.6	144.2	1.5	112.1	2.3	5.1	-3.76	C2
820725022	02:44:44	0.7	0.0	0.43	0.04	0.40	121.6	7.0	3.0	355.4	2.5	7.0	-2.23	A
820725023	02:54:50	-0.5	0.1	3.03	0.37	0.98	121.6	114.6	1.7	162.9	2.0	4.9	—	C2
820811001	23:02:32	1.4	0.1	0.29	0.04	0.99	138.7	39.3	1.5	151.4	2.7	7.5	-3.51	A
820811002	23:11:14	-26.1	—	1.04	0.13	1.01	138.7	13.2	2.7	175.1	3.6	6.6	—	C1
820811003	23:11:27	2.9	0.4	0.66	0.05	0.98	138.7	26.7	0.9	204.0	0.5	6.9	-2.80	C1
820811004	23:20:49	5.1	3.5	0.81	0.08	0.98	138.7	42.9	1.4	201.0	0.6	5.9	-2.99	C1
820811005	23:31:05	-395.8	605.9	1.00	0.08	0.96	138.7	109.8	1.3	152.7	2.2	5.5	-3.95	C2
820811006	23:31:55	1.0	0.0	0.08	0.00	0.90	138.7	21.1	0.9	65.2	4.6	7.8	-2.49	C1
820811007	23:38:08	2.7	0.2	0.62	0.02	1.00	138.7	30.3	0.5	196.3	0.2	6.2	-2.66	C1
820811008	23:53:00	23.2	—	0.99	0.03	0.26	138.7	27.7	11.1	299.9	3.9	6.2	—	-
820811009	23:54:47	7.6	3.2	0.94	0.02	0.44	138.7	27.3	1.5	279.7	0.5	5.9	—	C1
820811010	23:57:12	-2.8	0.7	1.35	0.12	0.96	138.7	120.3	2.2	155.6	4.2	5.6	—	C2
820812001	00:03:32	1.5	0.1	0.75	0.01	0.38	318.7	17.8	2.0	117.5	3.4	6.1	—	-
820812002	00:12:08	2.2	2.5	0.69	0.18	0.68	138.7	135.0	12.3	101.2	17.8	5.1	—	C2
820812003	00:16:25	-2.2	0.5	1.19	0.06	0.44	138.7	82.9	2.1	272.5	8.9	2.9	—	A
820812004	00:19:04	2.3	0.2	0.60	0.03	0.89	138.7	111.7	1.0	133.1	2.9	3.6	-2.98	C2
820812005	00:22:17	0.9	0.0	0.42	0.02	0.53	138.7	111.5	1.6	50.3	5.0	4.0	-3.28	C2
820812006	00:28:16	2.6	0.2	0.63	0.02	0.97	138.7	26.5	0.5	208.4	0.5	6.6	—	C1
820812007	00:33:32	2.7	0.2	0.67	0.02	0.89	138.7	24.2	0.5	225.8	0.5	6.3	—	A
820812008	00:38:48	10.3	5.1	0.93	0.03	0.70	138.7	18.1	2.4	249.4	1.8	5.5	—	C1

TABLE II. ISIT camera meteors.

I.D. No.	E.S.T.	a	da	e	de	q	Ω	i	di	ω	dω	Mag	log(mass)	Type
820812009	00:42:08	0.8	0.0	0.42	0.01	0.48	138.7	2.6	0.6	320.9	0.8	6.8	-2.36	A
820812010	00:44:26	0.8	0.0	0.51	0.01	0.41	318.7	1.7	0.5	139.6	181.3	7.0	-2.54	A
820812011	00:58:33	0.7	0.0	0.93	0.05	0.05	138.8	129.5	16.0	12.3	4.8	5.4	-3.46	C2
820812012	01:06:03	-1.3	0.6	1.76	0.31	1.01	318.8	139.1	10.6	356.1	8.7	4.6	—	A
820812013	01:07:15	0.7	0.0	1.00	0.00	0.00	318.8	97.3	24.6	182.5	181.0	4.9	-3.16	C1
820812014	01:12:44	3.1	1.3	0.71	0.09	0.90	138.8	112.6	2.0	137.3	6.2	5.3	—	C2
820812015	01:13:33	2.3	0.5	0.99	0.01	0.03	138.8	27.6	20.2	343.8	3.8	4.9	—	A
820812016	01:14:00	1.0	0.0	0.02	0.00	0.98	318.8	1.3	0.0	331.1	168.9	5.9	—	C1
820812017	01:16:24	2.2	0.3	0.94	0.01	0.14	318.8	31.1	4.5	141.1	5.0	3.0	—	A
820812018	01:29:34	5.4	2.9	0.83	0.06	0.92	138.8	139.9	1.6	142.4	2.5	4.6	—	C2
820812019	01:41:19	-1.5	0.1	1.47	0.05	0.69	138.8	32.8	1.3	117.3	0.6	5.5	—	-
820812020	01:45:27	1.8	0.2	0.45	0.05	0.99	138.8	47.6	1.4	201.1	1.2	6.7	-3.41	C1
820812021	01:50:48	3.4	0.9	0.97	0.01	0.09	138.8	57.3	7.5	327.3	4.8	5.3	—	A
820812022	01:52:53	1.5	0.9	0.62	0.17	0.56	138.8	111.0	10.1	80.7	22.3	5.5	—	C2
820812023	01:53:20	-3.2	1.5	1.27	0.22	0.86	138.8	106.5	2.2	223.5	5.4	6.6	-4.48	C2
820812024	01:54:32	-37.8	---	1.01	0.06	0.32	318.8	134.6	16.4	111.3	7.4	5.4	—	C2
820812025	01:57:28	1.1	0.0	0.35	0.01	0.68	138.8	110.3	1.1	74.9	6.1	3.8	-3.14	C2
820812026	02:03:14	0.7	0.0	0.36	0.02	0.45	138.8	35.4	4.2	5.6	1.9	6.9	-3.26	C1
820812027	02:06:48	2.6	0.5	0.62	0.06	1.00	138.8	57.3	1.2	197.6	0.9	6.8	-3.56	C1
820812028	02:08:22	2.4	0.4	0.61	0.05	0.93	138.8	121.6	0.7	141.9	2.4	5.2	-3.73	C2
820812029	02:22:09	-7.0	3.1	1.14	0.10	0.96	138.8	116.0	0.7	154.4	1.4	5.9	-4.07	C2
820812030	02:30:20	-2.5	0.8	1.38	0.17	0.97	138.8	116.2	1.6	158.8	2.0	4.5	-4.02	C2
820812031	02:34:02	-1.2	0.1	1.82	0.11	0.99	138.8	150.8	1.4	163.7	1.2	5.6	-4.32	A
820812032	02:35:54	2.4	0.3	0.93	0.01	0.16	138.8	43.5	3.4	42.3	3.2	5.8	—	-
820812033	02:38:13	-3.2	0.8	1.31	0.10	1.00	318.8	174.2	1.4	346.5	1.2	5.0	—	-
820812034	02:42:11	3.2	2.6	0.72	0.13	0.90	138.8	113.3	1.7	137.2	4.8	5.4	-3.93	C2
820812035	02:43:49	5.2	---	0.82	0.22	0.93	138.8	113.0	2.9	144.1	6.1	4.3	—	-
820812036	02:50:59	0.9	0.1	0.09	0.06	0.84	138.8	66.5	2.9	7.6	16.5	7.4	-3.74	C1
820812037	02:54:29	3.5	1.4	0.76	0.07	0.83	138.8	116.2	1.2	125.3	3.5	5.0	-3.72	C2
820812038	03:02:06	-8.1	4.1	1.12	0.12	1.00	138.8	168.5	2.3	169.8	1.6	5.5	-4.27	A
820812039	03:09:42	9.1	13.7	0.90	0.06	0.92	138.8	113.4	0.8	144.5	1.8	3.8	-3.33	C2
820812040	03:14:28	2.2	1.1	0.58	0.14	0.91	138.8	108.6	1.9	136.1	6.4	6.1	-4.18	C2

YYMMDDNNN where Y signifies year, M month, D day and N the number that day;

E.S.T. Eastern standard time in hours, minutes seconds;

a Semi-major axis (A.U.);

da Probable error in a;

e Eccentricity;

de Probable error in e;

q Perihelion distance (A.U.);

Ω Ascending Node (°);

i Inclination of the orbit (°);

di Probable error in i;

ω Argument of perihelion (°);

dω Probable error in ω;

Mag The absolute magnitude of the meteor;

log (mass) The logarithm to the base 10 of the pre-atmospheric mass of the meteoroid in grams;

Type Tentative classification according to Ceplecha's (1958) scheme.

The errors listed in Tabs I and II were obtained as follows: the differences introduced by the likely errors in right ascension, declination and geocentric velocity were calculated separately and the total error in each of the elements was then calculated by finding the standard deviation from the sum of the variances.

We have listed neither the errors in perihelion distance nor in ascending node in Tabs I and II since these were so small. Occasionally the measurement errors were such as to render the sign of the semi-major axis uncertain and in such cases we have left the entry for the error in this quantity blank.

Of all the errors in the orbital elements, probably that in the estimate of the semi-major axis is of the greatest interest because some of the meteors appear to have hyperbolic orbits. The uncertainty in the semi-major axis arises mainly from our estimates of the likely error in the meteoroid velocity. Because the image of the meteor on the TV frame is not a point but a short comet-shaped object there is some arbitrariness about how the position of the meteor should be measured. It is difficult to measure the brightest point because of effect of system noise on the measurement of such a diffuse image. Even the sharpest feature of the image, namely the leading edge, is not very sharp and we considered our measurements of its position to be accurate to about 3 pixels along the line of the meteor motion although they were usually good to about one pixel or better perpendicular to this line.

It was distinct impression that the apparent velocity of some meteors fluctuated as though the meteoroid were fragmenting or had already fragmented. In such cases the image did not seem to move uniformly on the monitor screen from frame to frame. It is possible that this was some effect of electronic noise in the system but whatever the cause it had the effect

that sometimes the probable uncertainty in the velocity obtained from the end points of the trail was underestimated.

Through this analysis we have considered our measurement errors in right ascension, declination and geocentric meteor velocity to be uncorrelated. This is almost certainly not the case but to incorporate these correlations would have complicated the analysis enormously and to do justice to the extra work involved we would have to list not only the variances in the elements but the cross-variances as well. We did not consider this to be warranted but prefer to suggest that the entries listed in Tabs I and II be taken as representative rather than absolute.

3. Cosmic Weights

As remarked earlier this survey does not constitute a random sample so that the observed distributions of orbital elements are likely to present a distorted view of the actual distributions. To minimize this as far as possible we have adopted the system of weights used by Jacchia and Whipple (1961) to obtain the weighted distributions of elements discussed later. The weighting function, CW which is given by the formula

$$\mathrm{CW} = V_g \sin(i)\,(2 - 1/a - p)^{1/2}/V_\infty^4 ,$$

in which

$$p = a(1 - e^2) .$$

is composed of two factors. The first account of the dependence of mass on velocity for a given luminosity, the mass distribution of meteoroids and the velocity dependence of the photographic technique (Whipple, 1954) while the second involves the probability of meteoroids in a given orbit colliding with the Earth (Öpik, 1951). We acknowledge that the first effect may be slightly different for television methods of observing but since the effect of the weighting turned out to be quite small in most cases it seems unlikely that it is sensitive to such fine details.

4. Orbital Element Frequency Distributions

a) *Semi-Major Axis*

Both the observed and weighted fraquency distributions of $1/a$ which are shown in Fig. 1 are very similar to those found for photographic and radar meteors. Our data confirm the trend reported by Lebedinec (1968) that the short period tail of the distribution

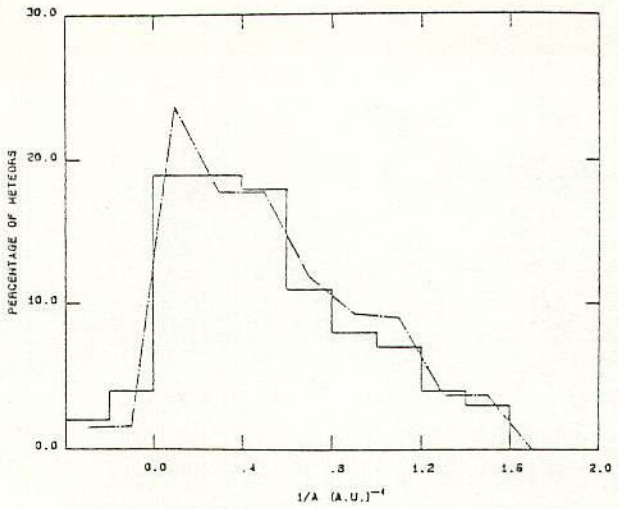

Fig. 1. Distribution of semi-major axes. Solid line — observed, dashed line — weighted.

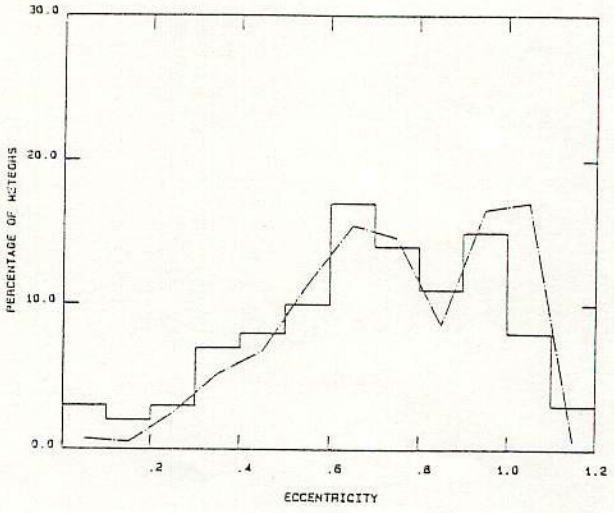

Fig. 2, Distribution of eccentricities. Solid line — observed, dashed line — weighted.

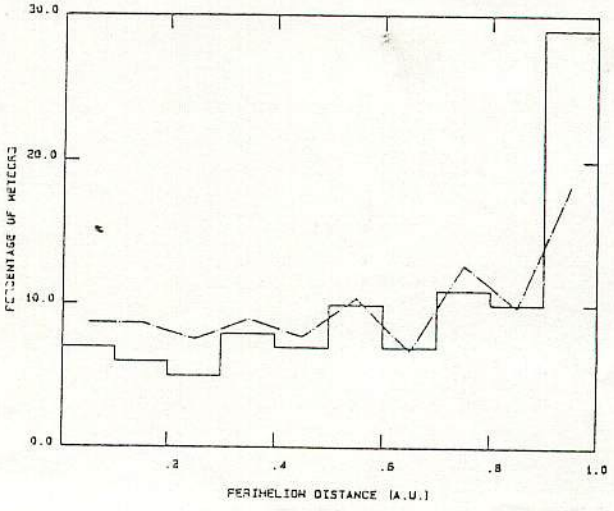

Fig. 3. Distribution of perihelion distances. Solid line — observed, dashed line — weighted.

becomes more pronounced for fainter meteors. This is possibly a result of the Poynting-Robertson effect but it could also be caused by the diffusion of the distribution as the result of inter-particle collisions.

Another feature which may not be significant is the occurrence of the peak of the $1/a$ distribution close to $1/a = 0{\cdot}2$ A.U. whereas for photographic and radar meteors this is usually found near $1/a = 0{\cdot}4$ A.U. This may be the result of the sample size coupled with the fact that, by their very nature the position of maxima are quite sensitive to "noise".

b) *Eccentricity*

Figure 2 shows the distribution of eccentricities of the TV meteor orbits. As before the observed and weighted distributions are very similar. Previous photographic and radar surveys have produced an essentially single peaked distribution with the maximum just below $e = 1{\cdot}0$. The TV meteors are markedly different in this respect displaying a bimodal distribution with an "extra" peak close to $e = 0{\cdot}7$. As yet we have investigated this in any detail but feel that it may be the result of non-random sampling or it may be associated with asteroidal type meteor orbits (see Section 5e).

c) *Perihelion Distances*

Perihelion distance is a quantity which can be calculated very precisely and so we might expect observational errors to be less effective in obscuring the true distribution than with the other orbital elements. Figure 3 shows the observed and weighted distribution of the ~~eccentricity.~~ perihelion As might be expected the distribution of the TV meteors is very similar to that obtained from the Super-Schmidt data with the exception that the sharp peak close to $q = 0{\cdot}1$ A.U. in the photographic data is absent. The radar data (Lebedinec, 1968) lead to very different distributions of perihelion distance and it seems likely that this may be the result of the masking effect of the "underdense ceiling" discussed by McKinley (1961).

d) *Inclinations*

It is in the distribution of orbital inclinations where the weighting function has its greatest effect. While it is clear that the formula will be unreliable at very small inclinations, Öpik (1951) has shown it to be accurate to better than 10 percent for $i > 0{\cdot}3°$. The distribution of the inclinations of the TV meteor orbits which is shown in Fig. 4 is very similar to that of the Super-Schmidt meteors with the possible exception of a minor peak close to $i = 70°$ which may be due to the non-random sampling. There also seem to slightly more retrograde orbits among the TV meteors than for the photographic meteors.

5. Two Dimensional Orbital Distributions

In this section we consider the correlations between pairs of orbital elements. Since it is very easy to present an observation as a point on a diagram but

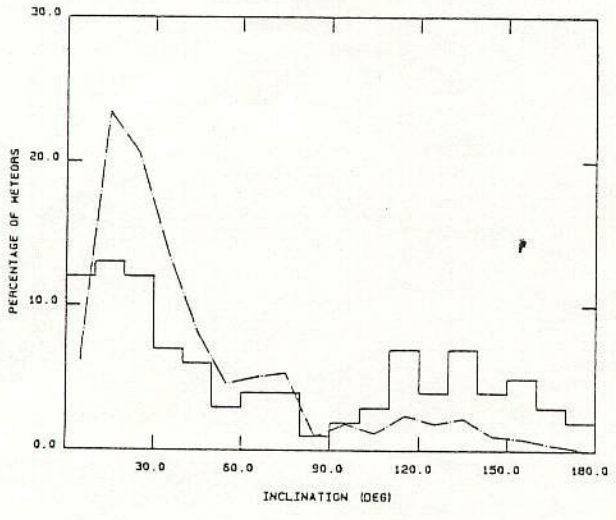

Fig. 4. Distribution of inclinations. Solids line — observed, dashed line — weighted.

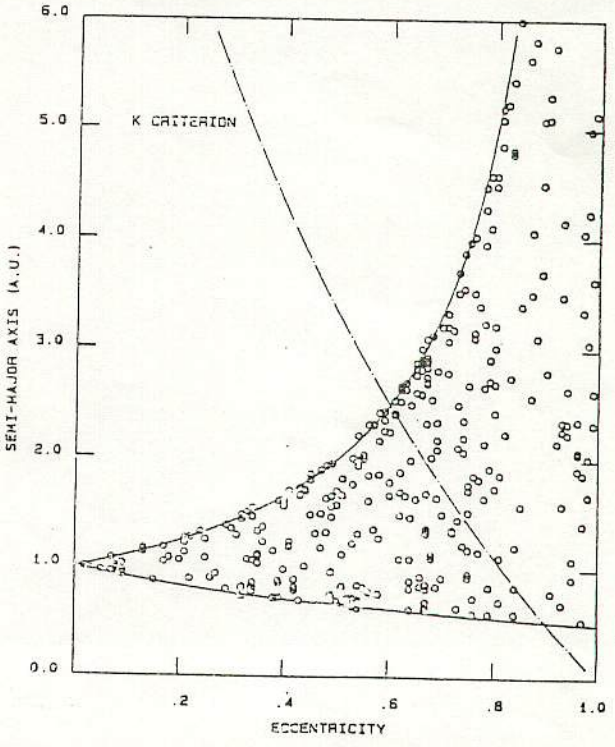

Fig. 5. Distribution of TV meteor orbits in semi-major axis and eccentricity.

much more difficult to display the cosmic weight assigned to that observation, we have presented only the observed distributions. We trust that this will give a fairly reliable representation of the distributions since the effects of the weighting seem to be small in Figs 1 to 4.

a) *Semi-Major Axis Versus Eccentricity*

Figure 5 shows the distribution of orbits in semi-major axis and eccentricity. The points necessarily fall inside the area for which

$$a(1 - e) < 1 < a(1 + e) .$$

A similar plot for Super-Schmidt meteors has been presented by Kresák (1967) which differs markedly from Fig. 5. Whereas the TV meteors are distributed fairly randomly over the allowed area, the photographic meteors cluster close to the upper bound in a for $0{\cdot}6 < e < 0{\cdot}8$. This clustering is also visible in the TV meteor data but on a much reduced scale. Kresák (1967) has identified two groups in this densely populated region: the asteroidal type of orbit which have e close to 0·6 and those with orbits similar to those of short-period comets (e close to 0·75). The asteroidal group is immediately evident in Fig. 5 and while the cometary group is difficult to discern. It therefore seems that the TV meteor population is either deficient in particles in these cometary orbits or that the cometary grouping is so diffuse as to go unnoticed.

Whipple (1954) defined an empirical criterion K given by

$$K = \log [a(1 + e)/(1 - e)] - 1 ,$$

which he found to be very effective for distinguishing between the orbits of comets and asteroids. Jacchia and Whipple (1961) found that 25 percent of their Super-Schmidt meteors were identified as being "asteroidal" on the basis of the K criterion. We have icluded a line corresponding to the K criterion in Fig. 5 — those points above the line are assigned cometary orbits while those below it are interpreted as being asteroidal according to this scheme. The K criterion divides the TV meteors about equally into the two classes but not into any obvious grouping and so does not seem to have much value in this size range as an indicator of meteoroid type.

The above discussion does not mean that most of the meteoroids are not of cometary origin but rather that their orbits have been so perturbed that they are difficult to recognize as such from their orbital elements. Kresák (1968) has also shown that the Poynting-Robertson effect causes the points to migrate to the bottom left hand corner of the $a-e$ diagram and so we might expect the points corresponding to the smaller TV meteors to be much more diffusely distributed than those associated with the larger photographic meteors. We might also expect a greater proportion of the smaller meteoroids to be products of collisions between larger meteoroids and this too will cause a diffuse distribution of points on the $a-e$ diagram.

b) *Perihelion Distance Versus Inclination*

The plots of perihelion distance versus inclination are shown in Fig. 6. As might be expected geometric selection results in high concentrations of meteors with large perihelion distances and also with low

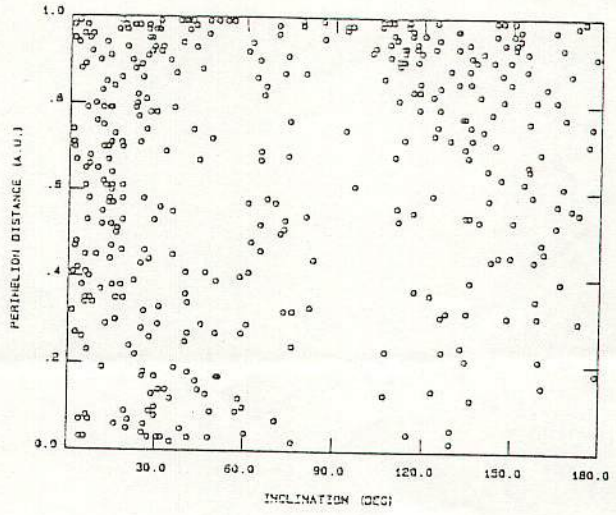

Fig. 6. Distribution of TV meteor orbits in perihelion distance and inclination.

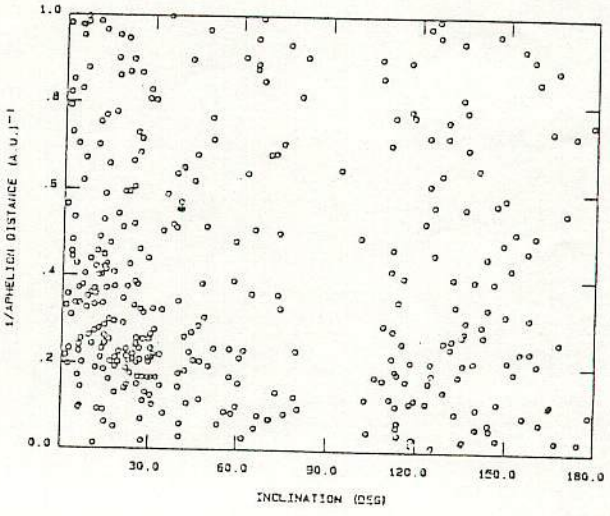

Fig. 7. Distribution of TV meteor orbits in aphelion distance and inclination.

inclination. There are no obvious gaps in the population except for orbits with inclinations close to 90° which probably results from the lack of comets in such orbits. Although there are few orbits with very small perihelia the proportion is more than for the Super-Schmidt meteors. It would appear that if the heat of the Sun is the cause of the paucity of photographic meteors in such orbits then possibly a plentiful source of TV meteors exists to make up for those lost to the heat of the Sun. Although solar heating must cause the loss of some particles, the density of particles should increase as we approach the Sun as the result of the Poynting-Robertson effect and this may to some extent make up for the losses of these very small particles.

c) *Aphelion Distance Versus Inclination*

It should be noted that the aphelion distance is not a well-determined quantity. Figure 7 shows the distribution of aphelion distance with inclination. This is to be compared with a similar plot by Jacchia and Whipple (1961). The two diagrams are very different, probably the most obvious feature being the much more uniform distribution of the TV meteors, although it should be remembered that observational selection results in a bias in favour of retrograde orbits (see Fig. 4). Like the Super-Schmidt data, the TV meteors show a high concentration of aphelia close to 2·0 A.U. The reason for this is not clear though we doubt that it is a result of perturbations by Mars. In strong contrast to the photographic data are many TV meteors with retrograde orbits with aphelia greater than 3·0 A.U. The absence of such orbits in the Super-Schmidt data was attributed to Jovian perturbations (Jacchia and Whipple, 1961) and if this is the case then a powerful source of TV meteors is required to balance the loss as in section c above.

d) *Semi-Major Axis Versus Inclination*

According to Whipple (1948), bright meteors have either near ecliptic asteroidal type orbits with relatively short periods or randomly inclined orbits with long periods. Figure 8 shows the distribution of TV meteor orbits in $1/a$ and inclination. Both of Whipple's groups of orbits are clearly visible with the "asteroidal" group containing orbits with $i < 30°$ and $a < 10$ A.U. as was found for the bright meteors but the overall appearance is that the cometary group embraces the whole range of inclinations i.e. near ecliptic orbits do not seem to be excluded from the cometary group.

e) *Eccentricity Versus Inclination*

In order to get some clue as to what the explanation of the double hump in Fig. 2 might be we have plotted the distribution of eccentricity versus inclination in Fig. 9. The peak close to $e = 1$ seems to be due to meteors with randomly distributed inclinations while the peak close to $e = 0{\cdot}6$ appears to be associated with meteors with near ecliptic (asteroidal) orbits.

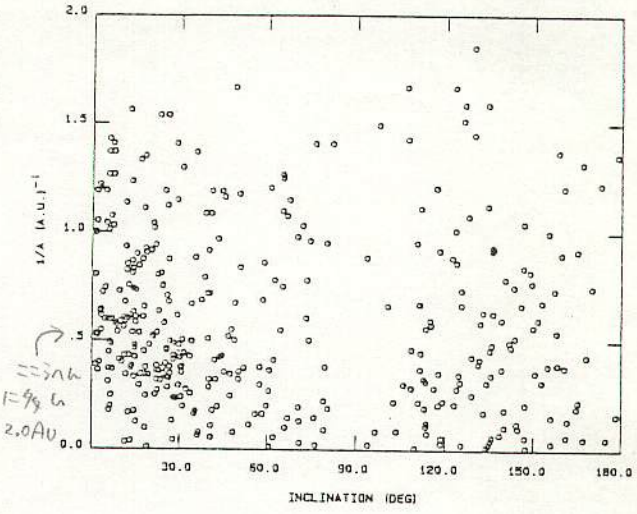

Fig. 8. Distribution of TV meteor orbits in semi-major axis and inclination.

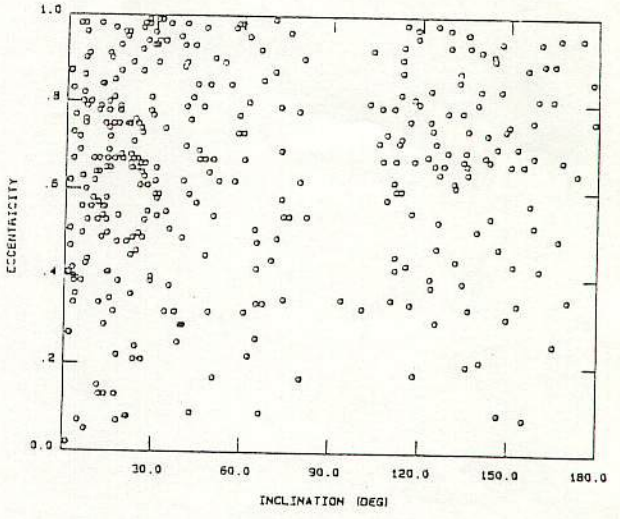

Fig. 9. Distribution of TV meteor orbits in eccentricity and inclination.

6. Hyperbolic Orbits

Of the present T.V. meteor orbits, 19 percent are hyperbolic. Undoubtedly most of these are probably elliptical orbits which appear to be hyperbolic as the result of observational error. It is interesting to see

how our data compares with the photographic survey of McCrosky and Posen (1961) which contained almost 13 percent hyperbolic meteors while that of Babadzahnov and Kramer (1967) contained almost 15 percent. If percentage of hyperbolic meteors is a measure observational accuracy, our TV meteors are not very much less precise than the photographic surveys. But for at least 8 of the TV meteors measurement errors do not seem large enough to account for the high value of the eccentricity. These "interstellar" meteors constitute almost 2 percent of our survey and this fraction is in good agreement with Öpik's (1958) value of 3 percent for visual meteors. The more recent work of McCrosky and Posen (1961) and of Babadzahnov and Kramer (1967) also contain a number of meteors with hyperbolic orbits but unfortunately we cannot asses their statistical significance since the probable errors in the orbital elements are not available. At least one meteorite, the Pultusk (Galle, 1868) had a well observed hyperbolic orbit.

In our sample we estimate that about 26 orbits are hyperbolic on the basis of 95 percent confidence limits. We have examined the original data for each of these and reject all but 8 because of uncertainties arising from difficulties in the velocities as mentioned in Section 2. These are listed in Tab. III below. There still remains the possibility that correlations between the errors, as mentioned in Section 2, would shorten this list even more.

Table III

List of hyperbolic meteors

Meteor number	Geocentric velocity (km/s)
810 730 003	67·9
810 924 007	31·3
811 104 057	74·5
820 720 001	65·6
820 721 020	76·3
820 724 018	72·3
820 725 009	43·3
820 812 031	76·6

It has often been remarked that if hyperbolic meteors are real then some should appear at geocentric velocities much less than the upper limit of 72 km/s. As can be seen from Tab. 2 at least 2 of our meteors fulfill this requirement. It is interesting to note that such slow yet hyperbolic meteors are found in the surveys of both Babadzahnhov and Kramer (1967) and McCrosky and Posen (1961). Observational selection would tend to enhance the observed rate of high velocity hyperbolic meteors, so that the observed proportion of slow hyperbolic meteors of 25 percent is not implausible.

The origin of these "interstellar" meteors – whether they really are particles from interstellar space or whether they are members of the solar system dust complex which have been shifted by planetary perturbations or knocked by collisions into these unbound orbits is not clear. But is does look as though Öpik's view may be correct that a small yet significant component of the sporadic meteor population may have these highly eccentric orbits.

Acknowledgments

This work was funded by a grant from the National Sciences and Engineering Research Council of Canada and also by an Academic Development Award from the University of Western Ontario. The authors gratefully acknowledge the help of Dr. Z. Ceplecha and Dr. I. Halliday for providing copies of their orbit calculation programs.

REFERENCES

Babadzahnov, P. B.; Kramer, E. N.: 1967, Smithson. Contr. Astrophys. **11**, 67.
Ceplecha, Z.: 1958, Bull. Astron. Inst. Czechosl. **9**, 54.
Galle, J. C.: 1868. Abhandl. Schles. Ges. f. vaterl. Kultur. Ableitung f. Naturwiss.
Hawkes, R. L.; Jones, J.; Ceplecha, Z.: 1984, Bull. Astron. Inst. Czechosl. **35**, 46.
Jacchia, L. G.; Whipple, F. L.: 1961, Smithson. Contr. Astrophys. **4**, 97.
Jacchia, L. G.; Verniani, F.; Briggs, R. E.: 1967, Smithson. Contr. Astrophys. **10**, 1.
Kresák, L.: 1967, Smithson. Contr. Astrophys. **11**, 9.
—: 1968, IAU Symp. 33, 391.
Lebedinec, V. N.: 1968; IAU Symp. 33, 241.
McCrosky, R. E.; Posen, A.: 1961, Smithson. Contr. Astrophys. **4**, 15.
McKinley, D. W.: 1961, in Meteor Science and Engineering (McGraw-Hill, New York), p. 204.
Öpik, E.: 1951, Proc. Roy. Irish Acad. 54 A, 165.
—: 1958, Contr. Armagh Obs. (No 26), 1.
Sarma, T.; Jones, J.: 1984, Bull. Astron. Inst. Czechosl. **36**, 9.
Whipple, F. L.: 1948, Astron. J. 54, 53.
—: 1954, Astron. J. 59. 210.

DOUBLE-STATION OBSERVATIONS OF 454 TV METEORS

III. *Populations*

J. Jones[1]), T. Sarma[1]), Z. Ceplecha[2])

1) *Department of Physics, University of Western Ontario, London, Canada. N6A 3K7*
2) *Astronomical Institute, Czechoslovak Academy of Sciences, 251 65 Ondřejov, Czechoslovakia*

Received 11 June 1984

НАБЛЮДЕНИЯ 454 ТЕЛЕВИЗИОННЫХ МЕТЕОРОВ С ДВУХ СТАНЦИЙ

III. *Составляющие населения*

В статье описываются результаты анализа населений, основанного на высотах точек появления 454 телевизионных метеоров, наблюдавшихся с двух станций. Присутствуют оба уровня A и C, ранее замеченные в данных Супер-Шмидтов и подтверждается существование группы C3, о которой предварительно сообщалось в малом обзоре телевизионных метеоров. Для C, или более высокого из двух уровней представляется основным механизмом отдачи тепла излучение, в то время как для нижнего уровня представляется более важным тепловой провод во внутрь метеорного тела. Свойства материала частиц верхнего уровня определяются с трудом, и эти метеорные тела могут быть как пористыми, так и камнеобразными, если они малые. С другой стороны сравнение теории и наблюдений ведет к требованию, чтобы метеорные тела A состояли из плотного материала с довольно высокой теплопроводностью, как камни. Обсуждается происхождение группы C3 и вероятное объяснение усматривается в зависимости от массы выбрасывания пыли из кометы родоначальницы.

This paper describes the results of a population analysis based on the beginning heights of 454 doubly observed TV meteors. Both the A and C levels previously seen in the Super-Schmidt data are present and the existence of the C3 group previously reported in a small TV meteor survey is confirmed. For the C or higher of the two levels radiation cooling appears to be the dominant heat loss mechanism while for the lower level thermal conduction into the interior of the meteoroid seem to be more important. The material properties of the particles in the upper level are difficult to determine and these meteoroids may be either porous or stony provided they are small. On the other hand comparison of theory and observation seems to demand that the A meteoroids be of a dense material with a fairly high thermal conductivity such as stone. The origin of the C3 group is discussed and a probable explanation is seen in the mass dependence of the ejection of dust from the parent comet.

1. Introduction

This paper constitutes the third in a series which has already dealt with the trajectories (Sarma and Jones, 1985) and orbits (Jones and Sarma, 1985) of 454 doubly observed TV meteors. The main impetus for this work came from a previous study (Hawkes, Jones and Ceplecha, 1984) which examined the populations and orbits of a relatively small number (84) of TV meteors which confirmed the existence among such faint meteors of the discrete level structure first discovered by Ceplecha (1958) and Jacchia (1958).

A particularly interesting parameter of the meteor trajectory is the beginning height because its interpretation is not complicated by the subsequent evaporation as is the height of maximum luminosity and the ending height. Depending on the meteoroid size this beginning height is determined either by radiation cooling for small bodies or by thermal diffusion limited conduction for large bodies which leads to

$$\varrho_B \doteq v_\infty^n \tag{1.1}$$

where ϱ_B is the air density at the onset of evaporation and v_∞ is the velocity of the meteoroid outside the atmosphere and $n = -3{\cdot}0$ for small meteoroids or $n = -2{\cdot}5$ for large meteoroids. (Hawkes et al., 1984).

Of course the actual situation may be complicated by the fact that some meteoroids may have already disintegrated into a cluster of much smaller particles before the onset of evaporation as has been suggested by Hawkes and Jones (1975). Nevertheless, it is a fact that the beginning heights of photographic meteors do conform to this simple model with $n = -2{\cdot}5$ as was found by Ceplecha (1967). Perhaps Ceplecha's most interesting finding was that there are two distinct levels separated by about 10 km for the onset of luminosity for photographic meteors and it was natural

Bull. Astron. Inst. Czechosl. 36 (1985), 116–122.

to suppose that this separation was the consequence of two populations of meteoroid of different density. Those associated with the higher level Ceplecha called 'C' meteors and those with the lower level 'A' meteors. In addition to this he also identified a small intermediate B group. Even within the two main levels subgroups were found to exist – the major division being in the C meteors which were found to be either C1 with short-period ecliptically inclined orbits or C2 which had long-period randomly inclined orbits. Ceplecha also found a large number of subgroups among the short-period ecliptically inclined A meteors.

It is understandable that the interpretation of these findings met with some criticism (Verniani, 1967) although the facts themselves are beyond question and confirmation of this structure in the beginning height was sought in the radio meteor data. Unfortunately no significant structure was seen (see for example Sekanina, 1978) and the matter was dropped until taken up again by Hawkes, Jones and Ceplecha (1984) with the study of TV meteors. Not only did they confirm the photographic results but they also found a new C3 group of meteors with short-period randomly inclined orbits. By this time it had become clear that the failure of the radar meteor method to detect the structure in the beginning heights was due in large measure to the severe observational selection effect of the so-called "under-dense" ceiling which has been discussed in detail by McKinley (1961).

The previous TV meteor sample was very small and the present paper describes the population analysis of 454 TV meteors which are not only on average 3 magnitudes fainter but are also considerably more accurate. The observational details are given in Sarma and Jones (1985) and Jones and Sarma (1985).

2. Discrete Levels of Beginning Heights

Since the scale height of the atmosphere varies considerably in the meteor region we prefer to work in terms of atmospheric density rather than height and Figure 1 shows a plot of beginning air densities versus v_∞ together with the lines corresponding to the A and C levels found in the photographic meteor data. The C line agrees remarkably well with the cluster of points at the top of the diagram and there seems to be a grouping of points round the A line though the concentration is less marked, containing mostly medium and high velocity meteors in contrast to the photographic meteors which exhibited a high concentration close to $v_\infty = 17$ km/s. Nonetheless, considering that the lines were obtained from the Super-Schmidt photographic data the agreement is noteworthy.

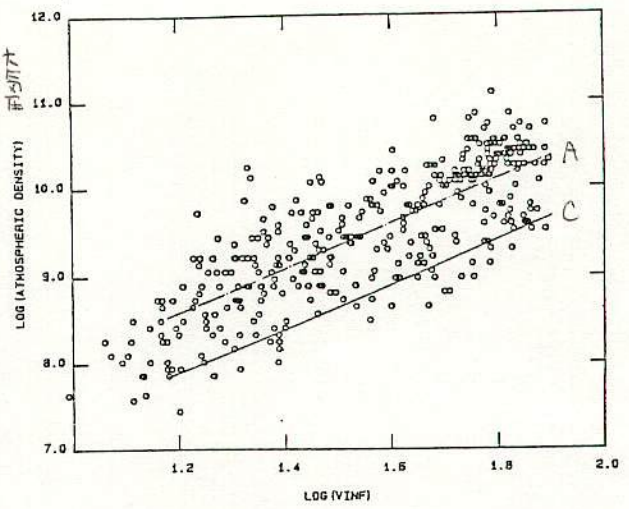

Fig. 1. Comparison of the atmospheric density at onset of luminosity of TV meteors with the Super-Schmidt A and C levels.

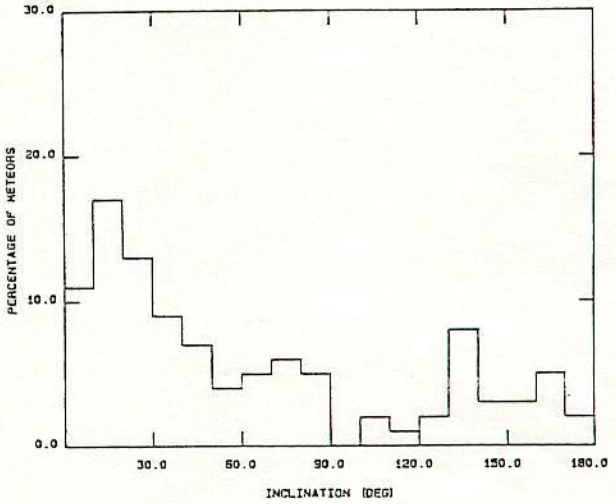

Fig. 2. Histogram of the orbital inclinations for the A meteors.

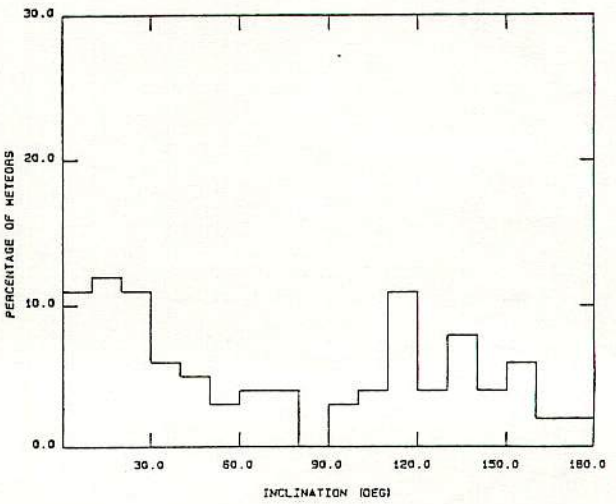

Fig. 3. Histogram of the orbital inclinations for the C meteors.

The absence of a high proportion of low velocity meteors confirms the findings of the earlier TV meteor study of Hawkes, Jones and Ceplecha (1984) who concluded that the deficiency is either real or the result of radiation cooling suppressing evaporation of the meteoric material. If real, it is possibly caused by the mass distribution index of these meteors being somewhat less than that of the rest of the meteoroid population.

In plotting Fig. 1 we have made no adjustments for the zenith angle of the meteor trajectory or mass because we judged these negligible in an earlier paper (Sarma and Jones, 1985).

On the basis of Fig. 1 we have classified our meteors according to Ceplecha's (1968) scheme and the classifications are listed in the appropriate tables presented by Sarma and Jones (1985) and Jones and Sarma (1985).

3. Inclinations

In Figs 2 and 3 we show the inclination (i) distributions of both the A and the C meteors. These are evidently similar to the corresponding distributions for the Super-Schmidt meteors (Ceplecha, 1967) in that few A meteors have retrograde orbits while among the C meteors there is both a large ecliptical component (C1, $i < 50°$) and a significant fraction with randomly inclined orbits (C2, $i > 50°$).

4. Semi-Major Axis Distributions

In Figs 4, 5 and 6 we present histograms of the reciprocal semi-major axis $(1/a)$ for the A, C1 and C2 groups. As for the Super-Schmidt meteors, the A and C1 groups have essentially short-period orbits but in the case of the C2 group the TV meteors differ markedly from the brighter photographic meteors. Whereas the Super-Schmidt C2 meteors all have long period orbits, the TV C2 meteors have in addition a considerable number of short-period orbits as is apparent from the long tail of the $1/a$ distribution show in Fig. 6. These are undoubtedly the same C3 meteors reported by Hawkes, Jones and Ceplecha (1984) although the shape of the distribution is different.

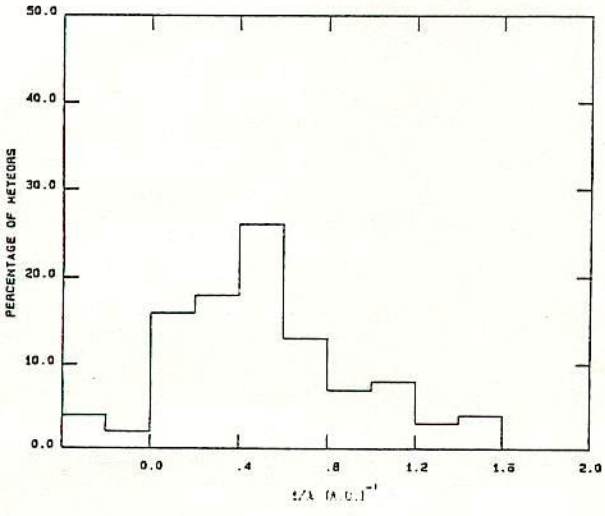

Fig. 4. Distribution of the orbital semi-major axes for the A meteors.

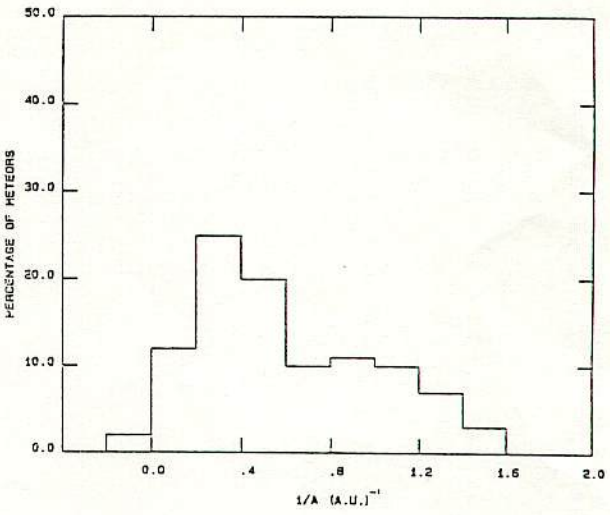

Fig. 5. Distribution of the orbital semi-major axes for the C meteors ($i < 50°$).

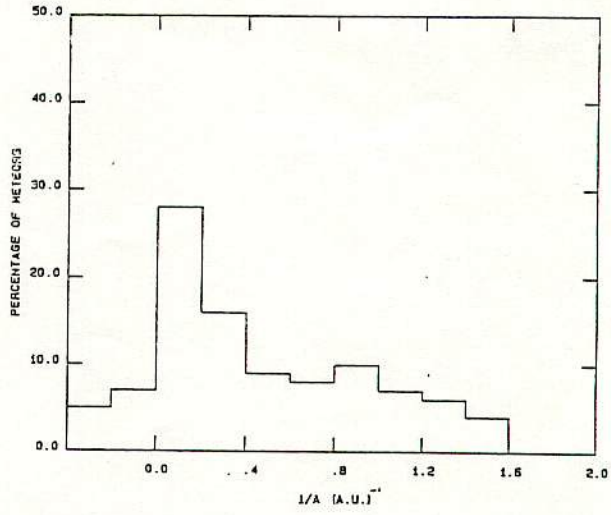

Fig. 6. Distribution of the orbital semi-major axes for the C meteors ($i > 50°$).

The bimodal distribution reported in the earlier paper was much more sensitive to sampling errors and because of inferior resolution the earlier system was less sensitive to fast moving meteors.

5. Semi-Major Axis — Perihelion Distance Distributions

Having presented the orbital size and inclination characteristics of the various groups we now wish to show the correlation of orbital size with perihelion distance among the groups. We feel this is best done by means of two-dimensional plots of perihelion distance (q) versus $1/a$. There are of course many other possible representations which convey essentially the same information but of those we have tried the $q - 1/a$ plot seems best suited to our purpose. These plots are given in Figs 7, 8 and 9 together with lines denoting the evolutionary paths of orbits decaying as a result of the Poynting-Robertson (PR) effect (this will be discussed in detail later).

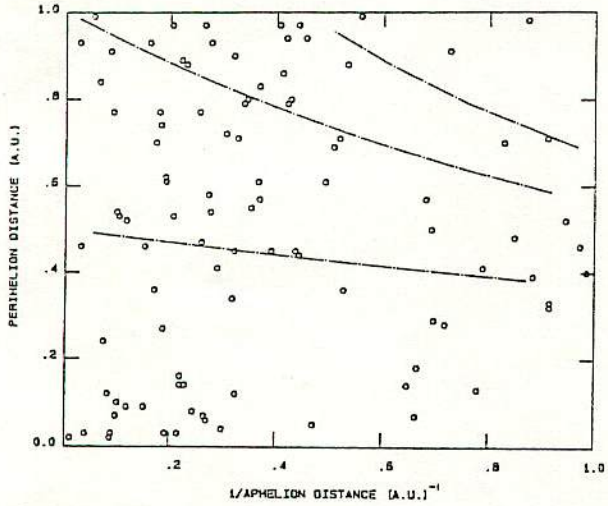

Fig. 7. Distribution of orbits in perihelion distances and semi-major axis for A meteors. The lines denote the evolutionary path of orbits decaying as a result of the Poynting-Robertson effect.

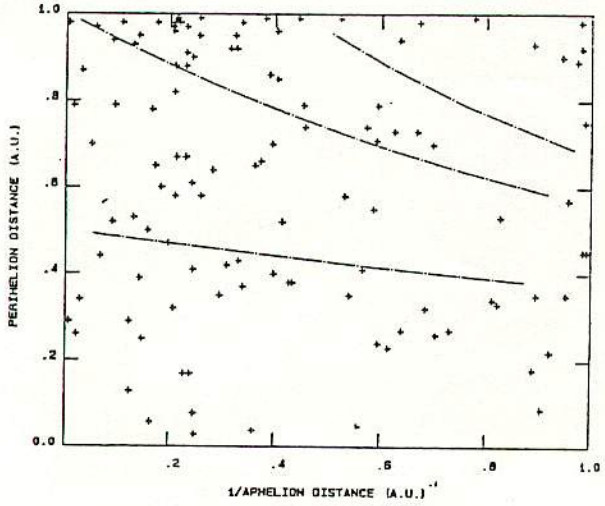

Fig. 8. Distribution of orbits in perihelion distance and semi-major axis for C meteors ($i < 50°$). The lines denote the evolutionary path of orbits decaying as a result of the Poynting-Robertson effect.

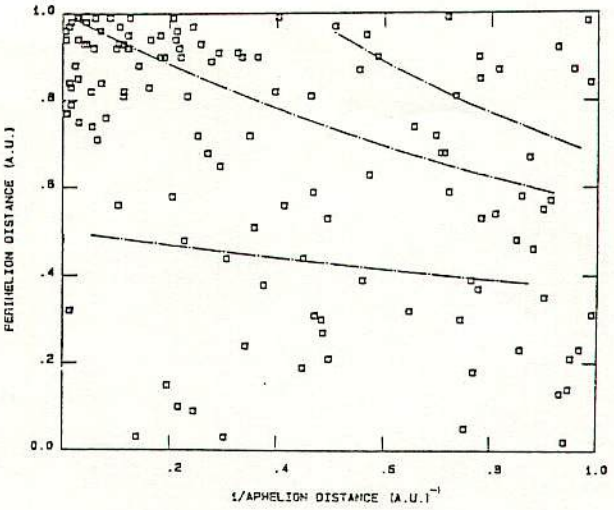

Fig. 9. Distribution of orbits in perihelion distance and semi-major axis for C meteors ($i > 50°$). The lines denote the evolutionary path of orbits decaying as a result of the Poynting-Robertson effect.

Perhaps the most evident feature of Figs 7 and 8 is their similarity and for TV meteors it would be difficult, if not impossible, to distinguish A from C1 meteors on the basis of their orbital parameters. Both groups contain meteors with eclipticaly inclined orbits and only on the average are the A meteor orbits somewhat smaller than those of C1 meteors.

In addition to their similarity, the two distributions are rather featureless, there being no significant concentrations of points anywhere on the diagrams which we might take as exemplifying that particular group. The situation for the randomly inclined component of the C group shown in Fig. 9 is quite different. The strong concentration of points in the top left hand corner of the diagram is very conspicuous and indicates that the core of the randomly inclined C group has very long-period orbits $(a > 5$ A.U.) which are observed close to their perihelion passage. It was this core that Ceplecha (1967) identified as C2 meteors and indeed almost all the randomly inclined photographic meteors belong to this group. As well as this long-period component Hawkes, Jones and Ceplecha (1984) discovered a short-period fraction among TV meteors and the present observations confirm this. This C3 group is seen in Fig. 9 as the diffusely distributed points which occupy the region $a > 5$ A.U. and which appear to be more or less uniformly scattered in perihelion distance.

6. Comparison with the Theory of Starting Heights

For very small bodies the surface area to mass ratio provides for efficient cooling by radiation. For larger bodies the thermal capacity of the meteoroids

becomes important but the transfer of heat into the interior is usually limited by thermal diffusion which has the effect that only the surface layer of the meteoroid experiences a substantial rise in temperature. The thickness of the surface layer is determined by the time constants of the energy flow and is proportional to v_∞. The net result of these two processes is that for very small bodies $n = -3$ while for large bodies $n = -2{,}5$ in equation (1.1). The energy balance prior to the onset of evaporation can easily be described by a differential equation whose solution is most conveniently obtained by numerical integration. An Appendix due to Ceplecha (Hawkes et al., 1984) describes the results of such calculations for a range of meteoroid sizes, densities and velocities. Of most interest to us are the limiting solutions for very small porous bodies (radiation cooling limited) and very large stone bodies (thermal conduction limited).

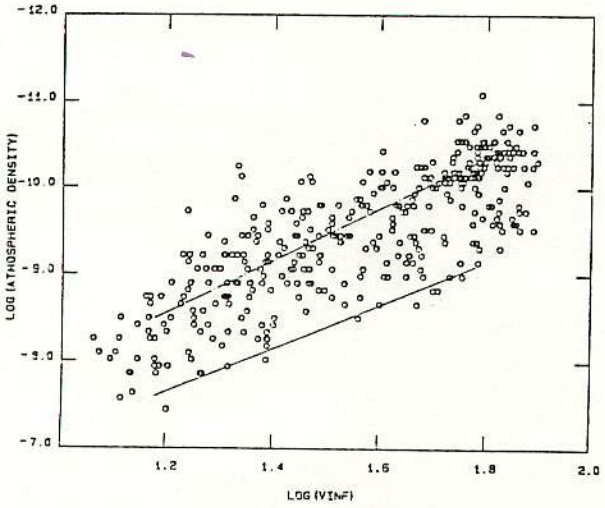

Fig. 10. Comparison of atmospheric density at onset of luminosity of TV meteors with theoretical predictions:
——— thermal condution limited,
—·—·— radiation cooling limited.

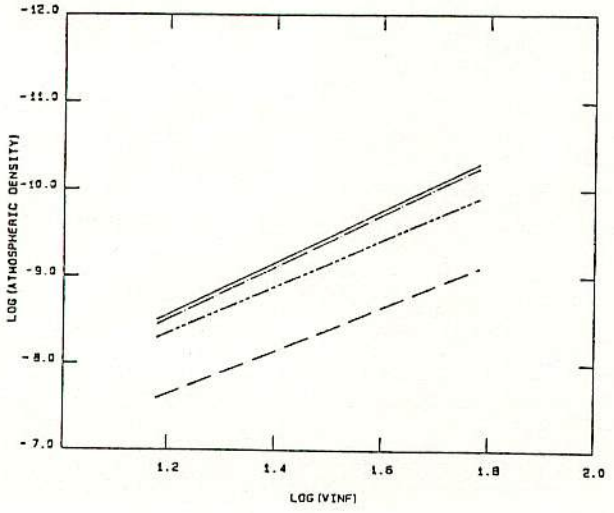

Fig. 11. Theoretical predictions for several meteoroid parameters:
——— stone, $r = 0.01$ cm.
—·—·— porous, $r = 0.01$ cm.
—··—··— porous, $r = 10$ cm.
— — — stone, $r = 10$ cm.

In Fig. 10 we show how these limiting values compare with our observational results for the starting heights. The clustering of the C meteors about the upper theoretical line in Fig. 10 cannot be overlooked while the lower line forms a convincing lower bound to the observed points.

It is also interesting to note that the numerical calculation also predicts that the starting height becomes independent of zenith angle for small meteoroids thus confirming our observational finding mentioned in Section 2. This comes about because the zenith distance does not appear in the heat balance equation when radiation cooling is the only heat loss mechanism.

Figure 11 shows some of the numerical predictions for the beginning height for both large and small, porous and stony bodies. It is clear that it is almost impossible to distinguish between very small stone and porous bodies on the basis of starting heights. The only way of achieving the observed spread in starting heights seems to be having stone particles as large as 0·3 cm. The inescapable conclusion follows that the starting heights show such a large spread because a considerable fraction of them (the A meteors) are stony particles in the size range 0·01 cm up to at least 0·3 cm. The C meteors may be either of stony or porous structure but if of stone then they are probably of radius less than 0·01 cm. On the other hand if they are porous then there is little restriction on their size, since their thermal conductivity is so low that significant transfer of heat into the body of the meteoroid is not possible and radiation cooling is the dominant heat loss mechanism even for large porous meteoroids.

It is a problem to explain how single particle of the same average mass could give rise to such a large scatter in starting heights. The present discussion does not exclude Ceplecha's original suggestion that the A meteors are stone while the C meteors are porous which is clearly quite consistent with Fig. 11. Much of the opposition to Ceplecha's (1967) paper seems to result from the notion that A meteors are of asteroidal origin, whereas in fact they are asteroidal only in as much that they behave like stone particles and have asteroidal-like orbits. While their origin is still a matter of debate, their resemblance to stone is well established and the problem is to explain how such

particles might have a cometary origin. Hawkes and Jones (1975) have proposed a meteoroid model which provides an attractive alternative explanation. According to this model, the meteoroid is a composite body of grains held together by a low boiling point "glue" which releases the grains when the temperature becomes high enough. The glue of meteoroids in very short-period orbits will evaporate or sublime as the result of solar heating thus releasing single particle stone meteoroids in interplanetary space. The orbits of photographic A meteoroids are significantly smaller than those of the C group but for TV meteors there is little difference. Even so these meteoroids might all start off as C1 meteoroids but change to the A group as the individual stony particles become detached from the original composite meteoroids because of the sublimation with age of the adhesive material. On the other hand, the composite meteoroids will release the grains only after they have been sufficiently heated in the Earth's atmosphere and the starting heights of such meteors will be determined by the smallest grains which we expect to be limited by radiation cooling.

7. The Evolution of the C3 Meteoroid Group

While most of the findings of the present study confirm the Super-Schmidt and previous TV meteor studies, our observations of the diffuse component of the short period fraction of the randomly inclined group do shed new light on the C3 group which was recently discovered by Hawkes, Jones and Ceplecha (1984). In their discussion they concluded that the histories of the C2 and C3 meteors must be intimately linked and they suggested two possible mechanisms for the production of C3 type orbits: 1) that C3 orbits are a consequence of the decay of C2 type orbits as a result of the PR effect or 2) that the mass dependence of the ejection velocity of the dust particles from the parent comets must cause the diffuseness of their orbits to increase with decreasing particle size. We will deal with each of these suggestions in turn.

According to Wyatt and Whipple (1950) the semi-major axis and eccentricity of an orbit under the influence of the PR effect are related by the equation

$$(7.1) \qquad e^{0.8}/[a(1-e^2)] = C$$

where C is a constant of motion determined by the initial conditions. It is therefore possible to calculate lines corresponding to fixed values of C on the $q - 1/a$ diagram such as those shown in Figs 7, 8 and 9.

In Fig. 9 the task is to explain how the diffuse distribution of points which are scattered almost uniformly over the diagram for $a > 5$ could have evolved from the dense cluster of points at the top left hand corner. It is very clear that the PR effect was not the agency since many C3 meteors fall outside the allowed evolutionary paths. It might be argued that observational selection might distort the distribution of points in Fig. 9 and although this is certainly true such distortion would only multiply the actual distribution by some two-dimensional function and could not generate those C3 meteors falling outside the allowed PR evolutionary paths. We must therefore reject the PR mechanism as the primary source of C3 meteoroids.

Since the C3 orbits are not the product of the PR decay of C2 orbits we are led to the conclusion that these two groups may share a common origin and that the orbital differences are simply a consequence of the process of ejection of dust from the comet. It is reasonable to suppose that the original cometary orbits were very similar to those of the C2 meteors, i.e. with $10 < a < \infty$ and perihelia close to 1 AU. We can calculate what ejection velocity is needed to explain the observed spread d in semi-major axis assuming the dust to be ejected at perihelion using the equation

$$(7.2) \qquad d(1/a) \doteq 2\mathbf{V}_c \,.\, \mathbf{V}_P/V_C^2$$

where V_C is 29·7 km/s, $\mathbf{V}_C$ is the heliocentric velocity of the comet and $\mathbf{V}_P$ is the ejection velocity of the dust particle relative to the comet. For long-period comets $|V_C| \doteq 42$ km/s and from Fig. 6 we see that $d(1/a) \doteq$ $\doteq 0.6$ AU which corresponds to $|V_P| \doteq 6$ km/s.

According to Whipple (1951) the value of V_P for a particle of radius r_m (cm) ejected from a comet of radius R_C(km) is given by

$$(7.3) \quad V_P = \left(\frac{1{\cdot}07 \times 10^5 R_C}{nT^{9/4}\varrho_m r_m} - 5594R_C^2\right)^{1/2} \quad [\mathrm{cm/s}]$$

where ϱ_m is the density of the particle (g/cm^3), r is the comet-Sun distance (AU) and $1/n$ is the fraction of incident solar energy used for sublimation of the cometary ices. With $R_C = 1$ km, $r = 1$ AU, $r_m = 0{\cdot}01$ cm and $\varrho_m = 1$ g/cm^3 we find $V_P \doteq 32$ m/s.

Whipple's model which is based on the continuous sublimation of the cometary ices such that the dust particles are accelerated by the escaping gases is obviously inadequate to explain the short-period tail of the $1/a$ distribution of the C2/C3 meteors by at least two orders of magnitude. But it is possible that the fault lies not with the mechanism but rather with the simplicity of Whipple's model. The work of Fox et al. (1983) supports the idea that the actual

ejection velocities are probably at least an order of magnitude greater than those predicted by Whipple's model since the duration of the Geminid shower is about 10 times as long as they predicted using Whipple's model. Whether such a factor is appropriate to other comets is uncertain but the possibility exists that since the Geminid stream is not representative, more typical comets may eject their dust faster than predicted by Whipple's model by even greater factors.

The reason for the possible failure of the Whipple's model to predict the high speed of dust ejection could be that the mechanism of dust release is much more complicated than envisioned by Whipple. Perhaps instead of being shed continuously, the dust is blown off in small explosions as the pressure of trapped gases becomes great enough to rupture the surface layer of the comet. The difficulty with this proposal is that since the material properties of the cometary surface are so unknown it is impossible at this stage to make any quantitative predictions about the likely ejection velocities and we will probably have to rely on observational data to fill this gap.

The idea that the C3 meteors result from velocity perturbations of C2 meteors as they pass close to perihelion prompts us consider whether any processes other than the escape of cometary gases could produce such perturbations. The main difficulty is to get velocity changes of the order of a few kilometres per second and it would seem that something quite violent is required. One such process is interparticle collisions. Because the relative energy in a collision is so great, the smaller of the colliding particles is always annihilated. If the larger survives the collision it is eroded somewhat and proceeds with little change in velocity since the mean velocity of the ejecta is likely to be only of the order of 0·1 km/s (Gault et al., 1963). It should be noted that the laboratory ejecta data refer strictly only to basalt targets but we consider the possibility of much greater velocities applying to meteoric material is remote. We must therefore reject the collisions as a means of converting C2 into C3 type orbits.

Acknowledgment

We wish to thank the National Sciences and Engineering Research Council of Canada for the grant which supported this work.

REFERENCES

Ceplecha, Z.: 1958, Bull. Astron. Inst. Czechosl. 9, 54.
—: 1967, Smithson. Contrib. Astrophys. 11, 35.
—: 1968, Smithson. Astrophys. Obs. spec. rept. 279.
Fox, K.; Williams, I. P.; Hughes, D. W.: 1983, Monthly Notices Roy. Astron. Soc. 205, 1155.
Gault, D. E.; Shoemaker, E. M.; Moore, H. J.: 1963, NASA TND 1967.
Hawkes, R. L.; Jones, J.: 1975. Monthly Notices Roy. Astron. Soc. 173, 339.
Hawkes, R. L.; Jones, J.; Ceplecha, Z.: 1984, Bull. Astron. Inst. Czechosl. 35, 46.
Jacchia, L. G.: 1958 Smithson. Contr. Astrophys. 2, 181.
Jones, J.; Sarma, T.: 1985, Bull. Astron. Inst. Czechosl. 36, 103.
McKinley, D. W. R.: 1961, in Meteor Science and Engineering (McGraw-Hill, New York).
Sarma, T.; Jones, J.: 1985, Bull. Astron. Inst. Czechosl. 36, 9.
Sekanina, Z.: 1978, Icarus 27, 265.
Verniani, F.: 1967, Smithson. Contr. Astrophys. 11, 61.
Whipple, F. L.: 1951, Astrophys. J. 113, 464.
Wyatt, S. P., Whipple, F. L.: 1950, Astrophys. J. 111, 134.

STUDIES ON SOME ASPECTS OF THE SOLAR Hα FLARES OF DIFFERENT VISUAL FEATURES

T. Chakravorti*), T. K. Das*), M. K. Das Gupta

Centre of Advanced Study in Radio Physics & Electronics, 92, Achsrya Prafulla Chandra Road, Calcutta-700009, India

Received 10 November 1984

ИССЛЕДОВАНИЕ НЕКОТОРЫХ АСПЕКТОВ СОЛНЕЧНЫХ ВСПЫШЕК В Hα С РАЗЛИЧНЫМИ ВИЗУАЛЬНЫМИ СВОЙСТВАМИ

Солнечные вспышки в Hα с различными визуальными свойствами анализировались с учетом их общих характеристик, связи с радиовсплесками и солнечными пятнами. Важными результатами полученными при исследовании являются: (I) среди разных типов T и A типы имеют соответственно наибольший

*) Narasimha Dutt College, 129 Belilios Road, Howrah, India.

DOUBLE-STATION OBSERVATIONS OF 454 TV METEORS

III. *Populations*

1987. 4/9
43rd M.S.S.
文献紹介
大西 洋

J. Jones[1]), T. Sarma[1]), Z. Ceplecha[2])

1) *Department of Physics, University of Western Ontario, London, Canada. N6A 3K7*
2) *Astronomical Institute, Czechoslovak Academy of Sciences, 251 65 Ondřejov, Czechoslovakia*

Received 11 June 1984

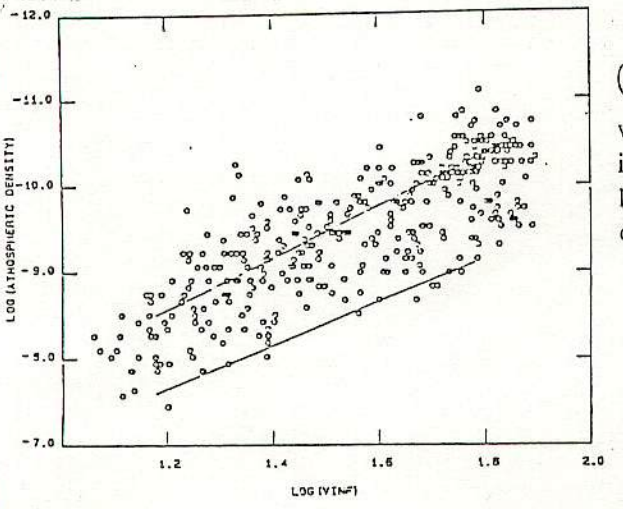

Fig. 10. Comparison of atmospheric density at onset of luminosity of TV meteors with theoretical predictions:
——— thermal condution limited,
—·—·— radiation cooling limited.

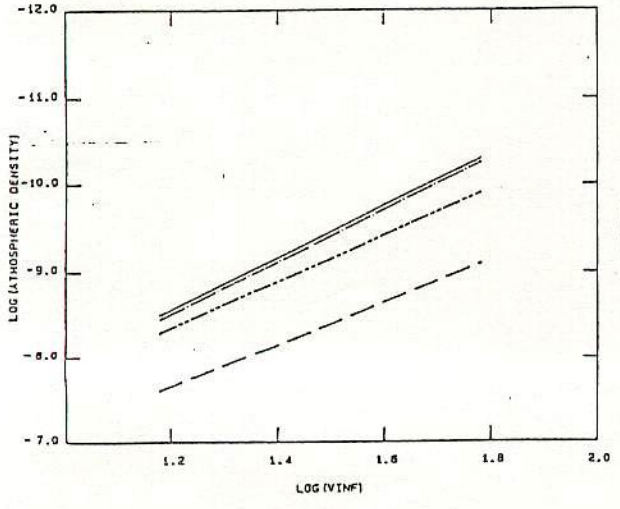

Fig. 11. Theoretical predictions for several meteoroid parameters:
——— stone, $r = 0.01$ cm.
—·—·— porous, $r = 0.01$ cm.
—··—··— porous, $r = 10$ cm.
— — — stone, $r = 10$ cm.

porous がかかしたもの
熱伝導率低い

$$e^{0.8}/[a(1-e^2)] = C \tag{7.1}$$

where C is a constant of motion determined by the initial conditions. It is therefore possible to calculate lines corresponding to fixed values of C on the $q - 1/a$ diagram such as those shown in Figs 7, 8 and 9.

$$d(1/a) \doteq 2V_c \cdot V_P/V_C^2 \tag{7.2}$$

where V_C is 29·7 km/s, V_C is the heliocentric velocity of the comet and V_P is the ejection velocity of the dust particle relative to the comet. For long-period comets $|V_C| \doteq 42$ km/s and from Fig. 6 we see that $d(1/a) \doteq$ $\doteq 0.6$ AU which corresponds to $|V_P| \doteq 6$ km/s.

According to Whipple (1951) the value of V_P for a particle of radius r_m (cm) ejected from a comet of radius R_C(km) is given by

$$V_P = \left(\frac{1{\cdot}07 \times 10^5 R_C}{\eta T^{9/4} \varrho_m r_m} - 5594 R_C^2\right)^{1/2} \quad [\mathrm{cm/s}] \tag{7.3}$$

where ϱ_m is the density of the particle (g/cm^3), r is the comet-Sun distance (AU) and $1/\eta$ is the fraction of incident solar energy used for sublimation of the cometary ices. With $R_C = 1$ km, $r = 1$ AU, $r_m = 0{\cdot}01$ cm and $\varrho_m = 1$ g/cm^3 we find $V_P \doteq 32$ m/s.

MSS-046

A triply-photographed meteor on July 28, 1985

Katsuhito Ohtsuka and Yoshihiko Shigeno ,Tokyo Meteor Network

Trajectory and orbital elements of a triply-photographed meteor on July 28, 1985 in Japan, are presented. This is a probable member of the Perseid meteor shower.

A meteor(TN 10) flared -4 magnitude was photographed simultaneously from three stations of Tokyo Meteor Network on July 29, 1985, at 2:49:14 JST (July 28, at 17 :49:14 UT) with equartorial drived 35mm-size cameras (1). Kodak 2481(High Speed Infrared film) and Hoya R-60 filter were used on account of a moonlight night. Positional and instrumental data are as follows :

Station	λ	φ	H	Lens	Rotating Sutter
Daisawa	−139°40′41″.1	+35°39′07″.4	36m	50mmF2.0	25 (breaks/sec)
Mikado	−140 22 09	+35 16 46	40	50mmF1.8	20
Ashigara	−139 10 47.3	+35 19 49.5	208	24mmF1.4	−

Standard Diviations from plate(film)-constants fit the order of 30 arc sec. Results of trajectory and orbital elements are listed, as follows :

No. TN 10 1985- 7-28.74252 UT $\lambda_{\odot(1950.0)}$ 125°.09

App.R.P.(1950.0) α 25°.11 δ +54°.87
(σ ± 0°.04 ± 0°.05)
Cor.R.P.(1950.0) α 24°.98 δ +55°.17

			Meteor	1862III(2)
		$\omega_{(1950.0)}$	155°.6	152°.8
		$\Omega_{(1950.0)}$	125°.1	138°.7
sinQ 0.915 a)	V_{obs} 59.1km/s b)	$i_{(1950.0)}$	109°.5	113°.6
H_B 106.9km	V_∞ 59.2± 0.6km/s	e	0.956	0.960
H_E 79.1km	V_G 58.0km/s	q (AU)	0.971	0.963
cosZ 0.868 c)	V_H 41.3km/s	a (AU)	22.27	24.33

a) Q is the angle between great circles of meteors from Mikado and Ashigara.
b) V_{obs} is mean observed velocity.
c) Z is the zenith distance of the apparent radiant point.

The Comet 1862III(P/Swift-Tuttle), of which orbital elements from Mersden's catalogue (2) are shown in the above, is known as a parent body of the Perseid meteor shower. Theoretical radiant point predicted from cometary orbit at $\lambda_{\odot(1950.0)}$ 125°.0 is :

R.P.(1950.0) α 30° δ +53° Δ 0.226AU V_G 58.8km/s
(Δ is closest distance between Earth-Comet orbits.)

The meteor TN 10 shows a similerity to the cometary values in radiant and orbital data. Therefore, TN 10 is a probable member of the Perseids in July.

References

(1) Sky Watcher, Vol.3, No.10, 1985, p.83 (in Japanese).
(2) B.G. Marsden, "Catalogue of Cometary Orbits" SAO, Cambridge MA, 1986.

MSS-046

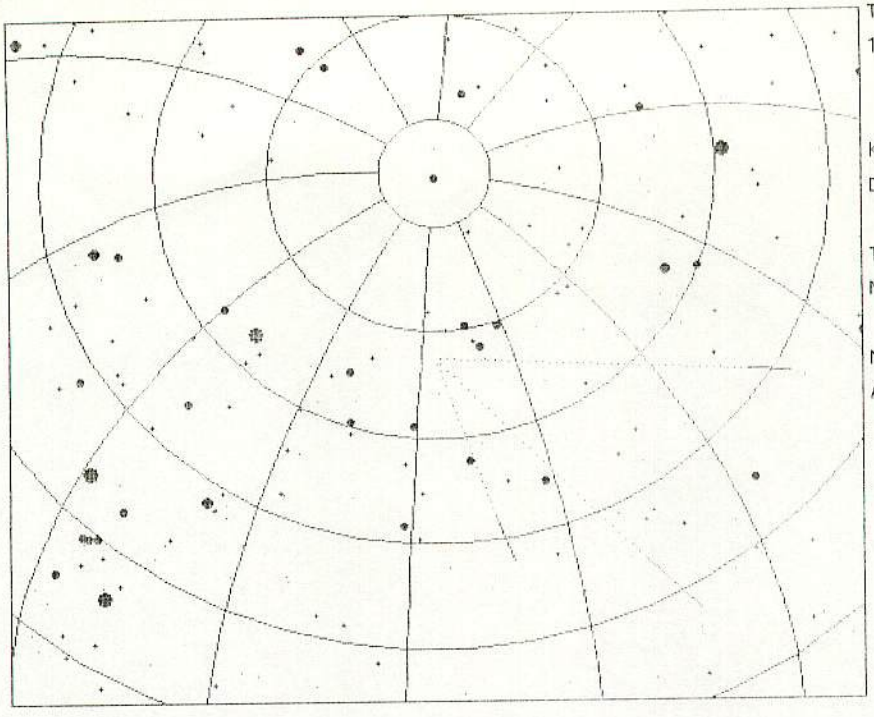

TN 10
1985年 7月 28/29日
2時 49分 14秒

K.Ohtsuka
Daisawa

T.S.U
Mikado

Meiji Unv.
Ashigara

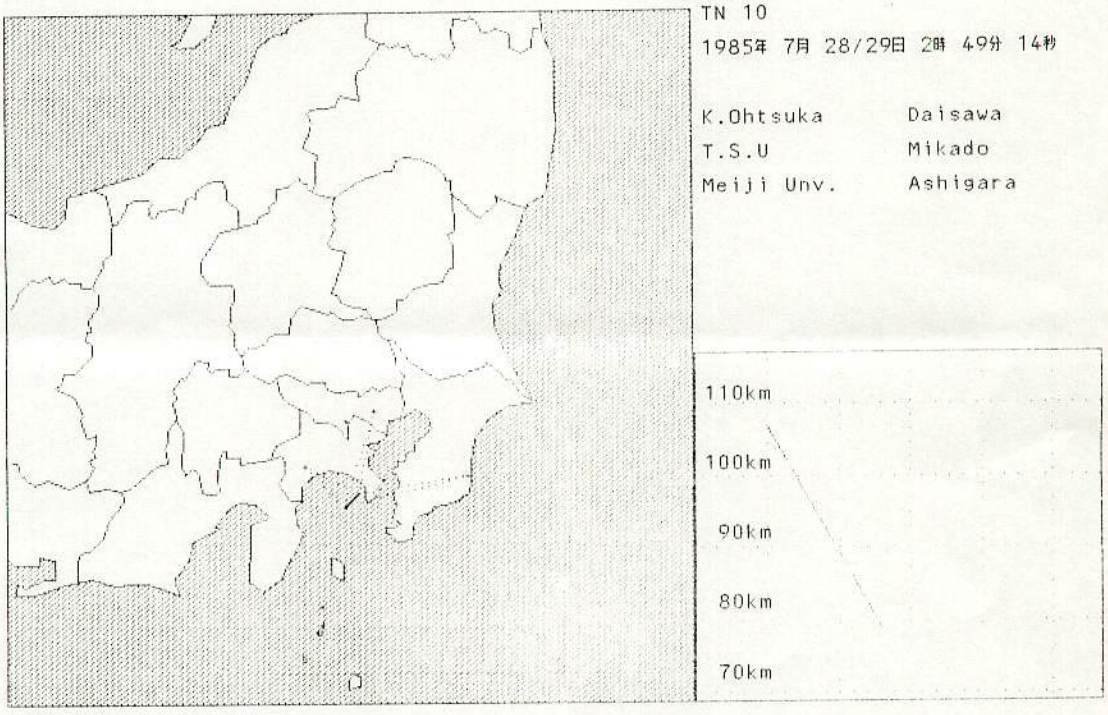

TN 10
1985年 7月 28/29日 2時 49分 14秒

K.Ohtsuka Daisawa
T.S.U Mikado
Meiji Unv. Ashigara

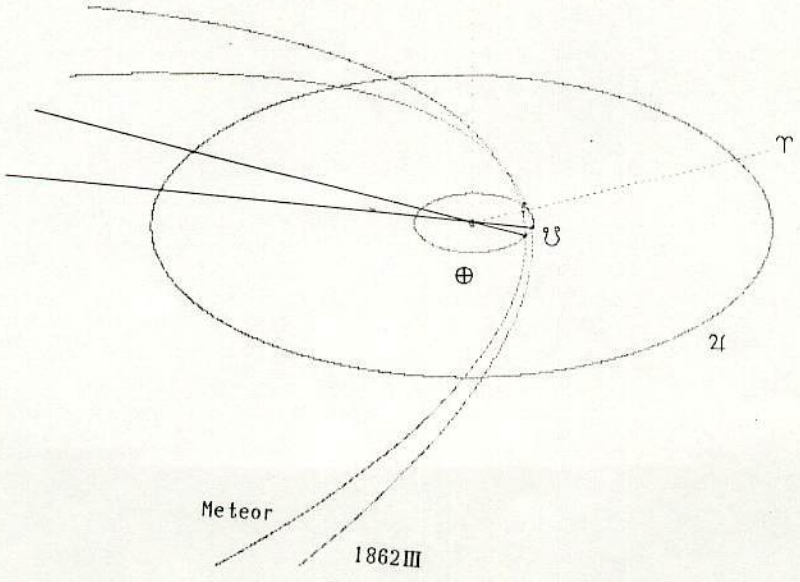

三門 47 MSS

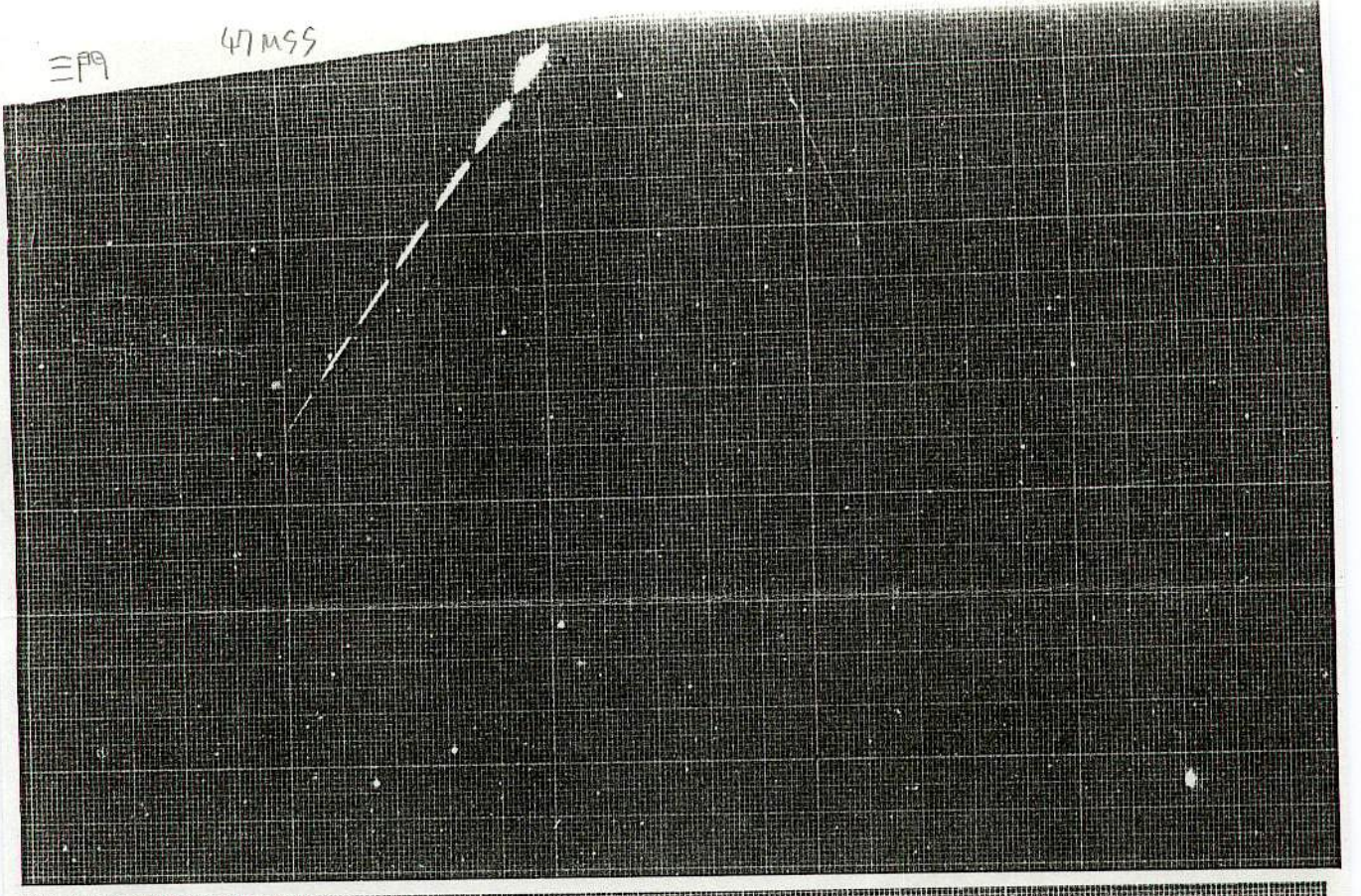

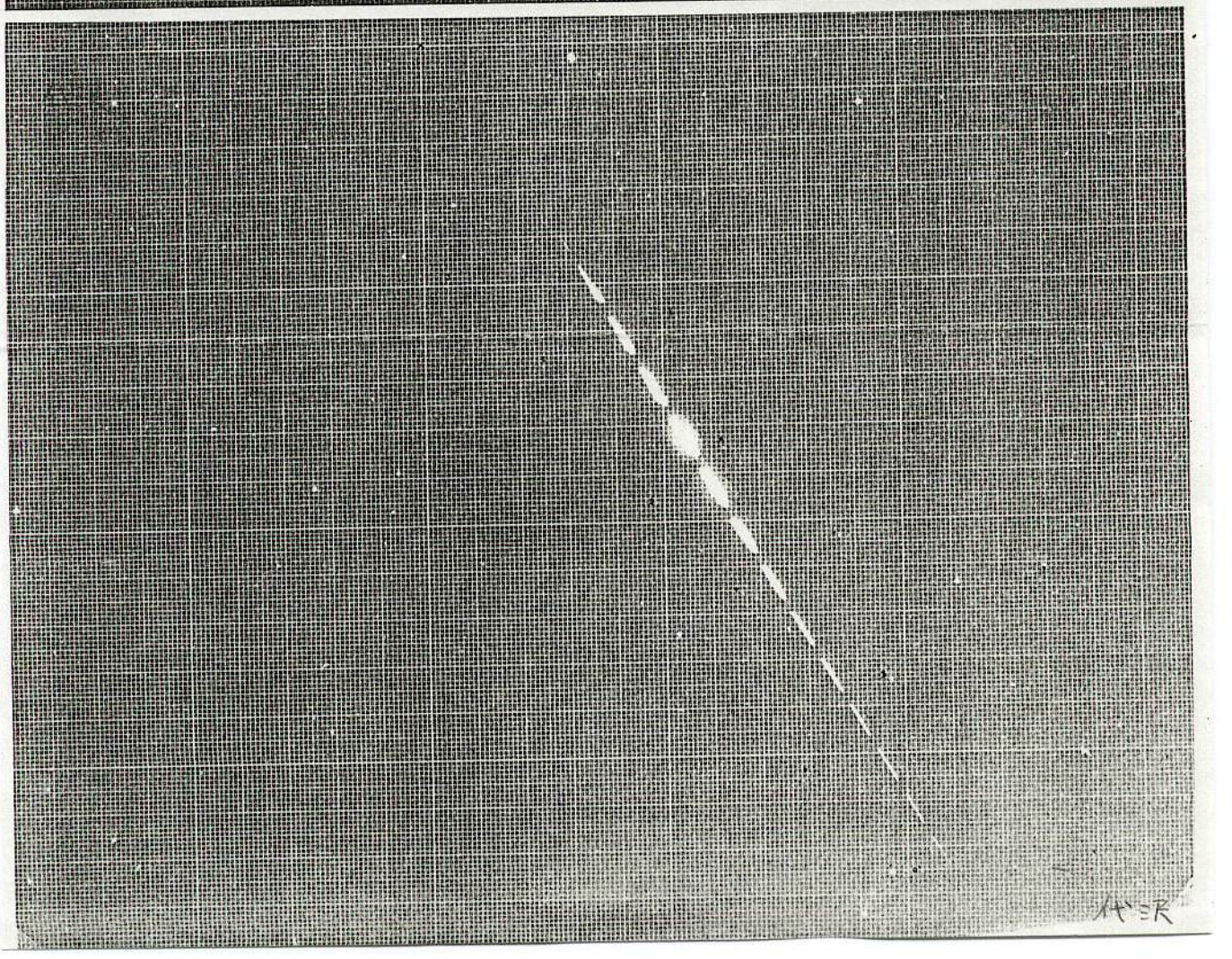

West Germany, 16 February 0200.46 GMT.

A fast moving fireball of -15 maximum absolute magnitude illuminated an area of about 1200 km diameter in central Europe. The fireball was photographed by 17 stations of the European network (11 in West Germany, 5 in Czechoslovakia, and 1 in East Germany). The time of fireball passage is based on two visual and one photoelectric timing with standard deviation of ± 6 seconds. The fireball travelled a 65-km luminous trajectory in 1 second and exhibited 2 flares: the main flare of -15 absolute magnitude lasted 0.3 seconds with brightness over -13 magnitude, and the terminal flare of -11 absolute magnitude, which lasted only 0.02 seconds, was followed by an extremely short decrease in brightness. One diffraction grating spectral record of the fireball with dispersions down to 10 angstroms per mm is also available showing many emission lines, mostly of ionized calcium, magnesium, and silicon, and of neutral iron, calcium, and magnesium.

The photographs were measured by J. Bocek. The following results are based on computations from the best records of 6 different stations and should be close to the final results.

48MSS 1988.7.3 from 大家

SEAN Bulletin, v. 13, no. 3 March 31, 1988

30 m/sec 急眠

1797 彗星 予想 RP 208, +8 60 km/s 2月15日 撮木

q 0.525 ω 279.9
e 1 Ω 331.4
λ 129.4

Fireballs (continued)

	Beginning	Maximum Light	Terminal
Velocity (km/s)	66.2	62.	47.
Height (km)	113.0	80.6	71.46
Latitude	48.948°N	49.22°N	49.302°N
Longitude	11.832°W	11.52°W	11.436°W
Absolute Magnitude	-4.4	-14.7	-4.6
Photometric mass (kg)	4.2	1.4	none
Z R	49.78°	-	50.22°

Fireball Type: IIIB (with some possibility of IIIA)
Meteorite fall is completely excluded

Radiant (1950.0)	Observed	Geocentric	Heliocentric
Alpha	213.72°	213.62°	-
Delta	4.89°	4.55°	-
Lambda	-	-	189.7°
Beta	-	-	27.0°
Initial velocity (km/s)	66.2	65.1	42.0

Orbit (1950.0)

A	30.0	A.U.	Omega	260.°
E	0.98		Ascending Node	326.086°
Q	0.58	A.U.	Inclination	144.°

The fireball was probably a late member of the stream of Coma-Berenicids.

Information Contacts: Z. Ceplecha and P. Spurny, Ondrejov Observatory, 251 65 Ondrejov, Czechoslovakia.

USSR/near Aral Sea, 19 February, 2359 GMT (20 February, 0459 local time)
Observer: F/O Wolf, Lufthansa No. 737 (Bangkok-Frankfurt)
Location: 46.83°N, 60.50°E, aircraft course 325° magnetic, alt. 10.6 km
1st sighting: Azim. 315°, alt. 15°
End sighting: Azim. 010°, alt. 14°
Duration: 15 seconds
Magnitude: Brighter than full moon
Color: White
Size: Half diameter of full moon
Termination: Fragmented into 3 pieces: 1 bright with tail; 2 bright as stars
Information Contact: Same as for Newfoundland, Canada.

Illinois, USA, 27 February, 0245 GMT (26 February, 2045 Central Standard Time)
Observer: Edwin Lacheta
Location: Chicago Heights (41.33°N, 81.38°W)
Path: In N-NW, alt. 50°-55°, nearly vertical descent
Duration: 8-9 seconds
Magnitude: Much brighter than full moon
Color: Bright blue with burning edges
Trail: Blue, halo-like on trailing edge
Termination: Fell behind buildings
Information Contact: Edwin Lacheta, Chicago Heights, Illinois.

Central Great Lakes, USA, 28 March, 0110 GMT (27 March, 2010 Eastern Standard Time).

Many people reported seeing a fireball traveling generally N-E or NW-SE at a low (20° 30°) altitude. The most northerly sightings were from the Milwaukee, Wisconsin

Meteor Luminosity at 160 km altitude from TV observations for bright Leonid meteors.

Yasunori Fujiwara, Masayoshi Ueda, Yasuo Shiba, Masatoshi Sugimoto, Masao Kinoshita, Chikara Shimoda
Nippon Meteor Society, Japan

and Takuji Nakamura
Radio Atmospheric Science Center, Kyoto University, Kyoto, Japan

Short title: METEOR LUMINOSITY AT 160 KM ALTITUDE

submitted to the Geophysical Reseach Letters Aug 1997

Abstract. Two atmospheric trajectories have been determined by simultaneous observations with image intensifier-fitted TV cameras and conventional photographic cameras for two bright Leonid meteors (fireballs) in 1995 and 1996. Beginning heights recorded by the photographic method are lower than about 130 km, but those observed by the TV systems are closer to 160 km. The primary reason for this difference is the sensitivity of the observing systems. However, the difference in the sensitive wavelengths (up to 900 nm for the TV systems) could be another factor contributing to the large difference between the two method. This result suggests that the beginning heights of high speed bright meteors such as Leonid meteors are much higher than previously expected.

1. Introduction

Meteor is a phenomenon of luminosity and ionization caused by the impinging of meteoroid into the earth's atmosphere. The height range of meteor luminosity is related to the physical characteristics of the meteoroid as well as the impinging velocity to the earth (Ceplecha, 1968). According to the data base of about 4,500 photographic meteors at the IAU Meteor Data Center (Lindblad, 1995), the average meteor beginning height is 96.2 km, and the maximum beginning height recorded was 138.3 km, with the meteors with beginning height of over 120 km and 130 km are 35 records (0.8%) and 7 records (0.2%), respectively. On the other hand, sensitive TV camera observations have recently become popular and have been used to determine the orbit of meteors (Hawkes et al,1984; Sarma and Jones,1985). Those studies indicated very few meteors at heights greater than 120 km. Ueda and Fujiwara(1995) have determined the orbits of meteors by the double station TV observations, and found that the average meteor beginning height is 107 km and few of them are observed to be above 120 km, with only two meteors to be above 130km (maximum height was 131 km). There are differences in limiting magnitude for different observation systems. For example, the 35 mm small camera can record up to 0 to +1 magnitude, and the super-schmidt camera can detect as faint as +4 magnitude(Hawkins, 1964). The limiting magnitude for TV camera observation is normally +6 to +8 magnitude(Fujiwara, 1993) and much more sensitive than the previous observation systems. Despite this high sensitivity of TV systems, the observational report mentioned above did not show a significant difference in the scatter-diagram of meteor velocities versus beginning heights(Hawkes et al, 1984). Woodworth and Hawkes(1996) stressed that there was a significant bias against very high (and low) meteors, since the optimum intersection height for previous multistation TV meteor studies was set to approximately 95 km and the relatively small fields of view result in a bias against high altitude meteors. TV observation is characterized by its high sensitivity. However, the objective lens used with the TV observation

usually project a fairly small field, such as 20 degrees in diameter. Because of this small field, bright meteors or fireballs are rarely recorded by the observations. In this study, we report two cases of the Leonid fireballs observed using TV camera systems with wide field areas, as well as the photographic measurement, and report the meteor beginning height determined by these instruments and discuss the effect of the different observation systems on the observed meteor height.

2. Observations

Multistation TV and photographic observations were carried out for three nights on 16-18 of November 1995 and 16-17 of November 1996, aiming at bright Leonid meteors. The observational sites and the equipments are given in Tables 1. The TV observation systems utilize the image intensifiers (I.I.) produced by Hamamatsu Photonics(V3287P) and 8 mm video recorders. Further details have been described elsewhere(Fujiwara, 1993; Ueda and Fujiwara, 1995). The objective lenses were wide-angle ones with the focal length of 24–28 mm, in order to observe bright meteors or fireballs with higher probability. For the photographic observation, both 35 mm and 6x7 size cameras were used, and some of them were equiped with rotating-shutters in front of their lenses. The wide-angle lenses were also used as the objective lenses. Two fireballs were observed by these observation systems; a Leonid fireball with visual magnitude of -7 at 18:05:44 UT on November 17, 1995 (Leonid 1) was observed by four photographic cameras and two TV systems, and another Leonid fireball with visual magnitude of -4 at 17:31:17 UT on November 16, 1996 (Leonid 2) was again recorded at two TV sites and two photographic sites. The images recorded by TV systems were digitalized by a PC with an image processing board, whereas most of the photographic meteors were analyzed with a film scanner or photo-CD by a PC software. The position of the meteor trail and of a number of surrounding reference stars (typically 15 for each meteor) were measured. The computer program to reduce positions of meteors from the digitized images was

developed by Hanaoka (1991, private communication). On some of the photographic meteors (Nos.5 and 6 of Leonid 1), on the other hand, positions were measured on the printed photographs. The standard deviation errors of the measured positions of each observations were also shown in Table 1. For the photographic meteors, the magnitudes were estimated by measureing the image density. However, these magnitudes could not be determined from TV images since these meteor images were saturated because of their brightness. The meteor trajectories in the atmosphere and the heliocentric orbits were calculated in a standard method (Hasegawa, 1983). The beginning and terminal heights of each meteor are determined by the combination of observational sites, independently, by intersecting the meteor trajectry by the angles observed from each site. Then the beginning and terminal heights are avereged on the observations at each site, and given in Table 2 and in Figures 1 and 2. Trajectory and orbital data are presented in Tables 3 , respectively.

3. Results and Discussions

As shown in Table 2 and Figure 1, the meteor beginning heights determined by the photographic observations were between about 130 and 110 km. In the photographic meteor file of IAU Meteor Data Center, 23 meteors are recorded as Leonid meteors, which have determinations of beginning heights. These beginning heights ranges from about 110 km to 128 km with an average of 114.4 km, which is very similar to our current analysis. On the other hand, the beginning heights obtained by the TV observations in the present study were about 160 km, which is much higher than those determined by photographic technique.

Ueda and Fujiwara(1995) have determined the trajectory of seven Leonid meteors. They further observed ten Leonid meteors by more recent observations (Ueda and Fujiwara, 1997, private communication). For these 17 Leonid meteors by TV observations with magnitudes of +0 to +7, they found that the average beginning height

was slightly higher than that of the photographic meteors, but the distribution itself, 128–106 km, was similar to that by photographic meteors.

These results suggests that the meteoroids threw off from comets with a large mass and a large impinging speed, which are easily broken, start luminating at a much higher altitude (about 160 km) than the beginning heights previously known by the photographic observations (up to 130 km). Since TV observations with I.I. system are sensitive to a longer wavelength (up to about 900 nm), the luminosity at very high altitudes as shown in this study could be due to the infrared luminosity in the upper atmosphere. Although we cannot make a clear conclusion by the only two examples shown here, we suggest that meteor observations with wide-field TV camera systems with an infrared sensitivity would be very valuable to clarify the luminosity mechanism of the meteors at very high altitudes.

4. Summary

We have observed two Leonid fireballs from simultaneous TV and photographic observations, and the beggining heights were found to be around 160 km, which were extremely higher than the previous observations. Thus, at least the luminosity of the Leonid fireballs starts at much higher altitude than is considered from the previous photographic observations.

Acknowledgments. The authors are grateful to U. Takeuchi, S. Ida and A. Inaka for providing their data.

References

Ceplecha, Z., *Smithson. Astrophys. Obs. Rep., 279,* 1968.

Fujiwara, Y., Television observations of meteors in Japan, *Meteoroids and their Parent Bodies,* 265, 1993.

Hasegawa, I., Determination of Orbits, Koseisha, Tokyo(in Japanese) , 1983.

Hawkes, R.L., J. Jones, Z. Ceplecha, The populations and orbits of double-station TV meteors, *Bull. Astron. Inst. Czechosl., 35,* 46-64, 1984.

Hawkins, G.S., Meteors, Comets, and Meteorites, *McGraw-Hill, New York,* 1964

Lindblad, B. A., The IAU meteor data center in Lund, *Earth Moon Planets, 68*, 405-408, 1995.

Lindblad, B.A., V. Porubcan and J. Štohl, The orbit and mean radiant motion of the Leonid meteor stream, *Meteoroids and their Parent Bodies,* 177–180, 1993.

Sarma, T., and J. Jones, Double-station observations of 454 TV meteors, I. Trajectories *Bull. Astron. Inst. Czechsl., 36*, 9–24, 1985.

Ueda, M. and Y. Fujiwara, Television meteor radiant mapping, *Earth Moon Planets, 68*, 585–603, 1995.

Woodworth, S.C., and R. L. Hawkes, Optical search for high meteors in hyperbolic orbits, *Astron. Soc. Pac. Conf. Ser., 104*, 83–86, 1996.

Y. Fujiwara, M. Ueda, Y. Shiba, M. Sugimoto, M. Kinoshita, C. Shimoda,Nippon Meteor Society, 2-16-8 Mikuni Honmachi, Yodogawa, Osaka 532, Japan. (e-mail: DHB15312@biglobe.ne.jp)

T. Nakamura, Radio Atmospheric Sciencen Center, Kyoto University, Uji, Kyoto 611, Japan. (e-mail: nakamura@kurasc.kyoto-u.ac.jp)

Received August XX, 1997

To be submitted in the *Geophysical Research Letters*, 1997.

Table 1. List of the observer, observing site and the equipment

Leonid 1.(1995-11-17 18h05m44s)

No.	Observer	Site	M	Lens	Field of view	L.M.	Error
1	Sugimoto	Shigaraki	TV	24mm F1.4	ϕ 48°	6.5	8.08
2	Takeuchi	Handa	TV	58mm F1.4	ϕ 25°	7.0	4.39
3	Ueda	Shigaraki	P*	15mm F4.0	fish eye	-	7.37
4	Ida	Youkaichi	P	35mm F2.0	53° x 37°	-	0.91
5	Inaka	Gifu	P	28mm F2.0	64° x 45°	-	2.45
6	Shiba	Sanda	P*	24mm F4.0	fish eye(6x7)	-	1.07

Leonid 2.(1996-11-16 17h31m17s)

No.	Observer	Site	M	Lens	Field of view	L.M.	Error
1	Nakamura	Shigaraki	TV	28mm F2.0	ϕ 45°	6.5	5.36
2	Kinoshita	Ohmihachiman	TV	24mm F1.4	ϕ 48°	6.5	5.22
3	Shiba	Tohjou	P*	24mm F4.0	fish eye(6x7)	-	1.02
4	Shimoda	Hario	P*	15mm F2.8	fish eye	-	2.07

M: methord of the observation(TV or P:Photograph, *:with rotating-shutter)

L.M.: the apparent limiting stellar magnitude

Error: the standard error in the position(arc minutes)

Table 2. Beginning and terminal points of Leonid 1 and Leonid 2.

Leonid 1(1995-11-17 18h05m44s)

No.	Observer	M	Beginning(λ , ψ ,H,c)		Terminal(λ , ψ ,H,c,**)	
1	Sugimoto	TV	136.84E 34.95N 159.9	B	136.08E 34.97N 89.4	J **
2	Takeuchi	TV	139.85E 34.94N 160.7	A	136.50E 34.96N 127.1	C **
3	Ueda	P*	136.31E 34.97N 108.1	F	136.12E 34.98N 90.8	H
4	Ida	P	136.50E 34.96N 128.5	D	136.05E 34.98N 87.9	K
5	Inaka	P	136.39E 34.97N 117.0	E	136.09E 34.98N 89.6	I
6	Shiba	P*	136.25E 34.97N 104.1	G	136.04E 34.98N 85.3	L

Leonid 2(1996-11-16 16h31m17s)

No.	Observer	M	Beginning(λ , ψ ,H,c)		Terminal(λ , ψ ,H,c,**)	
1	Nakamura	TV	135.53E 34.87N 160.5	A	134.58E 34.83N 91.6	F **
2	Kinoshita	TV	135.51E 34.87N 159.7	B	134.91E 34.85N 115.8	C **
3	Shiba	P*	134.86E 34.84N 113.1	D	134.53E 34.82N 90.1	H
4	Shimoda	P*	134.72E 34.84N 103.1	E	134.56E 34.83N 91.5	G

M: methord of the observation(TV or P:Photograph, *:with rotating-shutter)

λ :latitude in degrees, ψ :longitide in degrees, H:height(km)

c:letter code for beginning or terminal point plotted Figs.1 and 2.

**:last observed point in the field of the view

Figure 1. Ground path of the Leonid fireballs and observer sites. Letter coding of the path of each fierballs is set out in Table 2. Leonid 1(17 Nov.1995), Leonid 2(16 Nov.1996)

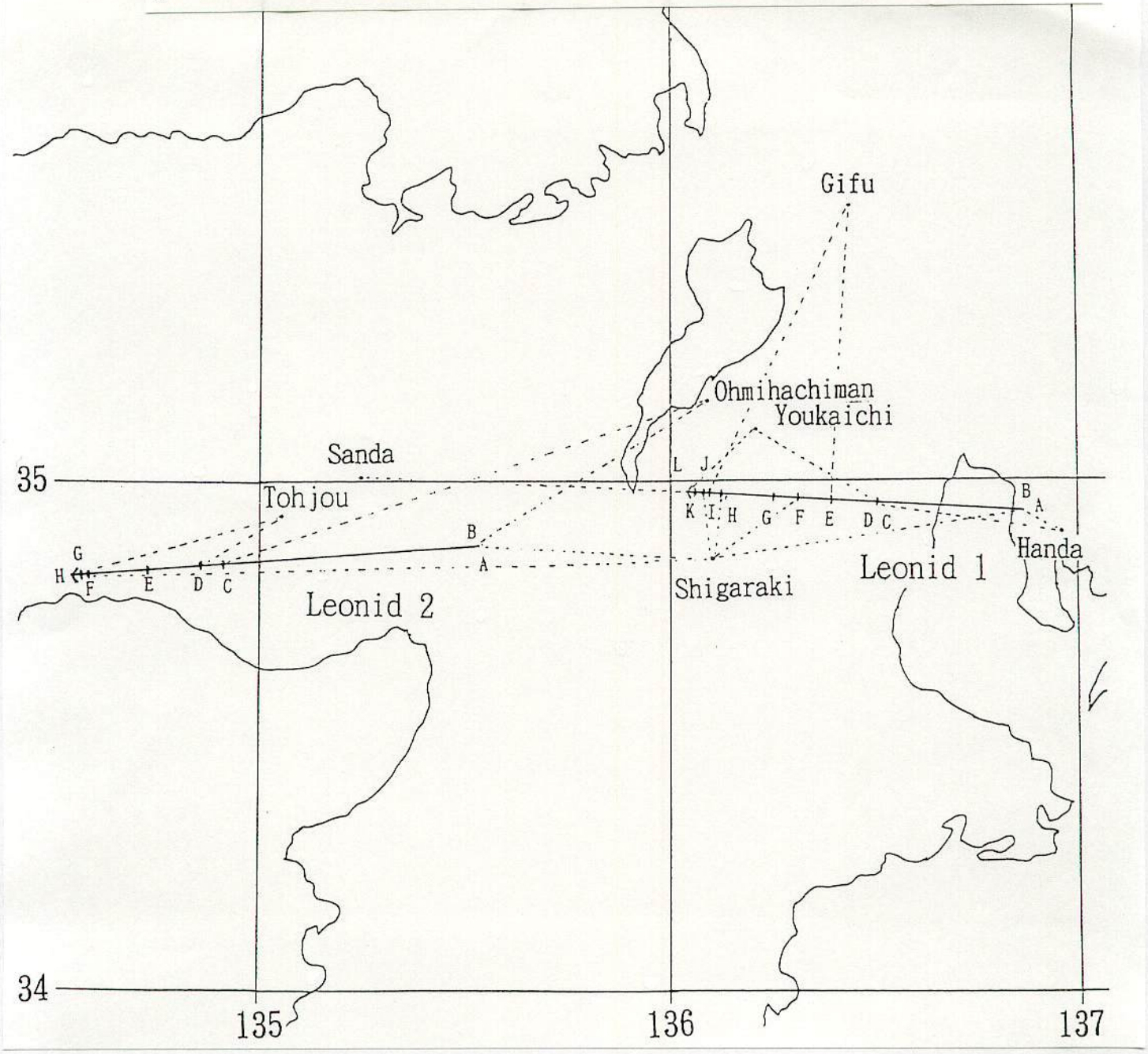

Table 3. Trajectory and orbital data(eq.2000.0) for each of the fireballs

No.	Leonid 1	Leonid 2
Date	17 Nov. 1995	16 Nov. 1996
Time(UT)	18h05m44s	17h31m17s
Apparent Radiant(°)	α =153.7	α =153.2
	δ =22.2	δ =22.2
Corrected Radiant(°)	α =153.7	α =153.4
	δ =22.2	δ =22.1
Observed Magnitude	-7	-4
Cos ZR	0.707	0.616
Beginning point	136.85E	135.53E
	34.94N	34.87N
	160.7km	160.5km
Terminal point	136.04E	134.53E
	34.98N	34.82N
	85.3km	90.1km
Velocity(km/s)	Vobs=72.1	Vobs=71.3
	Vg=71.0	Vg=70.1
	Vh=41.7	Vh=40.9
Orbital data	a=17.0	a=7.2
	e=0.94	e=0.86
	q=0.98	q=0.98
	Ω =235.0	Ω =234.7
	i=161.8	i=162.0
	ω =171.9	ω =171.3

α :right ascension, δ :declination
corrected radiant: corrected for diurnal aberration and zenithal attraction
cosZR: cosine of the zenith distance of the trajectory
beginning(terminal) point: (latitude in degrees, longitude in degrees, height)
Vobs: average observed velocity
Vg: velocity corrected for diurnal aberration and zenithal attraction
Vh: heliocentric velocity
a: semi-major axis(AU), e:eccentricity, q: perihelion distance(AU)
Ω: longitude of the ascending node(°), i: inclination of the orbit(°)
ω: argument of perihelion(°)

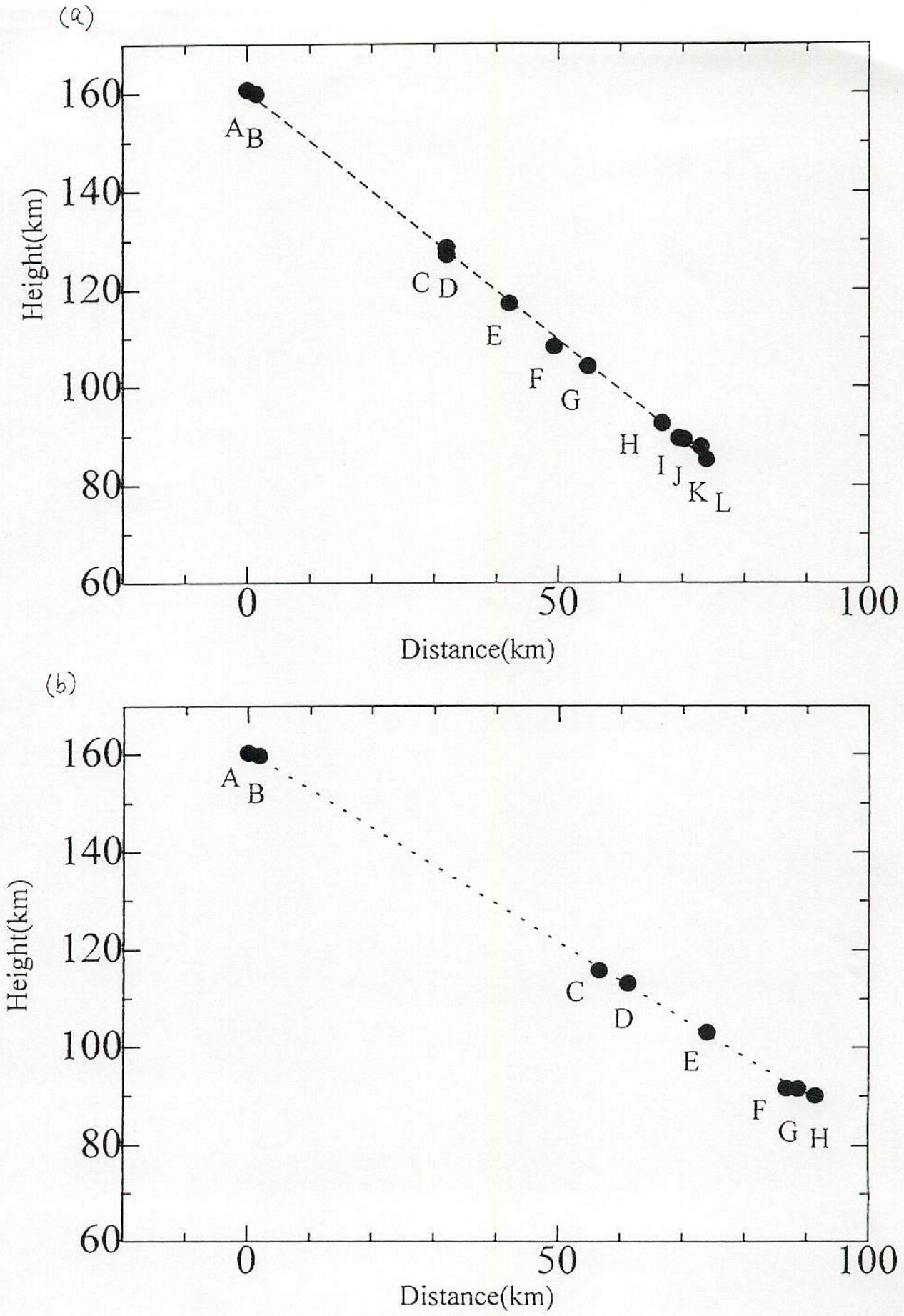

Figure 2. Reduced trajectory of the Leonid fireballs: (a) Leonid 1 (17 Nov. 1995). (b) Leonid 2 (16 Nov. 1996). The coding of letters plotted is given in Table 2. Note that the beginning of the emission was at 160 km.